A new annealing route for industrial processing of dual phase steels to obtain improved mechanical properties

A Dissertation submitted

in partial fulfillment of the requirements

for the degree of

Master of Engineering

in

Production Engineering

by

Virender Singh

Regd. No. 801482029

Under the supervision of:

Dr. Tarun Nanda
Assistant Professor, MED,
Thapar University, Patiala

Dr. B. Ravi Kumar
Principal Scientist, MST
CSIR-NML, Jamshedpur

MECHANICAL ENGINEERING DEPARTMENT

THAPAR UNIVERSITY, PATIALA-147004, PUNJAB, INDIA

July, 2016

Dedicated to my Grandfather

Ch. Sher Singh

Certificate

I hereby declare that the thesis entitled "**A new annealing route for industrial processing of dual phase (DP) steels to obtain improved mechanical properties**" is an authentic record of my study carried out as requirements for the award of the degree of **Master of Engineering** in **Production Engineering** at **Thapar University, Patiala** under the supervision of **Dr. Tarun Nanda**, Assistant Professor, Mechanical Engineering Department, Thapar University, Patiala and **Dr. B. Ravi Kumar**, Principal Scientist, MST Division, CSIR-NML Jamshedpur during July, 2014–2016. The matter embodied in this report has not been submitted in partial or full to any other university or institute for the award of any degree.

Date: 12/7/16

Virender Singh

It is certified that the above statement made by the student is correct to the best of my/our knowledge and belief.

Dr. Tarun Nanda
Assistant Professor
Mechanical Engineering Department
Thapar University, Patiala - 147004

Dr. B. Ravi Kumar
Principal Scientist
MST Division
CSIR-NML Jamshedpur

Countersigned by

Dr. S.K. Mohapatra
Sr. Professor & Head
Mechanical Engineering Department
Thapar University, Patiala – 147004

Dr. S.S Bhatia
Dean of Academic Affairs
Thapar University, Patiala - 147004

Acknowledgement

I would first like to thank my thesis advisor, Dr. Tarun Nanda. I have been amazingly fortunate to have an advisor with such a character and hardworking nature. His patience and support helped me overcome many crisis situations and finish this dissertation.

My deepest gratitude is to my co-advisor, Dr. B. Ravi Kumar. The door to his office was always open whenever I ran into a trouble spot or had a question about my research or writing. His support and un-ending encouragement made it possible for me to express myself and explore independently. His expertise was always available to steer me in the right direction whenever he thought I needed it.

A special Thanks to Mrs Manashi Adhikary and Mr. Anindya Das who created a friendly environment and helped me with their expert advice whenever I needed it. Without their passionate participation and input, the experimental work could not have been successfully conducted.

I am also indebted to the members of the *National Metallurgical Laboratory* with whom I have interacted during the course of my graduate studies. I would like to show my gratefulness to the technical staff of NML-Jamshedpur (Mr Lalit Gupta, Mr Lalan Patro and Mr Rajiv Jonko) for their consistent support during experimentation phase of the research work.

Finally, I must express my very profound gratitude to my parents and to my friend Mr. Arnab Chakraborty for providing me with unfailing support and continuous encouragement throughout the process of researching and writing this thesis. This accomplishment would not have been possible without them.

Virender Singh

Abstract

Dual-phase (DP) steels offer high potential of weight reduction without sacrificing mechanical properties for their application in automotive industry. They derive their properties through the second hard phase (martensite/ bainite) in a ferrite matrix. DP steels are mostly produced through the continuous annealing process route in the industry because of the requirement of high production rates, uniformity in properties, and leaner chemistry design feasibility. Important mechanical properties which are desirable for the final components include absence of yield point, low yield point to ultimate tensile strength, high strain hardenability along with high ductility etc.

The main objective of the present work was to improve the mechanical properties of a low carbon Si based ferrite-martensite DP steel by tailoring the second phase (martensite) morphology, distribution, and size in the ferrite matrix. An existing conventional continuous annealing process (CAL) route was modified to develop an improved annealing process route suitable for industrial usage. A custom designed annealing simulator (capable of simulating conditions similar to industrial continuous annealing lines) was used to simulate the various annealing processes. Several combinations of processing routes depending on the governing mechanisms such as, ferrite recrystallization, pearlite dissolution, and phase transformation etc. were investigated for their effect on the morphology, and distribution of the martensite phase and the resulting mechanical properties. The main focus of the current work was to study the effect of heating rates, isothermal annealing temperatures, and soaking time periods (with no changes in cooling regime of conventional CAL) on the morphology, and distribution of martensite phase. Further, the effect of combining thermal cycling as a pre-treatment to conventional CAL processing was also investigated. It was observed that by varying the above stated annealing parameters, it was possible to trigger the ferrite recrystallization, pearlite dissolution, and phase transformation at various stages of the annealing process cycle. All such changes resulted in change of martensite morphology, distribution, and even grain size and thus affected the final mechanical properties of DP steel.

This entire experimentation effort resulted in the development of a new processing route called “Continuous Heating Annealing Process (CHAP)” that gave strength levels of 625 MPa with ductility similar to that obtained with the conventional CAL process with a significant improvement in strain hardening exponent. Thus, the present research provided a new annealing route (without any major changes in the conventional CAL process) for processing of DP steels with improved strength-ductility combination.

Table of Contents

List of Figures

List of Tables

List of Acronyms

Acronym	Full name
AHSS	Advanced high strength steels
BH	Bake hardening
CP	Complex phase
DP	Dual phase
DIC	Differential interference contrast
EBSD	Electron backscatter diffraction
FG	Fine grained
HSLA	High strength low alloy
IF	Interstitial free
IQ	Image quality
LOM	Light optical microscopy
M-A	Martensite- austenite
MART	Martensitic
OM	Optical microscopy
Q&P	Quenching and partitioning
QT	Quenching temperature
SEM	Scanning electron microscope
TEM	Transmission electron microscope
TMP	Thermo mechanical processing
TRIP	Transformation induced plasticity
TS	Tensile strength
UTS	Ultimate tensile strength

XRD	X-ray diffraction
YS	Yield strength

List of Symbols

Symbol	**Meaning**
Al	Aluminum
Ac_1	Lower critical temperature
Ac_3	Upper critical temperature
B	boron
C	Carbon
Ca	Calcium
Co	Cobalt
Cr	Chromium
℃	Degree Celsius
Fe	Iron
H_2	Hydrogen
Mg	Magnesium
Mo	Molybdenum
Mn	Manganese
MnS	Manganese sulphide
N	Nitrogen
Ni	Nickel
N_2	Nitrogen

P	Phosphorous
S	Sulphur
Si	Silicon
V	Vanadium
V_f	Martensite volume fraction
α	Ferrite phase
γ	Austenite phase

Chapter 1
Introduction

1.1 Background

Steel can easily be called mankind's most important technological achievement as regard to structural materials thus facilitating newer engineering feats in the fields of infrastructure, energy and transportation. In a sense, steel helps feed and clothe the world by providing employment and making infrastructure, transportation, and construction possible. It is hard to find a material as versatile as steel and that can provide as many combination of strength and formability as steel does. Moreover, all these benefits become more meaningful and sustainable because of high recycling rate of steel which is well above 90 percent [1]. The industrial revolutions in the past wouldn't have been possible without the development of iron and steel [2].

1.2 Role of Steel in Automotive World

Traditionally, the vehicles were heavier in weight and consumed more fuel as compared to their modern counterparts thus resulting in excessive economic and environmental hazards. The safety of passengers was the prime concern at that time as it is now. So there was an inevitable need to trim down the weight of automobiles, but the biggest problem was to achieve this without compromising the safety of passengers [3]. The only way out was to improve the strength of steel without reducing its formability which was an absolute necessity for industrial forming of automotive parts. These conflicting demands of automotive industry increased engineering and scientific interest in the development of newer grades of steels with industrially accessible mechanical properties. The development of advanced high strength steels (AHSS) significantly fuelled technological progress in the field of automotive industry and completely revolutionised the automotive world. These modern steel grades provided high strength along with good ductility and also were very light in weight as compared to the conventional steels used for automobiles (see Figure 1.1). So the usage of these steels grew more and more in the modern automotive industry for achieving improved crash worthiness and fuel economy [4]. There are six main categories of AHSS that are gaining more popularity these days: Dual Phase (DP) steel, Transformation-Induced

Plasticity (TRIP) steel, Complex Phase (CP) steel, Ferritic-Bainitic (FB) steel, Martensitic (MS) steel, and Twinning-Induced Plasticity (TWIP) steel [4,5].

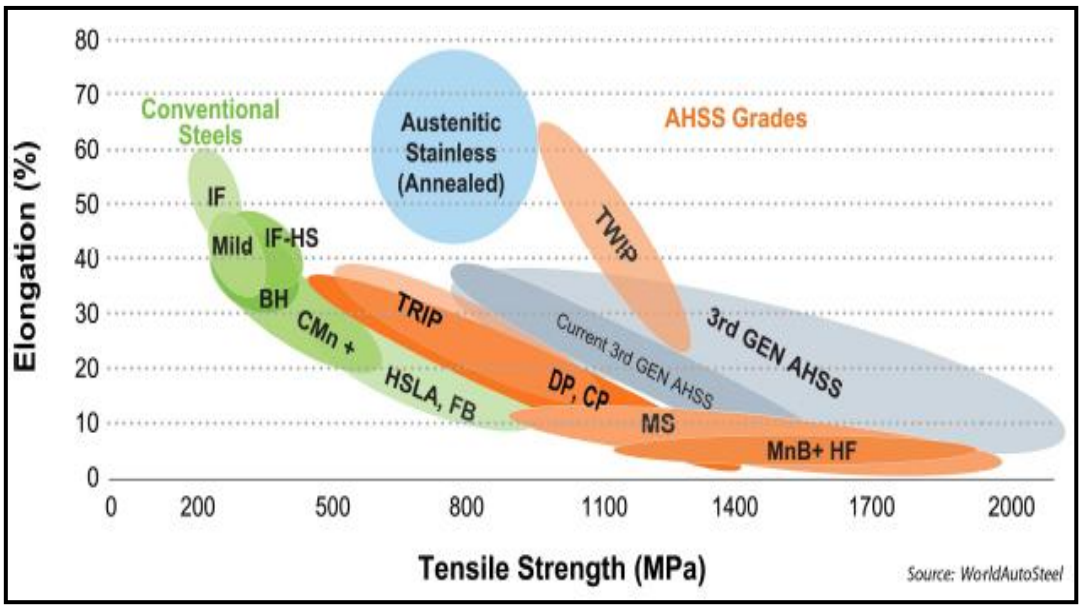

Figure 1.1 "Banana curve" showing the tensile strength with respective elongation of different steel microstructures [5].

These categories of AHSS provide solution for two distinct needs of automotive industry. The first need is of having higher strength levels along with improved formability and crash-energy absorption in comparison to HSLA (High Strength Low Alloy) grades. This necessity is fulfilled by the TRIP and DP grades of steel, which have improved values of work hardening exponent. The second need is to extend the availability of steel in strength ranges higher than the HSLA grades. This region is covered by the MS and CP grades [6]. Originally developed only for chassis, suspension system, and body-in-white components, advanced high strength steels are now being applied to doors and other body panels. A combination of different microstructural constituents that was not traditionally available in conventional HSS is possible with AHSS and gives a wide range of properties. This facilitates steel companies to tailor the processing routes to meet even more specific application requirements of automotive industry [5].

1.3 Dual Phase steels

DP steel first came into existence in 1960s but it did not gain much attention till 1970s. After energy crises in seventies, the fuel prices increased significantly and engineers turned towards DP steel. Following this, three major conferences were held between 1977 and 1981

on mechanical behaviour and processing of DP steel. The majority of research in this field was an outcome of results presented in these conferences. But till 2000s, DP steel was not used by automotive industry to a large extent. It was the beginning of 21st century that these steels found widespread applications in automobile industry.

In the last decade or so the interest of researchers and engineers has grown considerably in Dual Phase (DP) steel. This is well justified from the engineering perspective, owing to relatively straightforward thermo-mechanical processing and very few alloying requirements for the production of DP steels. Ferrite and martensite/ bainite are the main constituent phases in the microstructure of dual phase steel. This dual phase microstructure provides this steel with excellent combination of strength and ductility. Ferrite being a deformable phase provides ductility and martensite is responsible for its strength due to its hardness [7]. The dual microstructure of DP steel shows the following advantageous properties over the conventional high strength steels:

- Continuous yielding behaviour.
- High initial strain hardening rate due to plastic incompatibility of ferrite and martensite phases and due to generation of geometrically necessary dislocations in ferrite matrix.
- Low YS/UTS ratio makes them suitable for forming into different part shapes.
- Can be bake hardened.
- Very good weldability and can be welded with all conventional welding methods viz. arc welding, resistance spot welding, laser welding (which are mostly used in the automotive industry).

1.4 Production of DP Steels

The automobile industry has shown a great interest in the development of DP steels because of the ability of these steels to provide weight reduction by using inexpensive alloying and that too without losing the desirable mechanical properties [8]. Although, DP steels mainly consist of ferrite and martensite. However, in addition to martensite, small amounts of pearlite, retained austenite, and bainite may also be found in the microstructure depending upon the cooling rate employed and thermo-mechanical processing route followed [9]. Figure 1.2 illustrates schematic diagram of processing routes followed for the production of DP steels. One of the heat treatment methods that is widely used for the production of DP steels is by first heating the steel to a temperature above A_{C1} temperature (i.e. also called inter-critical temperature) and then fast cooling to room temperature from there, thus forming a

ferrite and martensite microstructure [10,11]. While another traditional method involves heating to full austenitic region and thereafter cooling slowly (air cooling from full austenitic region) up to the desired ferrite transformation from austenite and finally fast cooling (quenching) to transform the remaining austenite to martensite [12].

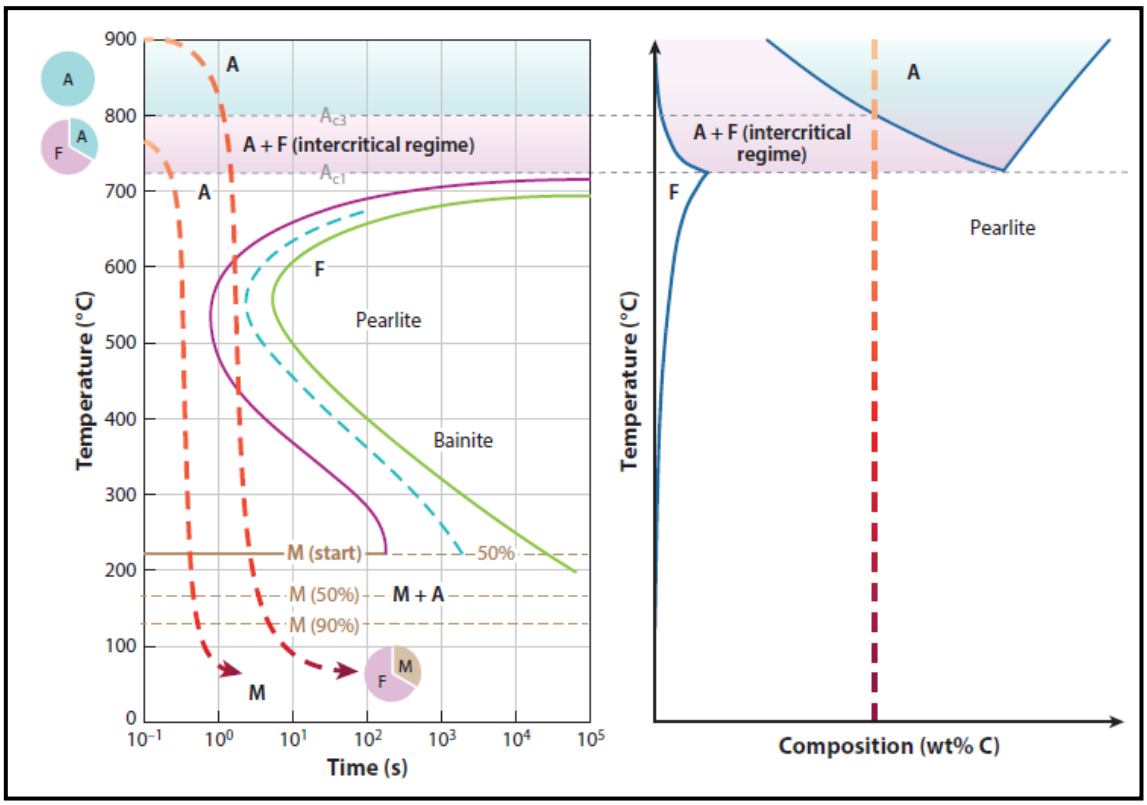

Figure 1.2 Basic heat treatment routes for production of DP steels [13].

But these days a continuous annealing processing route is employed that includes heating and soaking at different temperatures. Quenching and partitioning route is also gaining popularity due to tempering of martensite to give more uniform distribution in final microstructure.

1.5 Strengthening Mechanisms in DP Steels

Different methods are popular among researchers to impart the required microstructure/ properties to steels. Strengthening and hardening mechanisms are frequently used in different combinations to satisfy specific strength and formability requirements. Solid solution strengthening, grain refinement, and work hardening are some of the most universal means used for strengthening of DP steel [14,15].

1.5.1 Solid Solution Strengthening

The ease with which the dislocations can propagate in the crystal lattice of a material determines the strength of that material. These dislocations create stress fields within the material depending on their character. The solute atoms present in the metal matrix generate their local stress fields (because of difference in the size of metal and solute atoms) and hinder the movement of dislocations thus resulting in an increase in strength of the material (see Figure 1.3).

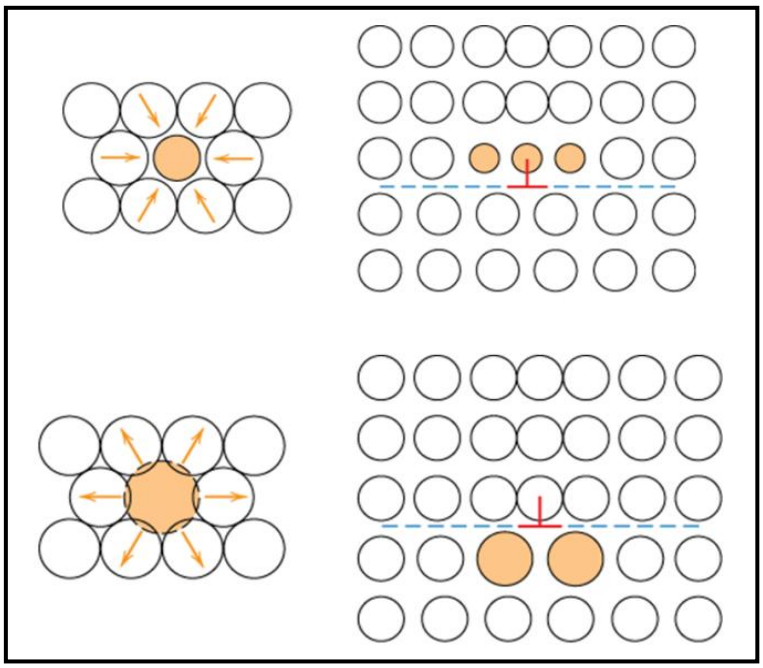

Figure 1.3 Mechanism of solid solution strengthening [16].

The result of the interactions of solute atoms and dislocation is pinning of the dislocations, and therefore, higher force is required to plastically deform the material and increase in strength is experienced.

1.5.2 Grain Refinement

Grain boundaries act as barriers to the movement of dislocations because of different orientation of atoms in different grains. So, grain boundary presents an obstruction to the slip phenomenon (see Figure 1.4). Thus, more the number of grain boundaries (smaller grain size) more will be the barriers to resist deformation which cause an improvement in strength of the material. Calcagnotto *et al*. [17] investigated the influence of grain refinement on the strength and toughness of DP steels and concluded that with the refinement of grains, the mechanical properties like strength and toughness are improved.

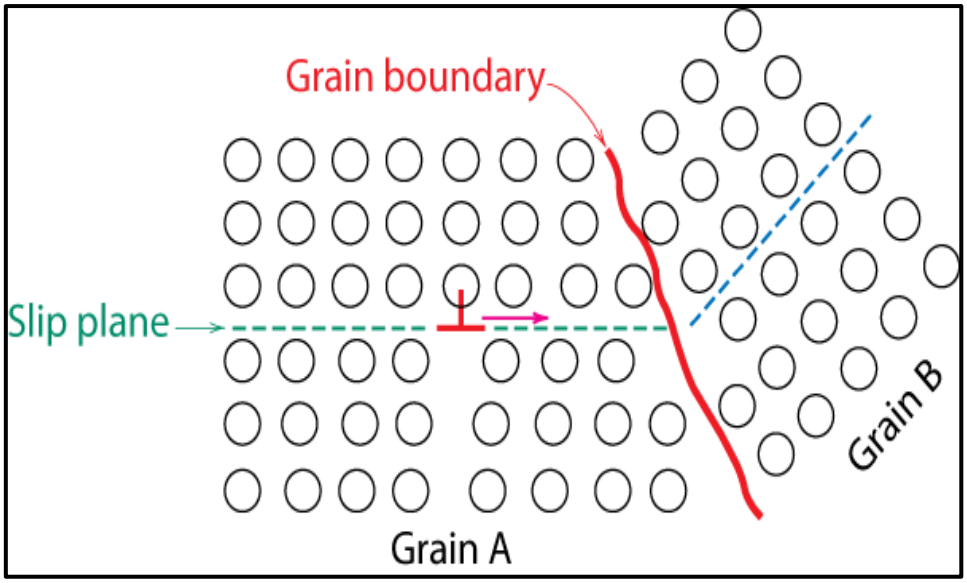

Figure 1.4 Movement of dislocations through grain boundaries [16].

Ultrafine grained DP steels are gaining popularity due to their superior properties in comparison to fine grained and coarse grained DP steels.

1.5.3 Work Hardening or Strain Hardening

When plastic deformation is applied to a single crystal it shows greater resistance to further deformation. This increase in stress required for further deformation of material is known as strain hardening. With increase in deformation, the movement of dislocations becomes difficult because of increase in dislocation density by generation of new dislocations. Due to dislocation pile-up and interaction among these dislocations, entanglement of dislocations occurs at grain boundaries. This accumulation of dislocations acts as a barrier to further deformation and increases the stress required for further deformation by locking of dislocations on slip planes [18].

1.6 Applications of DP Steels

Dual phase steels are mostly used in the light weight automobile structural components where high crash resistance is required. Figure 1.5 shows the main areas in the body structure of a car that play a vital role during crash conditions. Front and rear bumper structural components show potential areas where high energy absorption capability of DP steels can be utilized. Apart from that the cage like structure shown in Figure 1.5 has to have high strength along with high energy absorption capacity, so DP steels are being used these days in making B-pillar reinforcement, roof bow, A-frame reinforcements etc.

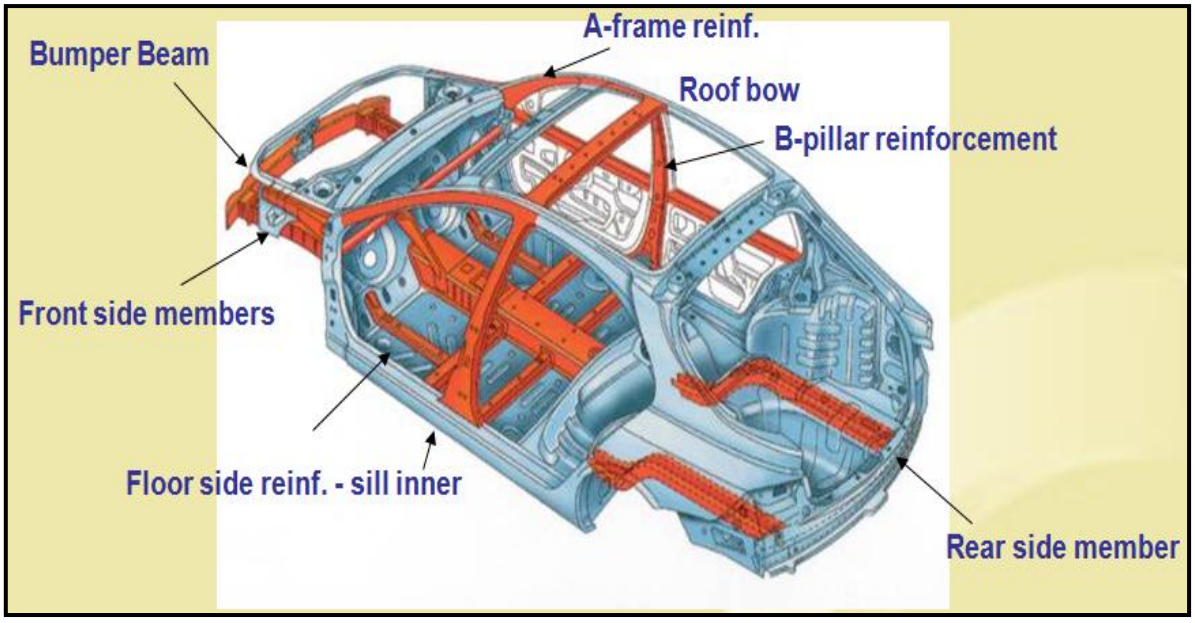

Figure 1.5 Crash sensitive areas of a car [5].

Some of the parts where DP steel is used include B-pillars of cars, anti-crash rods, bumper structures, rear side members, roof supporting structure of cars, suspension of vehicles and seat side components [5].

1.6.1 ULSAB and ULSAB-AVC Programs

To investigate the weight saving opportunities in automotive components, 35 car manufacturers from 18 countries came together in 1994 and started a program called, "Ultra Light Steel Auto Body (ULSAB)". The engineers were able to develop Steel car body with 90% of high strength steel (HSS).

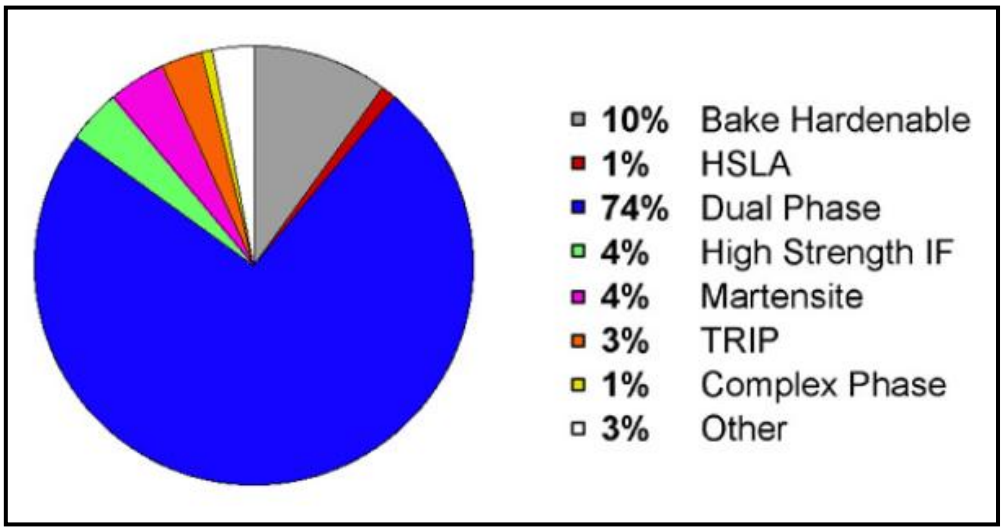

Figure 1.6: Contribution of Different grades of AHSS in ULSAB-AVC car body structure [19].

The car body had 25% lesser weight than conventional auto body structure along with 14 % reduction in manufacturing cost. DP steel played a crucial part in making all this possible. Furthermore, ULSAB program was extended to initiate a newer project with the name “Ultra Light Steel Auto Body-Advanced Vehicle Concept (ULSAB-AVC)” to supplement the improvement in fuel efficiency and passenger safety at an affordable manufacturing cost so as to minimize the environmental hazards. Figure 1.6 shows the contribution of different grades of AHSS in car body manufactured during ULSAB-AVC program [19]. Clearly, DP steel has the potential to transform the modern car industry with its superior strength-ductility combination along with continuous yielding and high strain hardening properties.

1.7 Summary of the Chapter

This chapter provides an insight into the growing world of steel especially that in the field of automotive industry. The role of advanced high strength steel (AHSS) in modern car body design has been discussed. An introduction of DP steel has been given with brief description of its applications.

Chapter 2
Literature Review

2.1 General

This chapter discusses the literature on Dual phase (DP) steels and various processes that have been used to produce these steels. This chapter provides an insight of the work done in the field of DP steels in the recent past.

2.2 Review of Dual Phase Steels

Patel *et al.* [20] investigated the influence of micro-alloying on a hot rolled multi-phase steel strips. The authors revealed that grain refinement can improve toughness considerably (the Hall-Petch relationship). Furthermore, a reduction in second phase (hard phase) also improves the cold formability along with toughness. Uniform elongation can also be improved by reducing sulphur content thereby achieving good cold formability. Excess sulphur content results in formation of large number of manganese-sulphide (MnS) inclusions, which causes component cracking and splitting during forming operations. The cracking was prominent when the sheet is bent parallel to the rolling direction due to the nucleation of voids at the particle-matrix interface. Sometimes calcium (Ca) is added to have globular shaped inclusions which have less plasticity at high temperatures and does not elongate during hot rolling operation. The globular-type inclusions reduce the chances of void nucleation during cold working of sheets. Ductility and weldability varies inversely with carbon content in the steel sheet. Steels with low carbon content exhibit good ductility and better weldability. Manganese strengthens the ferrite matrix by solid solution strengthening and reduces the transformation temperature (Ar_3) for austenite to ferrite transformation. However, the content of manganese is usually restricted to levels < 1.80 wt%. Niobium up to 0.07 wt% is added where high yield strength (up to 500 MPa) is required. But for heavier strips (above 6 mm gauge) vanadium is also added as a supplementary constituent along with niobium to achieve yield strength up to 500 MPa. However, niobium is first choice for alloying element because of its ability to help in grain refinement which improves both strength and toughness. This could be attributed to the fact that niobium (over other alloying elements) can raise the temperature at which austenite recrystallization stops. Furthermore, niobium forms secondary precipitates to further enhance strength via precipitation hardening effect. For conventional hot rolling process, the role of niobium is to refine grain size, and

that of vanadium is to provide precipitation hardening effect. Whereas titanium‘s effect is believed to lie between the two. The authors also revealed that partial dissolution of micro-alloying elements results in prohibition of these elements to act as grain refiner or to provide precipitation hardening. Although for majority of micro-alloyed steel grades, a reheating temperature of 1200 ℃ would be sufficient. In modern strip mills, a reheating temperature of 125 ℃ was normally applied, thus assuring a suitable finish rolling temperature. The determination of temperatures at which carbides and carbon-nitrides of niobium dissolve completely was done during the cooling of the cast slab. The temperature required for complete dissolution depends upon extent of micro-alloying and niobium, carbon and nitrogen content were determining factors.

Erdogan *et al.* [21] examined the influence of martensite size distribution on tensile fracture behaviour of a dual phase steel. Three specimens were made out of surface carburized steel sheet coded as A, B and C. Specimen A was inter-critically annealed at 731 ℃ followed by oil quenching thus producing dual phase microstructure with coarse martensite particles in ferrite matrix. Specimen B corresponds to oil quenching from a temperature of 900 ℃ followed by slow cooling to inter-critical temperature of 731 ℃ and finally oil quenching thus producing fine martensite in ferrite matrix. Specimen C was heated to 900 ℃ followed by oil quenching to produce fully martensitic microstructure. The authors observed that Specimen B showed higher tensile and yield strength as compared to specimen A due to the presence of finer martensite in microstructure of specimen B. In specimen B, at 25% martensite volume fraction (MVF) the martensite particles were almost isolated in the ferrite matrix as a result of different particle size and spacing and thereby providing greater strength levels. This could be attributed to the fact that finely dispersed martensite in ferrite matrix offered more barriers for the movement of dislocations and provided more strengthening compared to blocky martensite at same MVF. Moreover, initial work hardening rate and total uniform elongation was found to be higher in specimen B. Superior ductility of specimen B as compared to specimen A was attributed to better strain distribution between soft and hard phase along with higher number of void nucleation sites due to finely dispersed martensite. Whereas, specimen C showed higher yield strength comparing to specimens A and B but tensile strength was similar to specimen B. However, there was no difference between uniform and total elongation for specimen C. In specimen A with coarse microstructure, grain boundary martensite was found to be prone to cracking. However, martensite cracking was

less frequent in the fine microstructure (Specimen B) and voids were relatively smaller compared to specimen A. Fractography analysis for specimen B, showed ductile dimples on fracture surface and no cleavage facets were observed. Whereas, for specimen A, cleavage fracture was prominent failure mechanism with some void nucleation and growth. Completely cleavage type fracture was observed for specimen C.

Adamczyk and Grajcar [22] studied the influence of heat treatment parameters on the evolution of microstructure and mechanical properties of steel with Dual Phase microstructure. The steel (C:0.09; Mn:1.5; Si:0.26; Ni:0.07; P:0.014; S:0.009; B:0.003; Al:0.029; N:0.012: Fe: balance; all in wt %) was melted and slabs 100 x 100 mm were casted by continuous casting. Further, the slabs were hot-rolled and forged into rods of cross-section of 24 x 24 mm. Microstructural and mechanical properties were investigated for the samples prepared after heat treatment. Three different heat treatment regimes were followed and are shown in Table 2.1.

Table 2.1 Annealing process details.

Route	First stage	Second stage
I	Heating to a temperature of 910 ℃ (α + γ region) and holding for 30 min followed by air cooling to room temperature.	Reheating to 750 ℃ followed by water quenching.
II	Heating to a temperature of 910 ℃ (α + γ region) and holding for 30 min followed by water quenching.	Reheating to 750 ℃ followed by water quenching.
III	Austenitizing of steel at a temperature of 910 ℃ for 30 min.	Air cooling for 45 s to a temperature of 750 ℃ followed by water quenching

The steel processed by route I showed ferrite structure with an irregular cover of martensite on ferrite grain boundaries. Whereas, for route II martensite was mainly present as thin fibers located predominately in the vicinity of ferrite grain boundaries. Moreover, small ferrite grains (formed due to recrystallization) could be identified in surroundings of martensite, especially at the boundary region of large grains of ferrite phase. In route III Martensite was blocky in nature and was present at grain boundaries of ferrite phase. The fraction of martensite formed was comparable for all the heating treatment conditions and optimum range was found to be from 21% to 24% with grain size of ferrite phase ranging from 7 μm to 10 μm. The authors revealed that strength and ductility of steel varied significantly with morphology of martensite. The route II steel showed optimum strength and ductility

combination. The yield strength and tensile strength of this steel was about 520 MPa and 800 MPa respectively with a total elongation of 20%, and uniform elongation of about 16%.

Santofimia *et al.* [23] investigated the effect of partitioning temperature and time on the stability of austenite in a multi-phase steel. Steel having (0.19 C, 1.61 Mn, 0.35 Si, 1.10 Al, 0.09 P and bal. Fe (in wt. %)) gauge thickness of 1.2 mm with a complex microstructure containing ferrite, bainite, retained austenite, martensite was used for experimentation. The heat treatment route followed is shown in Figure 2.1 The partitioning of specimens was done by holding them at 125 ℃, 150 ℃ and 175 ℃ between martensite start and finish temperatures for 100 s, 10 s and 3 s respectively (as shown in Figure 2.1) and finally cooling them to room temperature.

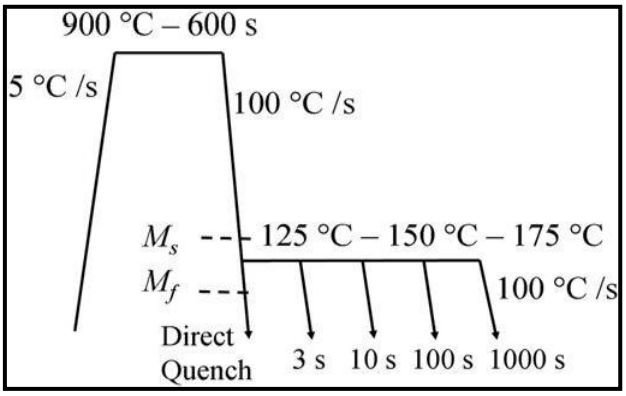

Figure 2.1 Quenching and Partitioning heat treatments applied to the given steel [23].

The different constituents in microstructure were analysed using Light optical microscopy (LOM) with differential interference contrast (DIC), image quality (IQ) analysis and electron backscatter diffraction (EBSD). It was observed that after the Q&P heat treatment ferrite, martensite were main constituents present in microstructures along with some retained austenite. Carbon content and volume fraction of retained austenite showed small increment after partitioning at 125 ℃ for 100 s, 150 ℃ for 10 s and 175 ℃ for 3 s respectively. This increase was attributed to the fact that at higher temperature carbon partitioning from martensite to austenite is relatively faster. Also, after partitioning for 1000 s at all the concerned temperatures, carbon content in retained austenite decreased slightly due to carbide formation in austenite. However, this carbon reduction and carbide formation was not large enough due to the presence of Al in the steel which retarded carbide precipitation. The authors concluded that at the chosen temperatures (175 ℃, 150 ℃ and 125 ℃) the partitioning time did not affect the microstructure significantly. However, volume fraction and carbon

content of austenite increased slightly with increase in partitioning temperatures (125 ℃, 150 ℃ and 175 ℃) for time periods of 100 s, 10 s, and 3 s respectively. A reduction in the C percentage of austenite phase was also reported by authors after soaking for 1000 s at concerned partitioning temperatures due to carbide precipitation.

Matlock *et al.* [4] examined recent developments in the field of Advanced High Strength Steels (AHSS). In the recent past, more emphasis has been given on weight reduction of automobiles to get better fuel efficiency with increased crash performance to ensure passenger safety. So throughout the world there is an increased research in the development of AHSS due to their high strength along with high ductility which is essential for automobile applications. In this paper the authors presented the excerpts from three papers namely "Strategies for third generation advanced high strength steel development", "Austenite stability effects on tensile behaviour of manganese-enriched-austenite transformation-induced plasticity steel" and "TRIP steels: historical perspectives and recent developments". Current commercially used steels have evolved from early work on dual-phase steels in late 1970's and early 1980's which showed a significant increase in elongation (ductility) of dual phase steels with nearly same ultimate tensile strength as that of HSLA steels (as shown in Figure 2.2a).

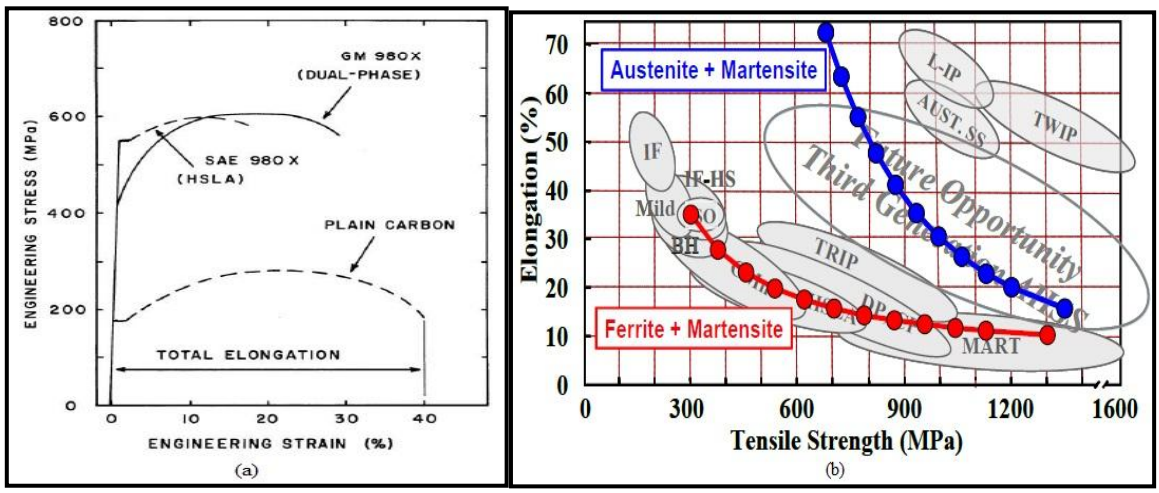

Figure 2.2 (a) Comparison of the stress strain curve for a dual-phase steel with those for a plain carbon steel and an HSLA steel, (b) superposition of predicted strength/ductility combinations of hypothetical ferrite/martensite and austenite/martensite mixtures [4].

One important finding was the increase in ductility with increase in the amount of retained austenite which formed the basis for transformation induced plasticity steels (TRIP). The transformation of retained austenite into martensite during deformation resulted in increased

strain hardening. The first generation of AHSS were developed in fairly lean compositions with ferritic-based multi-phase microstructures. First generation AHSS processed high ductility but the tensile strength of these steels was very low. This problem made way for the development of second generation of AHSS. The second generation of AHSS exhibited superior mechanical properties but was highly alloyed resulting in higher cost thus making them uneconomical for industrial applications. This problem diverted the research to third generation AHSS to get desired mechanical properties with lesser alloying and incorporating modified or novel processing routes. Furthermore, design considerations for third generation AHSS were based on varying the fraction of different phases in the microstructure of steel to get desired properties. Two hypothetical models, (i) ferrite & martensite and (ii) austenite & martensite were discussed. First approach assumed the absence of transformation of austenite during straining and the results obtained are shown in Figure 2.2b. The second approach considered that austenite transforms to martensite during straining with austenite stability as variable affecting the transformation. The results from this approach are shown in Figure 2.3a–b. By stability route D in Figure 2.2a, we observe that austenite transformation into martensite was the quickest, hence the curve corresponding to route D in Figure 2.2b showed higher strength at the cost of elongation (because of higher martensite and lower austenite content).

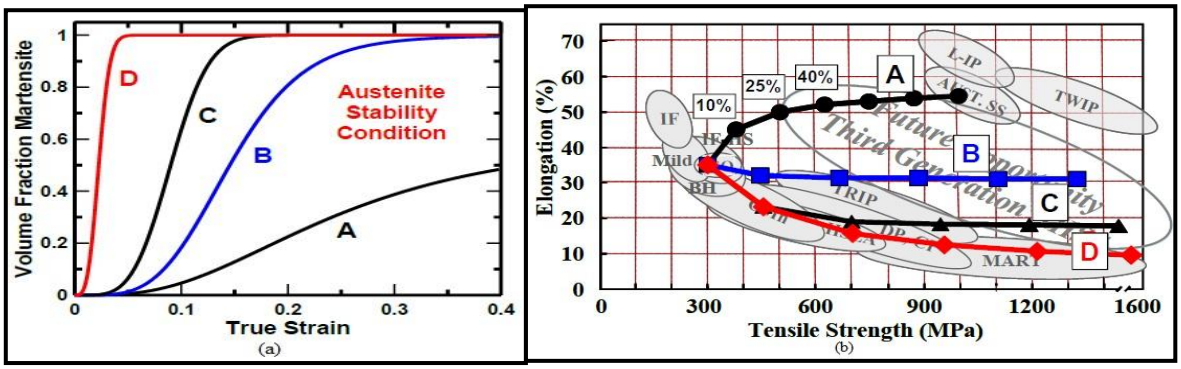

Figure 2.3 (a) Effect of austenite stability on predicted mechanical property combinations for (a) four different austenite stabilities identified as A through D, (b) predicted mechanical property combinations corresponding to ferrite plus austenite with the different austenite stabilities shown in (a), In (b) each data point on each curve corresponds to an initial austenite fraction, ranging from 0 to 85% [4].

Current research is focussed on improving the strength and ductility of AHSS by identifying the best possible composition of different alloying elements (e.g. Cr, Mn, V, Mo, C, Si etc.) and optimising the processing routes (heat treatment processes) so as to make these steels economically feasible for the industrial use in future light weight vehicles.

Sudersanan *et al.* [24] studied the variation of strength of dual phase steel with the percentage of carbon content in the martensite phase. The composition of steel used (wt %) was 0.13C, 1.18Mn, 0.01S, 0.001P, 0.3Si, 0.047Cr, 0.057Mo, 0.001B, 0.048Ni.

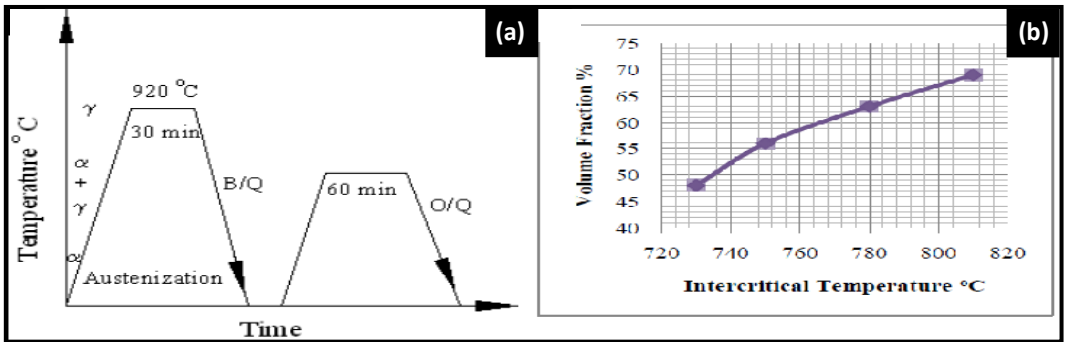

Figure 2.4 (a) Inter-critical annealing cycle, (b) volume fraction v/s inter-critical temperature [24].

All specimens were cut into sizes of 100 mm x 100 mm x 14 mm. The specimens were first austenized by heating to 920 ℃ and held for 30 minutes and then quenched in 9% iced brine solution at -7 ℃. The specimens are then heated to different inter-critical temperatures ranging from 730 ℃ to 810 ℃ before finally quenched in Servo quench 707 oil at 25 ℃ to obtain dual phase microstructure. The microstructures of the different specimens were obtained using metallurgical microscope at 1000X magnification. Thereafter, tensile test specimens were prepared from the different samples and tested for their yield strength and ultimate tensile strength. The heat treatment cycle adopted is shown in figures 2.4a. The percentage of martensite in the dual phase steel is influenced by the inter-critical annealing temperature. It is found that the volume fraction of martensite increases linearly with inter-critical annealing temperature.

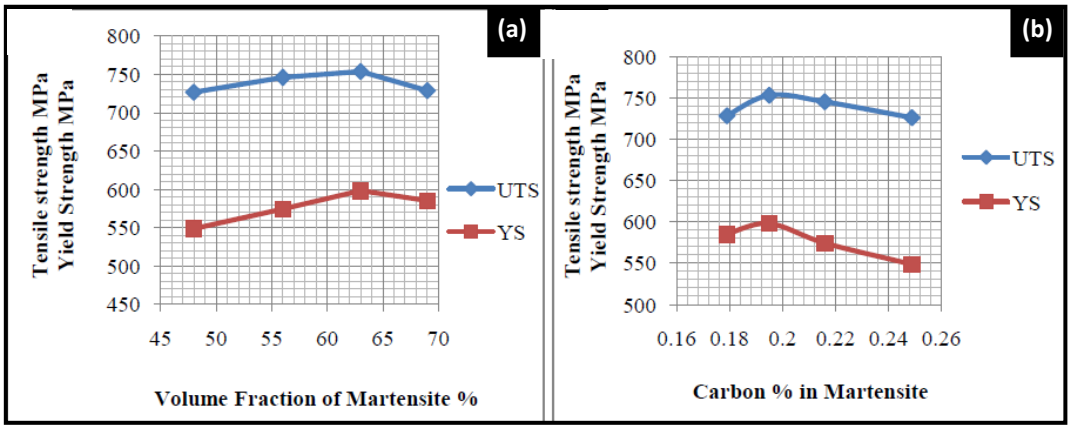

Figure 2.5 (a) Yield and tensile strength v/s volume fraction of martensite, (b) yield and tensile strength v/s carbon % in martensite [24].

Figure 2.5a shows the yield and tensile strength of steel plotted against the volume fraction of martensite. The strength increased with the martensite volume fraction initially and for higher percentage of martensite the strength is found to decrease. The yield strength and tensile strength showed a marginal improvement with the carbon content in martensite in the initial stages and then started to decline beyond 0.195 % (see Figure 2.5b). Since the solubility of carbon in ferrite is limited the carbon content in martensite decreased with an increase in volume fraction of martensite. An increase in carbon content in martensite to a certain limit increased both yield strength and ultimate tensile strength. The authors observed that yield strength and tensile strength increased initially with carbon content up to 0.195% and then decreased marginally thereafter with carbon content in the martensite phase. Finally the authors conclude that dual phase steels with high martensite volume fraction (>60%) showed an improvement in strength with an increase in carbon percentage in martensite.

Mittal [25] investigated the effect of inter-critical annealing parameters on the recrystallization kinetics, austenite formation and austenite stabilization in a dual phase steel. Experiments were performed on as-received cold rolled low carbon steel (0.08 C, 1.82 Mn, 0.40 Si, 0.042 Al, 0.017 P, 0.005 S, 0.0035 N and balance Fe wt %.). Metallography and SEM of as-received samples revealed presence of pearlite and pro-eutectoid ferrite. The annealing parameters viz. upper critical and lower critical temperatures were calculated using commercial software (JMat-Pro and Thermo-Calc). Thermo-Calc predicted the lower and upper critical temperatures to be 682.2 ℃ and 839.7 ℃ respectively and JMat-Pro predicted the TTT and CCT diagrams. To study the recrystallization kinetics, specimens ($15 \times 10 \times 1.6\ mm^3$) were heated to different inter-critical temperature ranges of 700–850 ℃ (with a step size of 25) with holding time in the range of 30–180 s (with step size of 30 s) followed by air cooling. Activation energy and ferrite recrystallization was determined using JMAK analysis. Metallography and recrystallization study revealed that time period of 0–30 s was the recovery time of the specimens and this time was dependent upon the annealing temperature. TTT diagrams revealed that for temperatures lower than 775 ℃, austenite was not formed in an appreciable amount. However, increasing the holding time to 3 min, austenite volume fraction of 33.19% was observed. It was observed that with increase in annealing temperature, or holding time, or both, the fraction of austenite formed in the steel increased. The appropriate amount of austenite (40–50%) was obtained at temperatures of 800 ℃ and 825 ℃ with soaking time periods of 5 min and 3 min respectively followed by

water quenching. In annealing simulator for (3 min soaking at 825 ℃ followed by quenching with N_2+H_2), dual-phase microstructure with martensite fraction of 35% was obtained which was less than that obtained by water quenching (cooling rate provided by water much higher than the gases used). Microstructure of the steel annealed in the simulator consisted of fine martensite phase dispersed in the recrystallized ferrite matrix. While for water quenching, a typical necklace type microstructure, in which martensite was observed on the ferrite grain boundaries was observed. As received specimen had a tensile strength of 810 MPa with elongation of 5.3%. However, the sample annealed under the optimum conditions in the simulator (having 35% martensite) showed high total elongation of 26.5% with a moderate ultimate strength of 610 MPa. Thus, by obtaining an appropriate microstructure through the selection of inter-critical annealing parameters, a good combination of strength and ductility was obtained in the given low carbon steel.

Sebek *et al.* [26] investigated the influence of annealing parameters on evolution of microstructure and mechanical properties of dual phase steel. The experimental material was produced in a laboratory resistance furnace in an inert atmosphere of argon. Subsequently, the hot rolling under laboratory conditions followed by cold rolling with the final reduction of 70% was performed. The chemical composition of studied material (in wt %) was 0.10C, 1.90Mn, 1.00Cr + Mo, 0.02P, 0.005S, 0.80Si, ≤ 2.0Al, 0.002V. To obtain the desired properties, the Cr and Mo content ratio was 1:1. Dual phase steel was annealed in laboratory conditions according to the three chosen cycles of annealing (see Figure 2.6): into inter-critical region (780 ℃), into austenite region (920 ℃) and into austenite region (920 ℃) by subsequently cooling into inter-critical region (780 ℃) with the hold at the temperature of 495 ℃. Simulation of annealing regimes by thermo-mechanical simulator Gleeble was done.

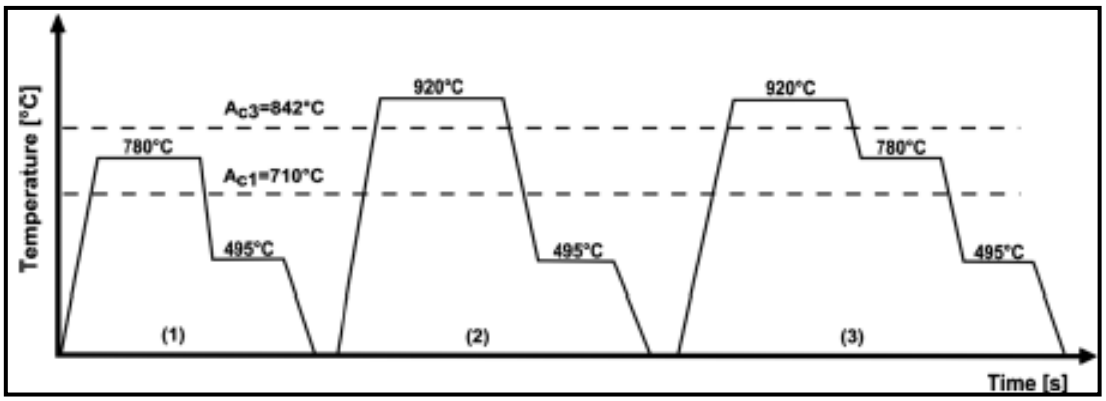

Figure 2.6 Annealing process routes for DP steels [26].

The microstructure of dual phase steel was documented by the optical microscopy and scanning electron microscopy. Figure 2.7 shows the microstructures of all studied regimes of annealing. For the first selected regime, the microstructure consists of ferritic matrix, austenite and areas suggested to be martensite. No typical martensite was observed in the microstructure. After the second selected regime of annealing, the microstructure formed by the ferritic matrix, austenite and martensite was observed. In this case, the partly martensite grains were found whereas the austenite was around.

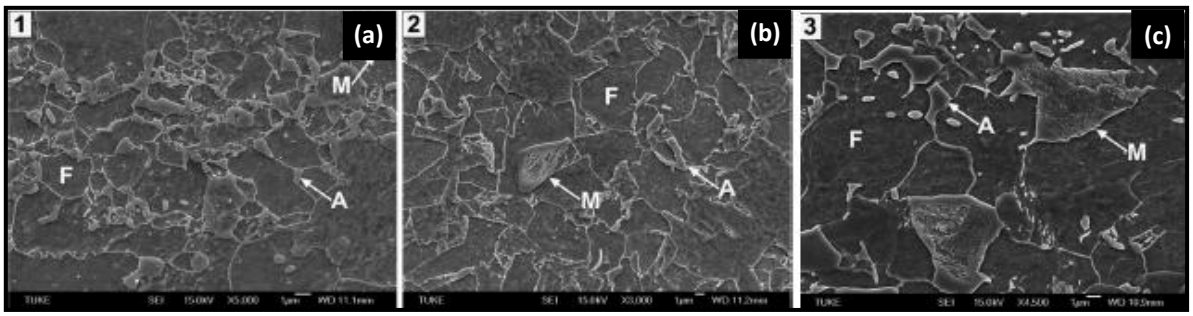

Figure 2.7 SEM micrographs of DP steel for (a) annealing regime 780 ℃─495 ℃, (b) annealing regime 920 ℃─495 ℃, (c) annealing regime 920 ℃─780 ℃─495 ℃ [26].

Moreover, grains of the needle like structure were observed. After the third annealing regime, the microstructure composed also of ferritic matrix, austenite and martensite, as observed in the case 2; however, in comparison with the regime 2, higher occurrence of martensitic grains, was observed. The TEM analysis was performed for two annealing regimes: 780℃─495℃ and 920℃─780℃─495℃ (see Figure 2.8).

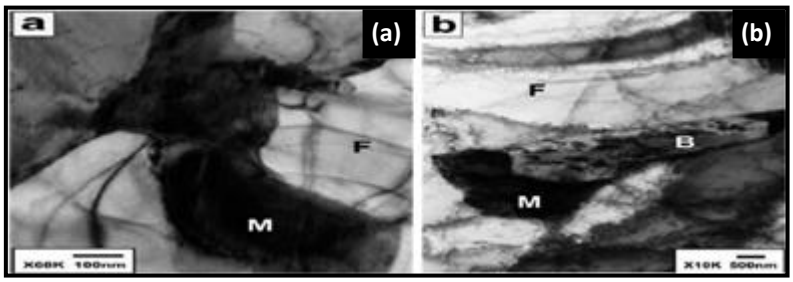

Figure 2.8 (a) Characteristic structure (annealing regime 780 ℃─495 ℃), (b) a partly transformed grain of bainite surrounded by martensite (annealing regime 920 ℃─780 ℃─495 ℃) [26].

Figure 2.8b shows the final characteristic microstructure of specimen after the 920 ℃─780 ℃─495 ℃ regime which consists of bainitic grains surrounded by the martensitic phase. The changes in mechanical properties of steels produced by three different processing routes are shown in Figure 2.9. Thereafter, nano indentation measurements were

carried out and Table 2.2 summarizes the results. Three different values of hardness were obtained. The hardness for ferrite was 2.5±1 GPa. By simulation of annealing regime at temperature 495 ℃, martensite is tempered and, therefore, the lower values of hardness were obtained (4.1 to 4.5 GPa).

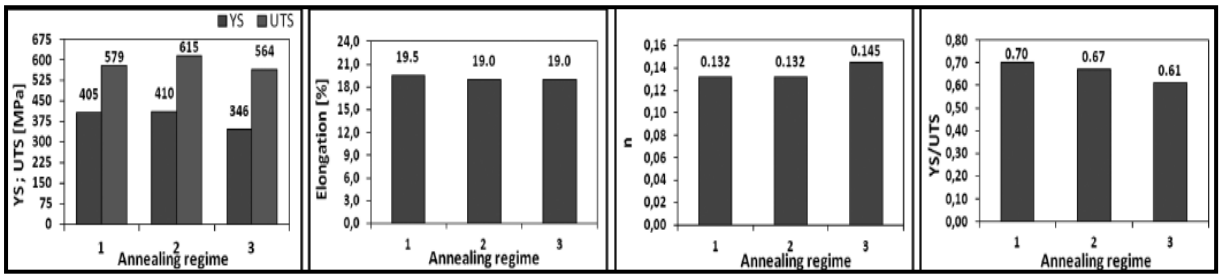

Figure 2.9: Mechanical properties of steels under investigation [26].

The hardness of mixed grains martensite/bainite (bainite surrounded by martensite), for the 920 ℃─495 ℃ and 920 ℃─780 ℃─495 ℃ annealing regimes, were 7.1 and 7.2 GPa, respectively.

Table 2.2 Results of the nano-indentation hardness testing [26].

Specimen	H_{IT} [GPa]	H_{IT} [GPa]	H_{IT} [GPa]
1. Annealing regime: 780°C-495°C	2.4	4.2	-
2. Annealing regime: 920°C-495°C	2.5	4.1	7.1
3. Annealing regime: 920°C-780°C-495°C	2.6	4.5	7.2

Kalashami *et al.* [27] investigated the effect of inter-critical holding time on microstructural evolutions, tensile behaviour and fracture mechanism of ultra fine grained DP steels containing Nb micro alloying element. The chemical composition of steel used was in (wt %) 0.12Nb, 0.14C, 0.95Mn, 1.00Cr, 0.30Si, bal. Fe. The samples were first homogenized at 1000 ℃ for 2 h and this was followed by furnace cooling and hot-forging at 1100 ℃ to a thickness of 4 mm (resulting in a ferritic-pearlitic microstructure). The samples dimensions were about 50 × 20 × 4 mm^3. The thermo-mechanical procedure used to produce the ferrite-martensite DP microstructures is schematically presented in Figure 2.10. The ferrite-pearlite microstructures were first heated to the austenitization temperature of 880 ℃ for 60 min and this was followed by inter-critical annealing at 770 ℃ for 100 min and water quenching. Then, the resulting duplex ferrite-martensite structures were subsequently cold-rolled up to 80% using a laboratory mill with a reduction of about 0.05 mm at each pass. Finally, the

cold-rolled samples were heated to the inter-critical temperature of 770 ℃ and held for 4 and 6 min and then water quenched. The DP steels were coded as the DP4 and DP6 depending on the inter-critical holding time of 4 and 6 min, respectively.

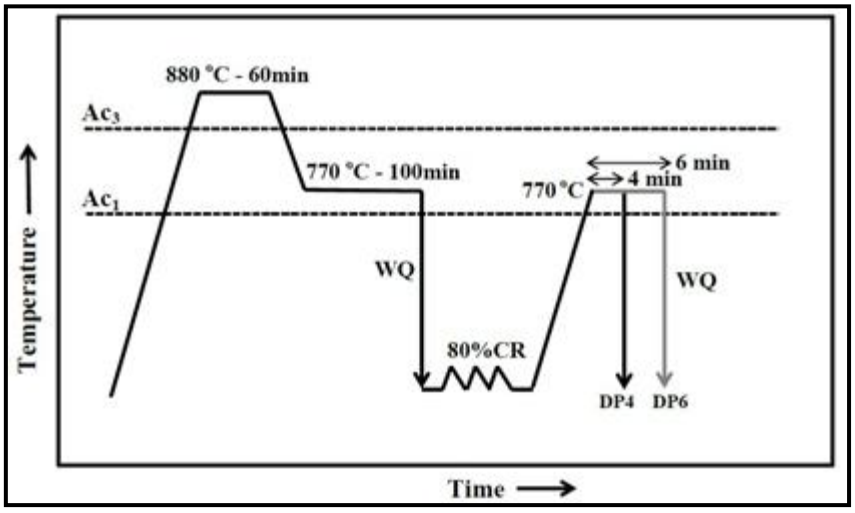

Figure 2.10 Thermo-mechanical cycle used to produce UFG-DP steels, A_{c1} and A_{c3}: austenite formation start and finish temperatures during heating respectively. WQ: water quench, CR: cold-rolling [27].

Cold-rolling of the duplex microstructure resulted in increasing the stored energy due to the high dislocation density, providing the driving force for the ferrite recrystallization upon inter-critical annealing. Figure 2.11 shows that, with increase in the holding time, the volume fraction of martensite (V_m) increased.

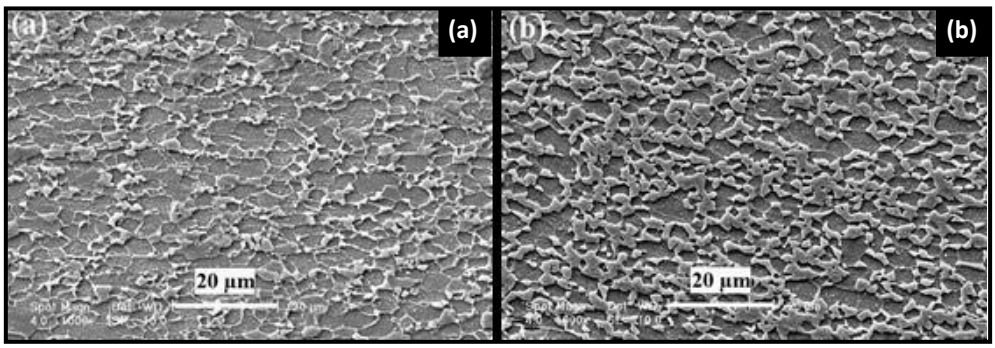

Figure 2.11 SEM micrographs of UFG-DP structures developed by 80% cold-rolling and inter-critical annealing of duplex microstructures at 770 ℃ followed by water quenching: (a) DP4, and (b) DP6 [27].

Moreover, average ferrite grain size (d_f) decreased by increasing the holding time. It was observed by the authors that higher amounts of the martensite phase caused finer ferrite grains. As shown in Figure 2.11, the martensite islands size was decreased by increasing the holding time. The effect of holding time on martensite islands size and morphology could be

attributed to the mechanism of the austenite formation during inter-critical annealing. When the duplex microstructure was cold-rolled and inter-critical annealed, the austenite nuclei at recrystallized ferrite/ ferrite interfaces resulted in fine martensite particles. Due to the lower inter-critical time in DP4 steel, austenite did not have enough time to be distributed uniformly throughout the microstructure, thereby resulting in the formation of some coarse martensite after quenching. Thereafter, tensile tests were conducted and the results are shown in Table 2.3.The investigated DP steels showed superior mechanical properties in terms of toughness (196 and 126 MPa for DP4 and DP6 steels, respectively) and energy absorption capacity (116 and 187 J cm^{-3} for DP4 and DP6 steels, respectively) compared to as-received sample.

Table 2.3 Microstructural quantification and mechanical properties of the studied steel specimens [27].

Steel	V_m (%)	d_f (μm)	YS (MPa)	UTS (MPa)	UE (%)	TE (%)	Toughness (MPa)	UTS×UE (J cm $^{-3}$)
as-received	-	-	350±15	540±13	7.5±0.80	17.22±1.72	86	40.50
DP4	45	2.82±1.82	430±12	665±20	28.15±2.90	32.18±2.14	196	187.20
DP6	62	1.40±0.37	621±17	1203±10	9.61±0.3	12.90±1.10	126	115.60

V_m: martensite volume fraction; d_f: average ferrite grain size; YS: yield strength, UTS: ultimate tensile strength; UE: uniform elongation; TE: total elongation.

The authors observed from fracture surface analysis that the fracture was ductile in nature. Furthermore, with increasing the inter-critical holding time, the average ferrite grain size and martensite particle size were decreased. Therefore, the fraction of ferrite/martensite interfaces increased resulting in formation of more voids. The increased number of voids caused the small and shallow dimples on fracture surface.

Concepción *et al.* [28] studied the effect of carbon content on microstructure and mechanical properties of DP steels. Four different conventional carbon steels were used, with nominal carbon contents between 0.05 and 0.35 wt%. The detailed chemical composition of investigated steels is shown in Table 2.4.

Table 2.4 Chemistry and inter-critical annealing temperatures for given DP steels [28].

Material	C	Mn	Si	P	S	Ac_1	Ac_3	Intercritical temperatures (°C)
S1	0.08	0.77	0.21	0.017	0.012	732	873	795; 810; 820; 840
S2	0.11	0.69	0.21	0.025	0.021	733	865	740; 750; 760; 770; 780; 790; 800; 820; 840; 860; 880
S3	0.20	1.45	0.40	0.015	0.028	720	776	740; 760; 780; 800; 820
S4	0.38	1.43	0.37	0.024	0.033	736	805	740; 750

The carbon content increased from material S1 to S4 from 0.08 to 0.38. Also, for S3 and S4 steels manganese and silicon contents were higher as compared to that of the S1 and S2 steels. Phosphorus and sulphur contents were similar for all the studied materials. Samples of each material were heat treated at different inter-critical temperatures (see Table 3) to obtain DP steel grades with different martensite volume fraction (M). The holding time at these temperatures was 30 minutes, followed by water quenching. Figure 2.12, 2.13, 2.14, and 2.15 shows the microstructure obtained after heat treatment of S1, S2, S3 and S4 respectively. The white coloured grains shows Ferrite phase and martensite is the brown one.

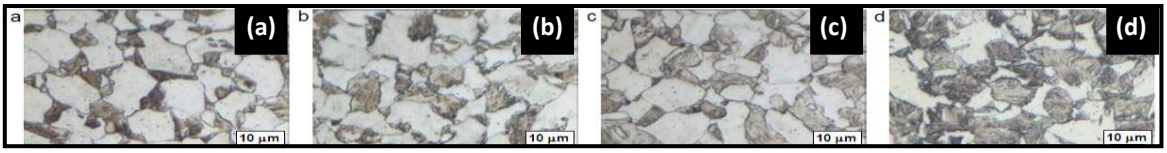

Figure 2.12 Microstructures of DP obtained from material S1 at the temperatures: (a) 795 ℃, (b) 810 ℃, (c) 820 ℃, (d) 840 ℃ [28].

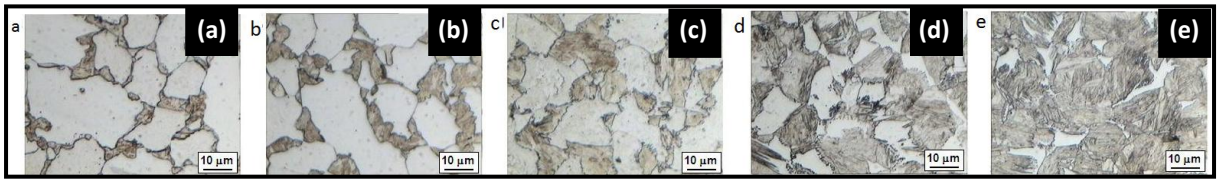

Figure 2.13 Microstructures of DP obtained from material S2 at the temperatures: (a) 740 ℃, (b) 770 ℃, (c) 800 ℃, (d) 840 ℃, (e) 860 ℃ [28].

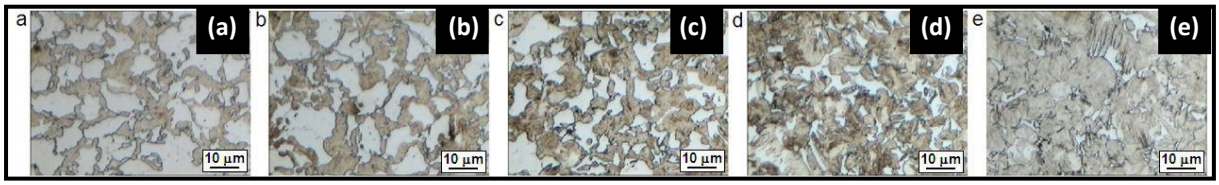

Figure 2.14 Microstructures of DP obtained from material S3 at the temperatures: (a) 740 ℃, (b) 760 ℃, (c) 780 ℃, (d) 800 ℃, (e) 820 ℃ [28].

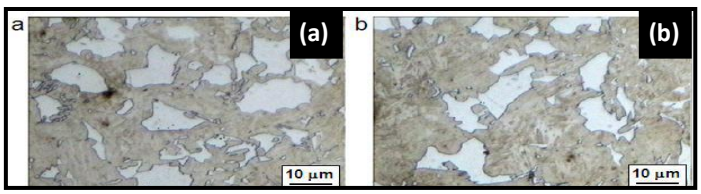

Figure 2.15 Microstructures of DP obtained from material S4 at the temperatures: (a) 740 ℃, (b) 750 ℃ [28].

It was observed by the authors that, in all the cases a dual structure consists of equiaxial grains of ferrite and islands of martensite. M increased with increasing temperature IHT, associated to a higher austenite fraction formed. Also, S3 steel presented smaller sizes of

ferritic phase than the rest of analyzed materials. The authors observed that for the steel S1, M was between 25–50%; for S2 was between 23–90%, being the wider range obtained. For steel S3, M was between 50–96%, and finally for S4, only two fractions of martensite could be achieved: 74 and 80%. It was observed that, for the same temperature, M increased with increasing carbon content. The highest difference was observed between steels S2 and S3.

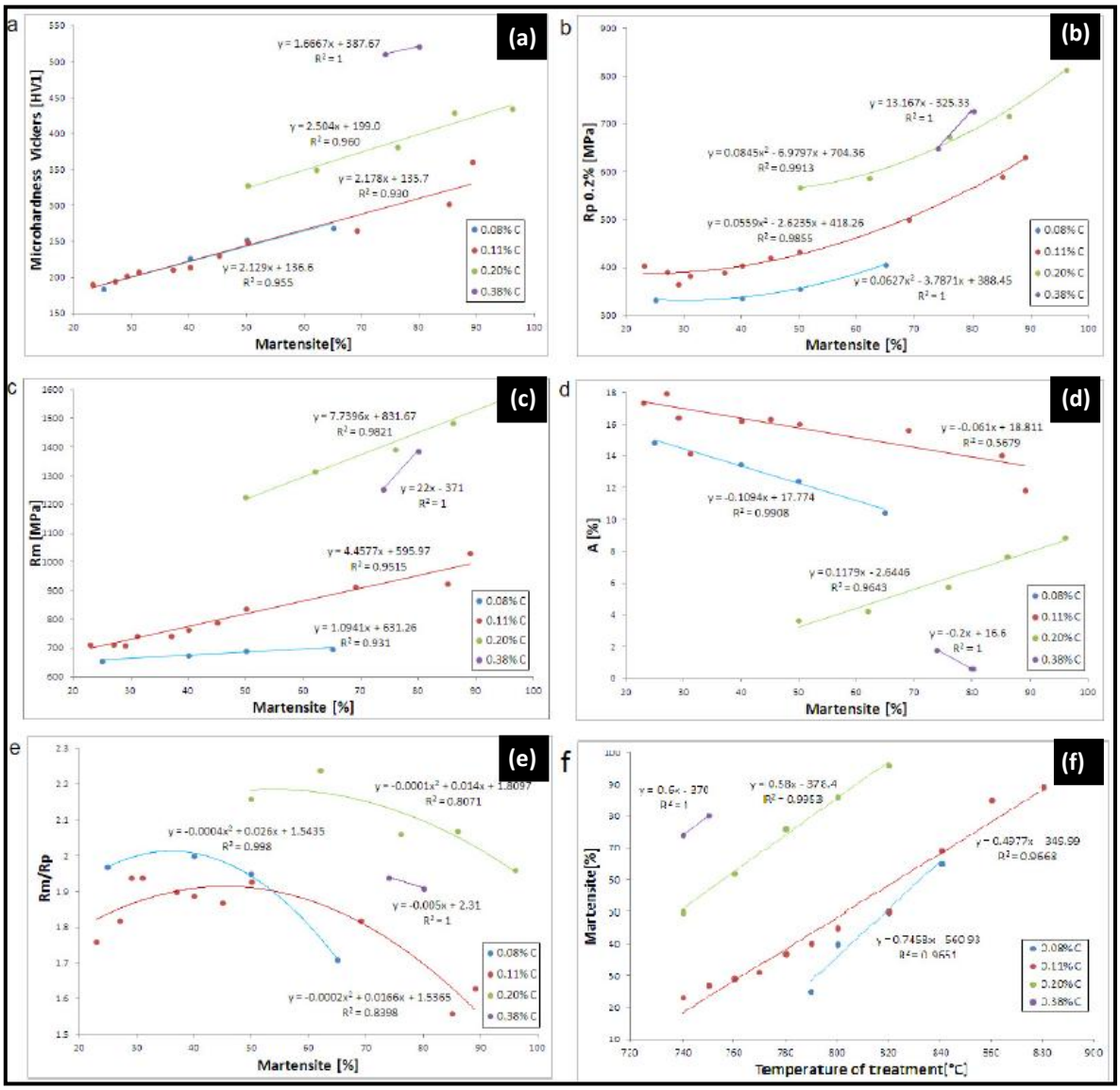

Figure 2.16 Mechanical properties of DP vs. M (martensite volume fraction) for different C: (a) HV, (b) R_p 0.2%, (c) R_m, (d) A%, (e) SR, (f) M vs. heating temperature [28].

Hardness increased with M, due to an increase of the carbon content in martensite phase. It can be observed that in all cases the rate of variation of hardness with M was almost the same (see Figure 2.16). Results for steels S1 and S2 were very similar (due to the similar C in both alloys). R_p 0.2% and R_m also increased with increasing C. The variation of the obtained

curves for R_p 0.2% with M was similar for all C values. R_m varied linearly with M, although the slope of the curve increased with the carbon content of the alloy. R_m for steel S3 was slightly higher than for S4, despite the difference in carbon content. As a general trend A% decreased with increasing C, as well as A% decreased with M for a certain carbon content in the steel, except for steel S3 where A% increased with increasing M. This anomalous behavior was be attributed by the authors to a balance of two effects: a decreasing of carbon content in martensite with increasing the volume fraction, and plasticity adopted by the martensite due to the stress partitioning in the DP. It was concluded that martensitic phase does not deform plastically until necking occurs in DP with low M. For high M (>50%), martensite is the matrix and supports most of the load, with small or none deformations of ferritic phase. SR showed high values that varied from 1.55 to 2.25, presenting a maximum value for M between 40 and 60%. Related with carbon content, maximum values were obtained for S3 steel, being always higher than 2. It was observed that for DP steels with low carbon content (0.08 and 0.11% C), the volume fraction of martensite had a higher influence in elongation to fracture, due to the decreasing carbon content of the martensite with the increase in its fraction. The opposite occurred for DP with 0.2% C. The best combination of mechanical properties in the analyzed DP can be obtained with carbon content between 0.1 and 0.15% and 50% martensite.

Zhang *et al.* [29] investigated the effect of martensite morphology and its fraction on strain hardening and damage evolution behaviour. The steel used in the experimentation was a commercial DP590 steel with an initial thickness of 1.5 mm. The chemical composition (in wt %) was 0.08C, 0.42Si, 1.83Mn, 0.16P, 0.002S, 0.0035N, 0.18Cr. DP microstructure with different martensite morphologies and fractions were developed by subjecting the steel to two different processing schedules: (a) *Cold rolling-inter-critical annealing (CR-IA):* The steel was cold rolled to 54.7% reduction and then heated to various inter-critical temperatures (750 ℃, 775 ℃, 800 ℃, 825 ℃, 850 ℃) in a furnace for 2 min, before water quenching to the ambient temperature. (b) *Intermediate-quenching (IQ):* In order to obtain near complete martensite, the steel was heated to 900 ℃ for 10 min followed by water quenching. Subsequently, it was inter-critically annealed, at temperatures identical to those listed in (a) above. Microstructure characterisation was done using scanning electron microscope (SEM) and transmission electron microscopy (TEM). The fraction of martensite was obtained using

the image processing software, Image Pro Plus. The SEM micrographs of steels processed by IQ and CR-IA treatments are presented in Figs. 2.17 and 2.18, respectively.

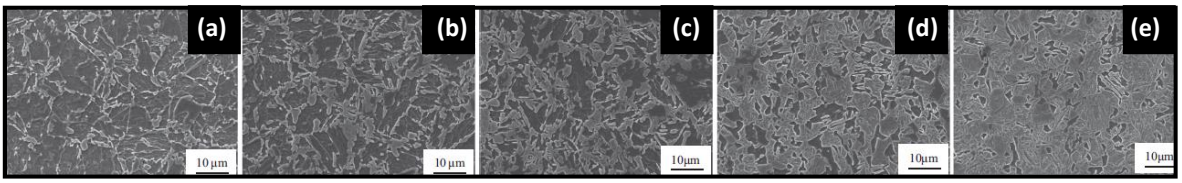

Figure 2.17 SEM micrographs of DP590 microstructure obtained by intermediate quenching (IQ) treatment at : (a) 750 ℃, (b) 775 ℃, (c) 800 ℃, (d) 825 ℃, and (e) 850 ℃ [29].

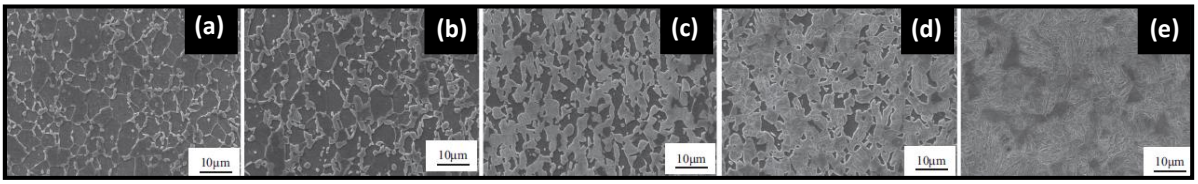

Figure 2.18 SEM micrographs of CR-IA samples treated at different inter-critical annealing temperature : (a) 750 ℃, (b) 775 ℃, (c) 800 ℃, (d) 825 ℃, and (e) 850 ℃ [29].

It was observed by the authors that both the treatments resulted into ferrite–martensite DP microstructure, but the morphology, size and distribution of martensite phase varied significantly with the heat-treatment schedules. The IQ sample inter-critically annealed at 750 1C (Figure 2.17a) yielded fine and fibrous martensite and the distribution of martensite laths was uniform. Additionally, some small polygonal martensite particles were present at the triple points of ferrite grains. With increase in the inter-critical annealing temperature, martensite grew gradually into block and there was significant increase in their content. CR-IA steels (Figure 2.18) indicated martensite islands along the grain boundaries while a small number of the islands with small size were present in grains and their fraction increased with increase in temperature. It can be noted in Figure 2.18a–b, ferrite grains have bimodal size distribution.

Table 2.5 Mechanical properties of (a) IQ samples, (b) CR-IA samples [29].

(a)

T (°C)	YS (MPa)	UTS (MPa)	Total elongation (%)	Uniform elongation (%)	Local elongation (%)	Martensite fraction (%)
750	471	675	16.79	11.68	5.11	39.79
775	445	753	14.92	10.90	4.02	44.21
800	456	795	14.09	10.69	3.4	58.21
825	509	830	13.26	9.45	3.81	66.31
850	554	880	8.27	5.93	2.34	81.00

(b)

T (°C)	YS (MPa)	UTS (MPa)	Total elongation (%)	Uniform elongation (%)	Local elongation (%)	Martensite fraction (%)
750	240	538	22.82	18.66	4.16	17.36
775	294	616	19.95	15.51	4.44	22.94
800	370	747	17.15	13.16	3.99	53.49
825	487	863	11.06	9.72	1.43	71.09
850	527	882	8.15	6.76	1.39	81.38

TEM studies were carried out to obtain superior contrast of martensite and ferrite phase. The martensite morphology in the two samples had distinct features. The fibrous martensite in IQ sample exhibited feather-like microstructure along the ferrite grain boundaries, while blocky martensite in CR-IA sample was distributed along the ferrite grain boundaries. Thereafter, tensile tests were conducted to study the mechanical properties of IQ and CR-IA samples (see Table 2.5).Thereafter, fracture analysis was done and a significant difference was observed in fracture surface of IQ and CR-IA samples. In the IQ sample, cleavage facets were observed, while only dimples were present in the CR-IA sample. From the investigation it was observed that there was not much difference in nature of fracture surface with change in martensite fraction. So the authors concluded that the fracture surface is governed by the morphology of martensite rather than its fraction. Firstly, unlike the IQ samples, which showed a significant decrease in the number density of micro voids, in the CR-IA samples, as the martensite fraction increased, the number density of micro voids experienced a small change. Secondly, in the CR-IA samples, martensite cracking was not frequently observed in comparison to the IQ samples and the micro-voids induced by ferrite–martensite interface de-cohesion were the primary cause of damage present in the material. So, it was concluded by the authors, that martensite cracking occurs easily at fibrous martensite and causes the cleavage facet. However, micro- voids are easy to form, when martensite is blocky.

Li *et al.* [30] investigated the effect of overaging temperature on microstructure and mechanical properties of DP590 steel in the conventional overaging and a proposed overaging process of continuous annealing. The annealing process of DP590 steels was simulated by continuous annealing simulator. The material used was cold rolled DP590 strip steel with 1.2mm thickness. The chemical composition (wt %) of the experimental steel was 0.08C, 0.479Si, 1.81Mn, 0.014P, 0.004S, 0.162Cr, 0.004N, 0.04Al and bal. Fe. Firstly, the continuous slab with thickness of 220 mm was heated to 1190–1200 ℃ and hot rolled to a thickness 20–25 mm. Subsequently the slab was rolled from 20–25 mm to 4–6 mm by finising rolling mill. Rough rolling temperature was 1120–1170 ℃. Entrance temperature of finishing rolling was 950–1030 ℃ and delivery temperature was 850–870 ℃. Coiling temperature was controlled at 600–620 ℃. After acid pickling, the hot rolled strip was cold rolled to the thickness of 1.2 mm. Figure 2.19 shows the schematic illustration of two types of annealing processes used during the investigation. “HS”, “SS”, “SCS”, “RCS”, “OAS” and “FCS” correspondingly denote the stage of heating, soaking, slow cooling, rapid cooling,

overaging and final cooling, while “LHS”, “RHS” and “OAS1” represent the low temperature holding stage after rapid cooling, the reheating stage and the overaging stage, respectively. The detailed annealing parameters are given in Table 2.6.

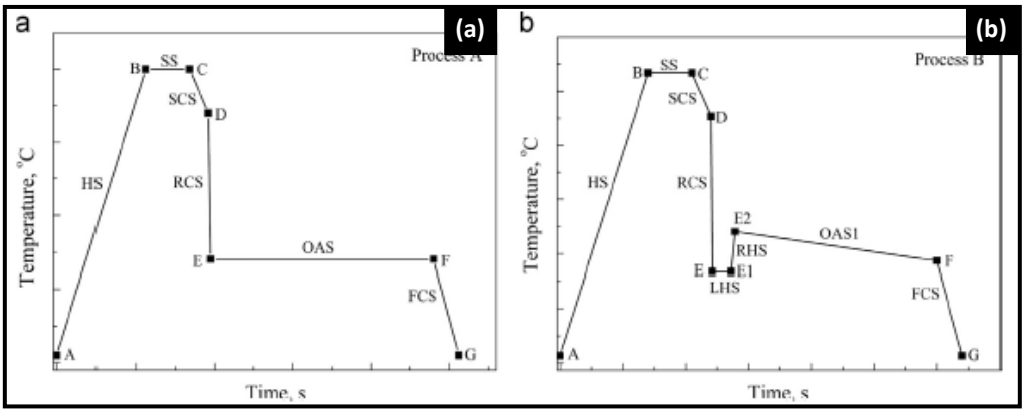

Figure 2.19 Schematic illustration of (a) conventional overaging, and (b) a proposed overaging process of cold rolled strip continuous annealing [30].

In order to investigate the effect of overaging temperature on the microstructure and mechanical properties, the experimental steels were rapidly cooled to various overaging temperatures of 280 ℃, 320 ℃, 350 ℃ and 400 ℃ in process A.

Table 2.6 Experimental parameters for continuous annealing experiments for process A and B [30].

Sections	Process A	Process B
HS (A→B)	30 ℃/s, 20→800 ℃	30 ℃/s, 20→800 ℃
SS (B→C)	800 ℃, 110 s	800 ℃, 110 s
SCS (C→D)	2 ℃/s, 800→680 ℃	2 ℃/s, 800→680 ℃
RCS (D→E)	30 ℃/s; 680→280, 320, 350, 400 ℃	30 ℃/s, 680→250 ℃
OAS (E→F)	280, 320, 350, 400 ℃; 420 s	–
LHS (E→E1)	–	250 ℃, 50 s
RHS(E1→E2)	–	50 ℃/s; 250 ℃→310, 330, 350, 400 ℃
OAS1(E2→F)	–	310, 330, 350, 400 ℃→280 ℃; 400 s
FCS (F→G)	280 ℃→20 ℃, 80 s	280 ℃→20 ℃, 80 s

However, in process B samples were rapidly cooled to 250 ℃ and held for 50s, and then heated at a rate of 50 ℃/s to various overaging temperatures of 310 ℃, 330 ℃, 350 ℃ and 400 ℃. The microstructure of experimental steels was observed by scanning electron microscopy and transmission electron microscopy. The volume fraction of martensite phase was measured and analyzed by Image-pro Plus software. Additionally, the tensile tests were performed on specimens with a gauge length of 50 mm. Furthermore, in order to observe the microstructure adjacent to the fracture surface, fractured tensile specimens were sectioned through-thickness along the mid-width plane in the longitudinal direction. The authors

observed that in conventional annealing process with the increase in overaging temperature (OT) from 280 ℃ to 400 ℃ the amount of retained austenite increased and volume fraction of martensite decreased because of austenite stabilisation due to higher carbon diffusion from ferrite to untransformed austenite at higher OT. Moreover, there is decrease in density of geometrically necessary dislocations (GNDs) due to recovery of ferrite from residual stress at high OT. Whereas, in the proposed annealing process similar trend was observed (with increase in reheated overaging temperature (ROT) the amount of retained austenite increased). In addition to that, TEM analysis showed that some cementite was also present in the martensite. This was because some martensite was formed during isothermal holding at 250 ℃ before reheating to overaging temperature (ROT). This formed martensite got tempered and cementite began to precipitate when the steel was reheated to higher temperature for overaging. Thereafter, tensile testing was done to compare the mechanical properties of steels obtained from annealing process A and B. Figure 2.20 shows graphs depicting the trend of strength with overaging temperature.

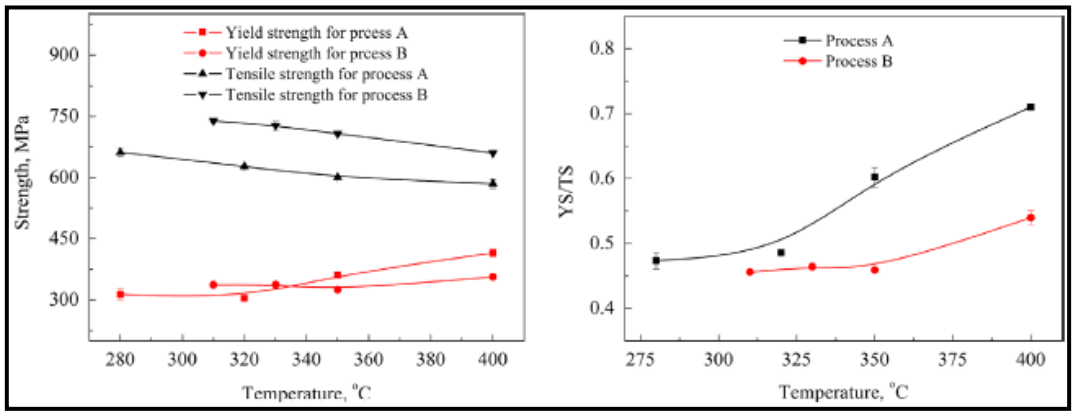

Figure 2.20 Yield strength, tensile strength and ratio of YS/TS for the experimental steels [30].

Tensile strength obtained in process B is higher than that from process A because of larger carbon content in martensite. For process B, most of the martensite is formed at the temperature of 250 ℃, at which the carbon diffusivity is lower. However, most of the martensite in process A is formed at the temperature higher than 280 ℃, at which the carbon is more likely to diffuse towards the neighbouring untransformed austenite or ferrite. Furthermore, the overaging temperature in process B decreases with time slowly, which means the solubility of carbon in ferrite will decrease. As a result, during overaging, for process B, the carbon in ferrite tends to diffuse towards the untransformed austenite. During the subsequent final cooling, some of the untransformed austenite will transform in to

martensite, which has higher carbon content than that formed in process A. In addition to the higher carbon content, higher volume fraction of martensite and the formation of nano-scale cementite in process B (due to decrease in ROT with time), also contributed to the higher tensile strength. For process A, the yield strength increased with increase in OT which resulted in increase of the ratio of YS/TS. Whereas, for process B these parameters changed slightly (increasing slightly at higher overaging temperatures). Finally, after fracture analysis it was observed by the authors that at lower overaging or reheated overaging temperature, the micro voids were easy to nucleate. As a result, the dimples on fractured surface were relative small and shallow. Whereas, the density of micro voids decreased with increase in overaging temperature due to which dimples on fractured surface were large and deep.

Maresca *et al.* [31] investigated, how retained austenite present in-between martensite laths affects the strain partitioning among the individual phases and the overall deformation behaviour of dual phase steels. Two simulation models were prepared using crystal plasticity approach. The overall objective was to study the strain partitioning behaviour of different phases of DP steel when a small fraction of retained austenite films (approximately 2% in the whole steel) is present in the inter-lath spacing of the martensite phase. It was observed by the authors that, presence of small fraction of about 2% inter-lath austenite films increases the heterogeneity of strain in both martensite islands as well as nearby ferrite phase. The authors confirmed these observations by comparing them with experimental observation from the previous literature, which showed that the local deformation/ mechanical response of martensite is anisotropic and depends upon the lath orientation. The authors concluded that for industrial production of dual phase microstructure (where retained austenite could be as high as 10%), the retained austenite could play a vital role and can drastically affect the stress-strain response of the DP steel. The results emphasise the potential key role played by inter lath austenite films in microstructures involving lath martensite.

Zhang *et al.* [32] investigated the influence of microstructure on the evolution of mechanical properties of a dual phase (DP980) steel. The chemical composition of the steel used for this study is shown in Table 2.7. To investigate the effect of annealing on the dislocation density and morphology of phases present recovery annealing experiments were conducted. The experiments consisted of three groups wherein the samples were heated for 60 minutes at the annealing temperature of 200, 400, and 550 ℃ respectively, referred as DP980-250, DP980-400, and DP980-550 respectively. In order to characterize and identify the individual

phase (martensite and ferrite) present in the microstructure EBSD (Electron backscatter diffraction) and nano-indentation hardness testing was done. To measure the mechanical properties at macroscopic level tensile testing and Vickers hardness tests were employed. The results from these experiments were correlated to understand the relationship between morphology of ferrite and martensite phases and strength of the metal.

Table 2.7 The chemistry of the DP 980 steel [32].

Chemical component	Al	C	Cr	Cu	Mn	Mo	Ni	P
wt%	0.05	0.12	0.25	0.01	2.47	0.36	<0.01	0.014
Chemical component	**S**	**Si**	**Ti**	**B**	**N**	**Nb**	**V**	**Zn**
wt%	0.004	0.03	<0.01	0.01	0.009	0.02	<0.01	<0.01

It was observed by the authors that when the annealing temperature was increased to 250 ℃ to 550 ℃, the martensite hardness decreased significantly. Whereas, the hardness of ferrite phase (measured at the centre of ferrite grain) remained approximately same before and after the annealing processes. Also, it was observed that hardness values at the inter-phase boundaries decreased with increase in the annealing temperature due to the relaxation of the dislocations at high temperature. The yield strength of the steel samples increase from 730 MPa to 850 MPa when tempering was done at a low tempering temperature (DP980-250 and DP980-400) as compared to the high temperature aging (at 550 ℃), which did not affect the yield strength much. However, a significant decrease in the UTS value was observed.

Ayatollahi *et al.* [33] used experimental and numerical methods to study the micromechanical behavior of DP steel. A steel plate of the given DP steel was annealed inter-critically to obtain different microstructures. Three different models with different microstructures were prepared from the optically determined surface of the steel plate (inter-critically annealed) and these microstructures were used for numerical simulations. The authors used three models namely: the 2D plane strain model, the uniformly extruded 3D model and the randomly extruded 3D model. It was observed that, the 2D microstructure based simulation model (which was constructed from real DP980 microstructure) could not simulate acceptable deformation behaviour under the conditions of tensile loading. Further, a

3D model was developed by extruding the 2D model uniformly through the thickness. However, no significant improvement was observed in the ability of the model to reproduce the tensile loading behaviour. Finally, a 3D model was prepared by extruding the 2D microstructure in the direction of thickness but this time the martensite and ferrite phases were redistributed in different layers with similar proportion of each phase in every layer. This randomly extruded 3D model showed promising results and was able to estimate the tensile loading behaviour of DP980 steel under actual experimentation conditions.

2.3 Summary of the Reviewed Literature

- Several authors have worked on the processing of first generation of DP steels to achieve high strengths as compared to conventional high strength steels but ductility of such steels was not enough for industrial forming. Some researchers used expensive micro-alloying (second generation advanced high strength steels) to achieve higher ductility along with high strength, but poor weldability due to excessive alloying caused problems. Finally, some work on third generation DP steels was reported by a few researchers in which first generation dual phase steels were modified by controlling the heat treatment routes, resulting in improved ductility without compromising on strength and toughness. Also, the carbon content and overall alloying content was reduced to improve weldability [4,9,13,14,20,34]
- Majority of the authors have reported that DP steels can be produced by initially inter-critically annealing the steel followed by water quenching. Although, a few authors have also obtained the dual phase structure from the fully austenitic region, followed by slow cooling and then finally quenching [1,11,14,17,25,35,36].
- Several authors have investigated the influence of inter-critical annealing parameters on the evolution of microstructure and mechanical properties of dual phase steels. The authors have studied the effect of different isothermal holding temperatures and holding times in the inter-critical region on the final microstructure, tensile behaviour and fracture mechanisms etc. [25,26,35,37].
- Some of the authors have studied the interaction of ferrite recrystallization and phase transformation during the heating stage of annealing process and have investigated the resulting microstructure for changes in morphology of phases present along with comparison of mechanical properties of low carbon steels processed under different annealing parameters [35,38–40].

- Some of the authors have investigated the effect of carbon content, morphology, and fraction of martensite on the mechanical properties and damage evolution behaviour of DP steels [27–29].

2.4 Gaps in the reviewed literature

- Most of the literature on DP steels has focused mainly on ferrite/martensite microstructure. Very limited literature is available on dual phase steels with ferrite/ bainite microstructure.
- Limited research is available to explain as to how the different physical phenomena of pearlite dissolution, ferrite recrystallization, and phase transformation etc. interact with one another during the heating stage of continuous annealing with change in annealing parameters. Further, these phenomena have not been investigated by simulating actual industrial continuous annealing conditions.
- For most of the research available on annealing simulations, Gleeble simulator has been used to simulate the continuous annealing process using water as the quenching medium. However, these are not the actual industrial continuous annealing line conditions wherein a gas mixture is used as a quenching medium.
- Most of the authors have attempted to improve the mechanical properties of DP steels by varying the martensite volume fraction, and/ or the ferrite grain size. However, very limited research is available showing the influence of martensite morphology and distribution on the mechanical properties of DP steels.
- Though, some literature is available on the use of thermal cycling to alter the morphology and distribution of martensite phase, but this concept has not been combined with continuous annealing cycle to investigate change in the mechanical properties of DP steels.

Chapter 3
Design of the Study

3.1 General

The objective of this chapter is to outline the detailed design of the research work presented in this report. It provides an insight into the research methodology followed, and the experimental procedure adopted during the research work. In addition, a brief description of the machines and equipment used has been provided.

3.2 Establishment of the Objective Function

DP steels are mostly produced through continuous annealing process route in the industry because this route allows for high production rates, uniformity in properties, and leaner chemistry design feasibility. The critical tensile deformation characteristics desired in DP steels (viz. absence of yield point, low yield point to ultimate tensile strength, high strain hardenability along with high ductility etc.) can be obtained by using continuous annealing process with optimized parameters. DP steels derive their properties via their second hard phase, namely; martensite or bainite which is present in the ferrite matrix. The important parameters affecting the martensite fraction and morphology are heating rate, isothermal annealing temperature, soaking time, and the subsequent cooling rate. All these process parameters can be controlled to trigger pearlite dissolution, recrystallization, and phase transformation at various stages of annealing process cycle. There could be several combinations of processing routes depending on the governing mechanisms such as, pearlite dissolution, recrystallization, and phase transformation, which can affect the morphology and distribution of the martensite phase. Also, the initial condition of austenite nucleation during inter-critical/ full annealing can significantly affect the spatial distribution and size of ferrite and martensite in the final microstructure and thus, subsequently affect the mechanical properties. Therefore, controlling the kinetics of austenite formation becomes an important aspect from an industrial point of view.

Extensive research is available on the process of transformation of austenite (into ferrite, pearlite, bainite, and martensite) during continuous cooling. However, scant literature is available on the kinetics of austenite formation from initial ferrite-pearlite microstructure during heating stage of continuous annealing. In the recent past, several models have been proposed to describe the austenite formation during heating. Nevertheless, these theories are

not as expansive as those for the austenite transformation during cooling stage and need further investigation. The present study deals with the experimental simulation of above parameters to control evolution of microstructure by using a custom designed annealing simulator with annealing conditions similar to that used in industrial practice. Through these simulations it was possible to tailor the microstructure and consequently properties of dual phase steel.

The main objective of the present research was, "to modify the martensite morphology and distribution in a DP steel when processed under actual industrial CAL conditions for improved "strength-ductility combination".

The sub-objectives of the presented work were:

- To study the effect of different heating rates during continuous annealing on the kinetics of ferrite recrystallization and pearlite dissolution for a cold-rolled low carbon steel.
- To understand the effect of extent of pearlite dissolution and ferrite recrystallization on austenite nucleation and growth kinetics during continuous annealing simulations.
- To develop a modified continuous annealing cycle that can be used for commercial production of DP steel with enhanced strength-ductility combination.

The key issues to be taken up during the research work were as follows:

- To investigate the microstructure of the as-received cold rolled low carbon Si based DP steel using optical microscopy and SEM.
- To obtain the annealing parameters (critical temperatures, austenite phase transformation kinetics etc.) for the given steel using Gleeble dilatometry studies.
- To perform annealing experiments on annealing simulator with conditions similar to that used in industrial practice for the production of DP steel grade.
- To characterize the resulting microstructures during different annealing regimes and investigate the influence of annealing parameters on microstructure evolution.
- To compare the mechanical properties of the processed samples using tensile testing and nano-indentation hardness testing.

3.3 Experimental Procedure

The experimental procedure followed during the present study is as follows:

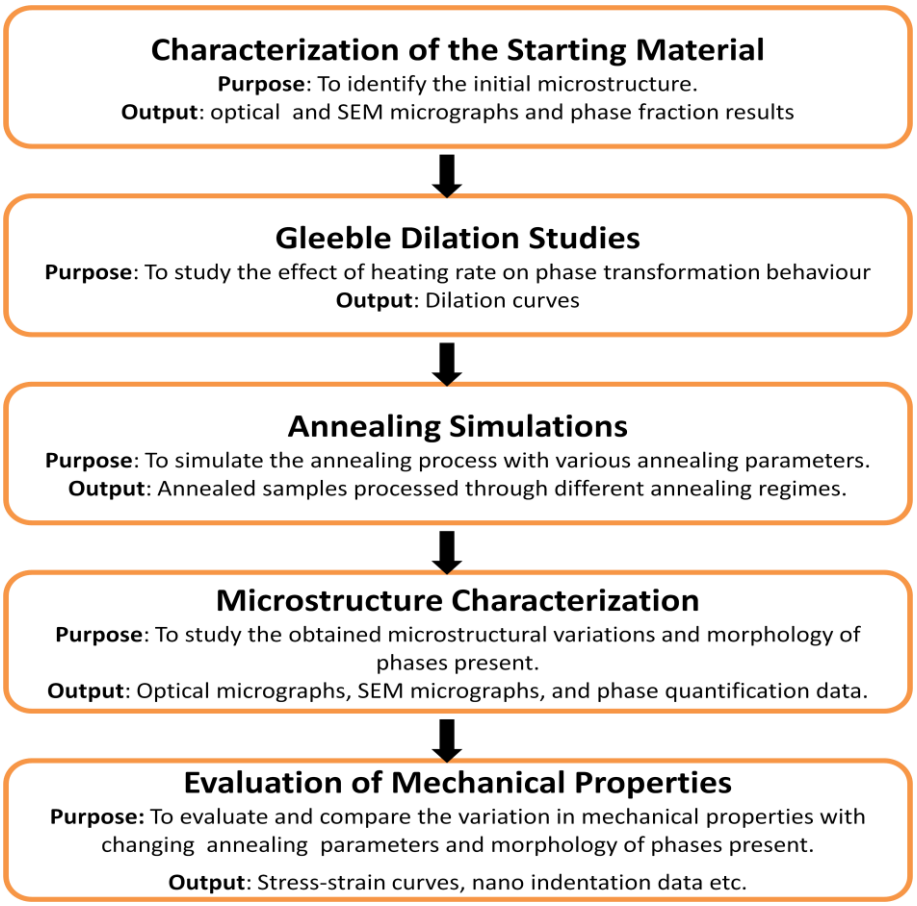

Figure 3.1 Experimental procedure followed for the research work.

3.3.1 Starting Material

The starting material was a low carbon Si based steel received from Tata Steels Pvt. Ltd, Jamshedpur. The chemical composition of this as-received material is presented in Table 3.1.

Table 3.1 Chemistry of the as-received Si based steel.

C	Mn	P	S	Si	Al	N	Fe
0.07	1.82	0.015	0.006	0.47	0.032	0.0025	Balance

The as-received material was industrially cold-rolled (67%) ferrite-perlite steel with a finishing gauge thickness of 0.82 mm. Microstructural analysis of the as-received material was conducted using both, optical microscopy and SEM analysis to observe the phase types, their fractions, and distribution.

3.3.2 Prediction of Annealing Process Parameters

In the actual industrial continuous annealing lines, the heating rates followed vary between 10–15 $℃/s$ [12,41]. Keeping this in view, dilatometery experiments (to determine the Ac_1 and Ac_3 critical temperatures of the given steel) were carried out at two different heating rates of 5 $℃/s$ (lower than the actual industrial heating rates) and 20 $℃/s$ (higher than the actual industrial heating rates) to study the effect of heating rate on the phase transformation behaviour. Rectangular steel strips, 100 mm in length and 10 mm in width were cut from the as-received steel sheets for these investigations. Figure 3.2 shows one such steel strip.

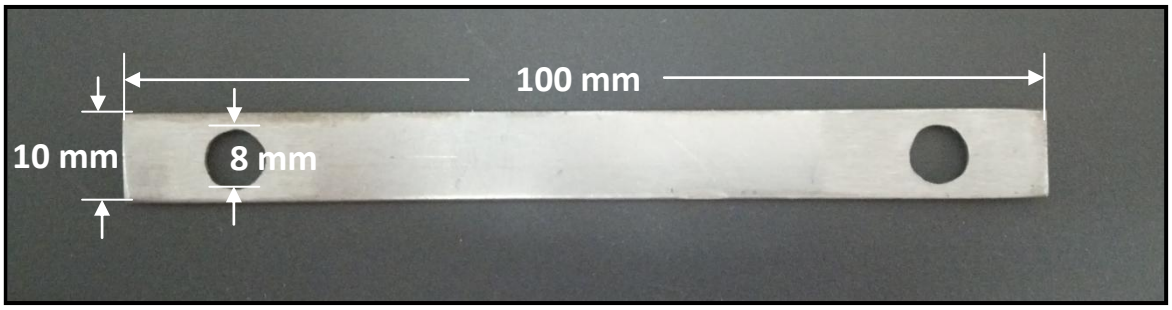

Figure 3.2 Gleeble dilation study sample.

3.3.3 Annealing Simulations and Microstructure Characterization

Tensile samples of 25 mm gauge length (see Figure 3.3) were prepared from the as-received steel sheets as per ASTM standard E-8M and annealing simulations were carried out in a custom designed annealing simulator (see Figure 3.4). A mixture of 10% H_2 gas in N_2 was used as inert annealing atmosphere and also as a quenching medium, which was similar to the annealing conditions used in industrial production of dual phase steels. The gas mixture discharge and injection pressure were varied to achieve different levels of cooling.

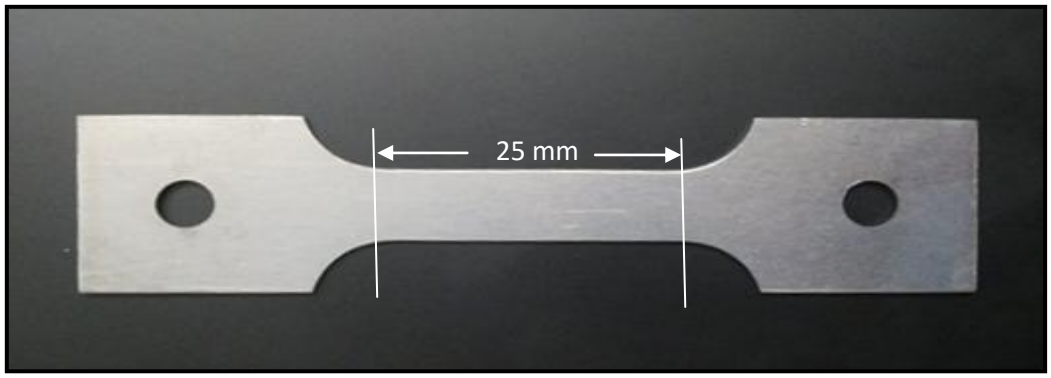

Figure 3.3 Tensile samples for annealing simulation and subsequent tensile testing.

Small samples were cut from these tensile samples subjected to annealing simulations for microstructural investigation. Standard metallographic techniques were employed to prepare the samples for microstructure characterization. The metallographic techniques used are discussed in detail in subsequent sections. Optical microscope and scanning electron microscope (SEM) were used to investigate the morphology i.e. shape, size, and distribution of phases present in the final microstructure. An etchant of 2% nital was used for revealing microstructure for optical and scanning electron microscope (SEM) studies. Further, quantitative analysis of the resulted micrographs was carried out using commercial software viz. Image J (version 1.51a, National Institutes of Health, Maryland, USA), and analySIS FIVE (Olympus, Waterloo, Australia).

3.3.4 Tensile Testing and Nano-Indentation Hardness Testing

Finally, to investigate the effect of annealing parameters on the mechanical properties (strength and ductility), the steel samples processed through different annealing regimes were subjected to tensile tests. Further, to determine the second phase hardness (and to clearly establish the second phase type i.e. martensite), nano-indentation studies were conducted. Indents were made both, at the globular/ polygonal as well as at the lath type martensite phase. A need for nano-indentation hardness testing arose due to the very fine size of martensite grains and laths. By this technique, it was possible to make indents exclusively on individual phases (i.e. martensite grains/ laths). This technique enabled to measure martensite hardness without the interference of ferrite phase. This could not have been possible by using conventional micro-hardness technique due to its large indent size.

3.4 Machines and Equipment

This section describes a brief outline and characteristic features of various machines, and equipment used in the present work.

3.4.1 Annealing Simulator

Annealing simulator is a custom designed experimental set-up developed jointly by CSIR-NML and Tata Steels, Jamshedpur (see Figure 3.4). In this simulator, the samples to be annealed can be heated in an inert environment ('N_2+ H_2' gas mixture) and quenched under controlled cooling conditions.

Figure 3.4 Annealing simulator (a) during the annealing process, (b) section details (Courtesy: NML, Jamshedpur).

The annealing simulator consists of:

a) *Heating System*

The simulator consists of a high speed heating system. The furnace of this simulator is capable of providing heating temperatures upto 1200 ℃. The heating chamber is heated to the desired annealing temperature by inserting it in the furnace using a motor guided system. Further, at the other end of the heating chamber, a cooling chamber is connected. Samples are mounted on a tray in the cooling chamber that can slide on guide ways and can be manually moved in and out of the heating chamber using a long handle protruding out of the cooling chamber. Two thermocouples, one mounted at the sample surface and the other mounted in the surrounding atmosphere near the mounted samples (though within the heating chamber only) measure the change of temperature of specimen and atmosphere around it for accurate measurement of temperature-time data.

b) *Quenching System*

A gas mixing chamber is used to prepare a mixture of H_2 and N_2 gases (with 10% H_2 and remaining N_2). Two lines connect this cooling chamber to this mixing chamber. The first line is used mainly for maintaining an inert atmosphere during annealing and additionally also for slow cooling (through small discharge of gas). The second line is used for obtaining high cooling rates. Different rates of cooling can be achieved by varying the gas discharge and purging pressure. An exit line from the cooling chamber allows the used gas mixture to escape to the environment.

c) *PLC based Digital Control System*

A PLC based digital controller, which is considered as the heart of annealing simulator, controls different annealing variables to achieve desired annealing process conditions. The furnace parameters viz. heating temperature, soaking time, heating rate etc. can be controlled either from inbuilt touch screen panel provided on the PLC controller or by an integrated computer system connected to the system. The system is highly versatile with multiple operating modes.

3.4.2 Gleeble Simulator

The Gleeble 3800 (Make: Dynamic System Inc, *Poestenkill,* New York, USA) is a fully automated thermal and mechanical testing system (see Figure 3.5). It uses a 'Windows' based computer software that allows the user to create, run, and analyze data from physical simulations and thermo-mechanical tests in a user friendly maner. The Gleeble has a direct resistance heating system which is capable of heating the specimens at heating rates of up to 10,000 $℃/s$, or even at a steady-state equilibrium temperature. The highly conductive grips enable the simulator to achieve high cooling rates of up to 10,000 $℃/s$. The mechanical system of Gleeble 3800 consists of a hydraulic servo system which is capable of applying loads of 20 tons in compression and 10 tons in tension. Displacement rates, as fast as 2000 mm/s can be achieved. The mechanical system is capable of allowing changes from one control mode to another during any given test; this provides the flexibility necessary to simulate many thermo-mechanical processes necessary during the test. A 'Windows' based workstation and a powerful embedded processor is used. Once the simulation has been finished, the results are automatically loaded into the 'Origin' software, a flexible and powerful data analysis package included with every Gleeble 3800 System.

Figure 3.5 Gleeble 3800 simulator (Courtesy: NML, Jamshedpur).

3.4.3 Equipment Used for Sample Preparation

In order to prepare samples for metallography, some basic steps need to be followed carefully. These include mounting, planar grinding, rough polishing, final polishing, etching and microscopic analysis. The equipment used for these steps are discussed in brief as follows:

a) Precision Cutter

To cut the samples accurately, a precision cutter (Make: MICRACUT 125, *Metkon Instrumens Inc*., Bursa, Turkey) was used. The cutter consists of an aluminium vice on which the specimen to be cut (into small samples) is mounted. A micrometer screw on the machine allows the user to locate the specimen accurately relative to the cutting wheel. The mounting arm has a dead weight at one end and the samples are cut by lowering the specimen over cutting wheel under the effect of dead weight. Figure 3.6 (a) illustrates the precision cutter used in present work.

b) Mounting:

The use of mounting of samples is to facilitate their easy handling. Mounting is done either with copper or with bakelite. Copper is used for mounting when specimen is to be used for SEM analysis. Specimens are hot mounted at a temperature of 160 ℃ by following the

procedure of powder metallurgy. The edges of the mounted samples are rounded off to minimize the damage to grinding/polishing discs. The mounting press (Make: BAINMOUNT METCO, *Chennai Metco Pvt. Ltd.*, Chennai, India) was used in the present work and is shown in Figure 3.6 (b).

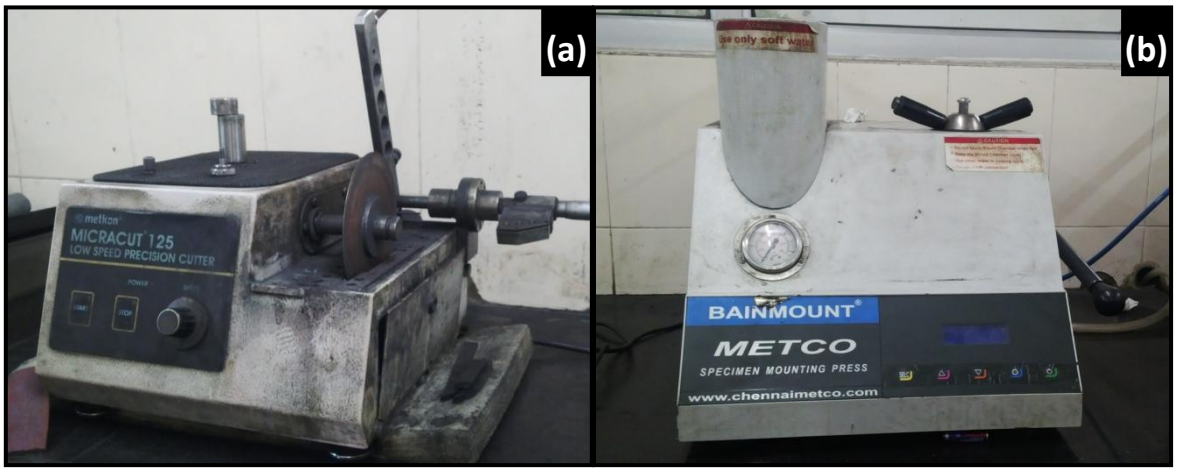

Figure 3.6 (a) Low speed precision cutter, (b) mounting machine (Courtesy: NML, Jamshedpur).

c) Grinding

The surface to be examined by microscope is polished with abrasive papers of successive finer grades such as 80, 120, 220, 320, 400, 600, 800, 1000, 1200, 1500 and 2000 mesh abrasive paper as shown in Figure 3.7 (a). Each time the sample is rubbed on SiC paper, scratch marks are introduced, therefore polishing is continued till all the scratches are in one direction. Then, the next paper with finer grade is used with direction of rubbing switched perpendicular to previous scratches. Similar process is repeated from the coarse grade paper (80 grit size) up to fine grade paper (2000 grit size). Over-heating of sample is avoided so that no modification in the microstructure occurs. Pressure needs to be adjusted, as high pressures can introduce deep scratches, whereas low pressures result in long time consumption.

d) Polishing

The next step is polishing on a horizontal rotating wheel. Polishing wheels are covered with a soft cloth (velvet, canvas, suede or selvet etc.) which need to be soaked with a polishing medium (alumina or colloidal). The polishing cloth is washed thoroughly with water before the start of polishing to remove any chances of introduction of contaminants which may cause deep scratches on surfaces. Polishing medium is spread on to a well washed cloth and as soon as the specimen starts to stick or friction starts to act between the specimen and the

cloth, water is poured on to the rotating wheel. The specimen is held on the rotating disc in order to obtain a scratch free surface with mirror like finish. Polishing machine (Make: BANIPOL METCO, Model No: PMV018, *Chennai Metco Pvt. Ltd.*, Chennai, India) of 0.37 kW capacity was used and is shown in Figure 3.7 (b).

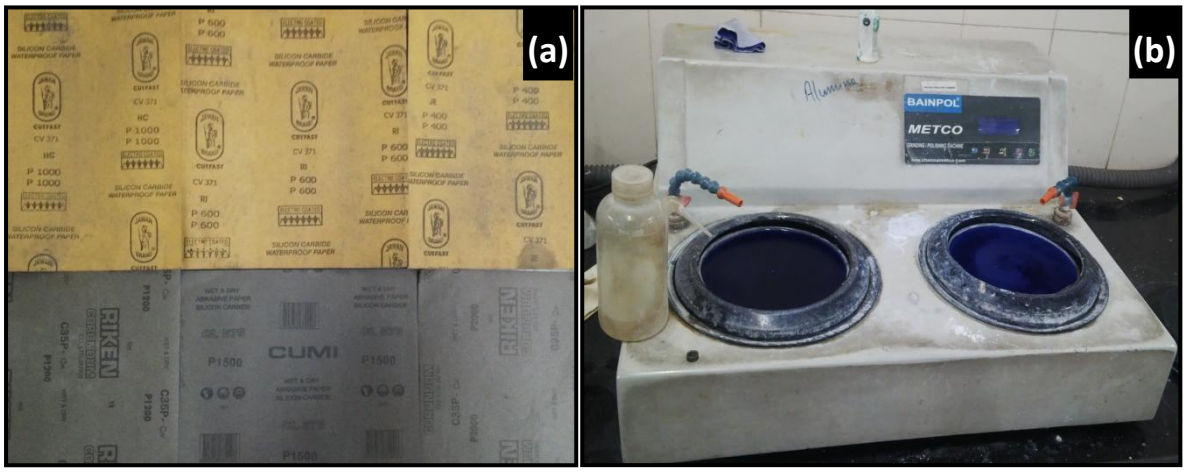

Figure 3.7 (a) Abrasive papers, (b) polishing machine (Courtesy: NML, Jamshedpur).

e) Etching

Etching is done in order to reveal the microstructure of the metal/ alloy system through selective chemical attack. The sample must be thoroughly cleaned before etching. Etchant must be selected and prepared accurately. Etchant may be applied using a cotton bud wiped over the surface for a few times (necessary precautions must be taken while etching, as very small difference occurs between etching and over-etching). Nital (2% nitric acid in ethanol) was used as the etchant. The specimens were immediately washed with alcohol after applying the etchant and were then dried.

f) Levelling

The surface to be examined optically should be perfectly flat and levelled. If not, then the viewing area would be out of focus i.e. if the centre is focused, the sides would go out of focus and vice versa. By using a specimen levelling press, this problem can be avoided, as it presses the mounted specimen into clay on a microscope slide, making it levelled. A small piece of paper or cloth covers the surface of the specimen to avoid scratching. A levelling machine is shown in Figure 3.8.

Figure 3.8 Levelling machine (Courtesy: NML, Jamshedpur).

3.4.4 Microstructural Evaluation

Mechanical properties of steels are strongly influenced by the microstructure, so microstructural evaluation is important. In the present research work, optical microscopy and scanning electron microscopy (SEM) were used for microstructural evaluation.

a) Optical Microscope

An optical microscope is used to fulfil two major basic functions:

- Magnification of small specimen to produce a magnified image
- Illuminating a specimen

Optical microscope uses visible light to illuminate the specimen and a system of lenses to generate a magnified image of the area under observation. The magnified image can be viewed from the eyepiece or the microscope can be integrated with a computer system that can convert optical images into digital form and can be stored on a hard drive. In metallography, metallic materials (generally opaque) are first prepared using standard metallography techniques and thereafter etched using a suitable etchant before viewing them under an optical microscope for microstructural investigations. The difference in the refractive indices of etched phases in specimen causes the light to get reflected back to the eyepiece at different angles and intensity. Thus, different micro-constituents appear to have different grey or colour shades when viewed through eyepiece and this difference enables the user to identify different phases.

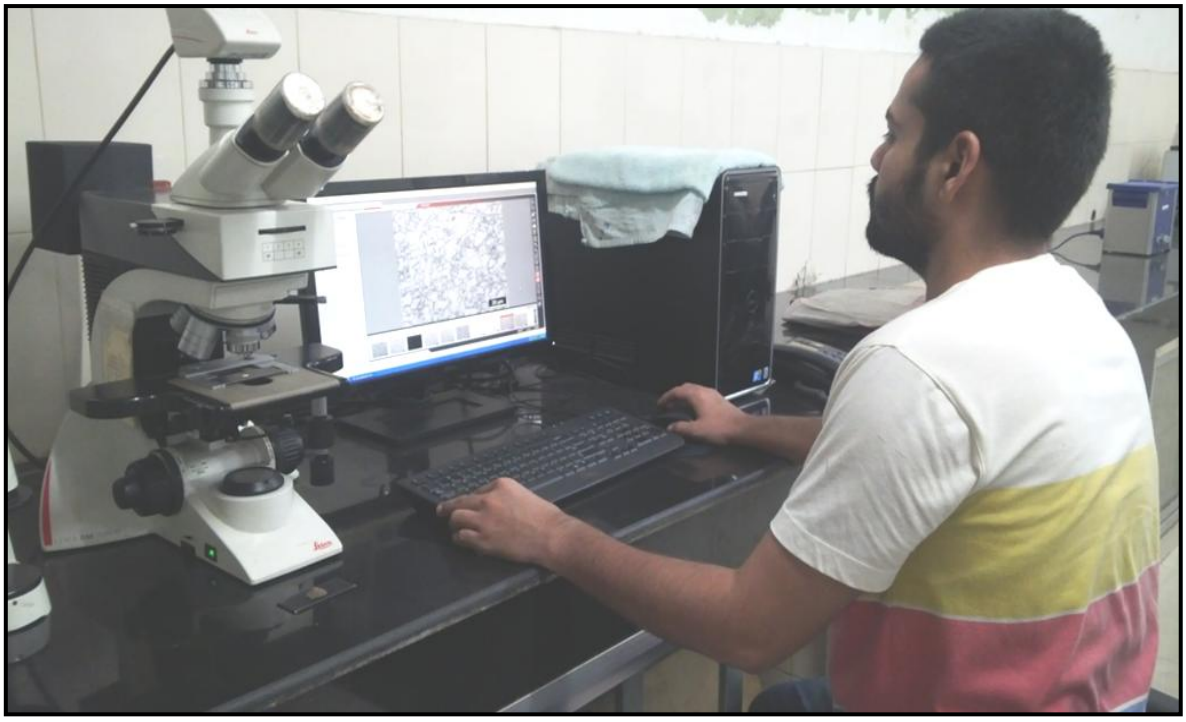

Figure 3.9 Optical microscope (Courtesy: NML, Jamshedpur).

To reveal useful information from optical microscopy, sample preparation is a critical step and sample should be levelled to get good images. The optical microscope (Make: Leica DM2500 M; *Lieca Microsystems,* Wetzlar, Germany) was used in the present study for microstructural investigations and is shown in Figure 3.9.

b) Field Emission Scanning Electron Microscope (FE-SEM)

A focused beam of high energy electrons (carrying significant amount of kinetic energy) is made to incident on solid sample and its energy gets dissipated in electron-sample interactions as the accelerated electrons hit the sample surface. These interactions produce a variety of signals that reveal information regarding morphology (texture), orientation of constituents, and crystalline structure. The main forms of signals produced are secondary electrons, backscattered electrons, diffracted backscattered electrons, photons, visible light and heat. Secondary electrons are detected and used to produce SEM images. The width of areas that can be scanned in a scanning mode using conventional SEM techniques ranges from approximately 1 cm to 5 µm with magnification range from 20X to approximately 1,000,000X. Figure 3.10 shows a field emission scanning electron microscope (Make: Nova Nano SEM 430; *Field Emission Inc.,* Hillsboro, USA) used in the present study.

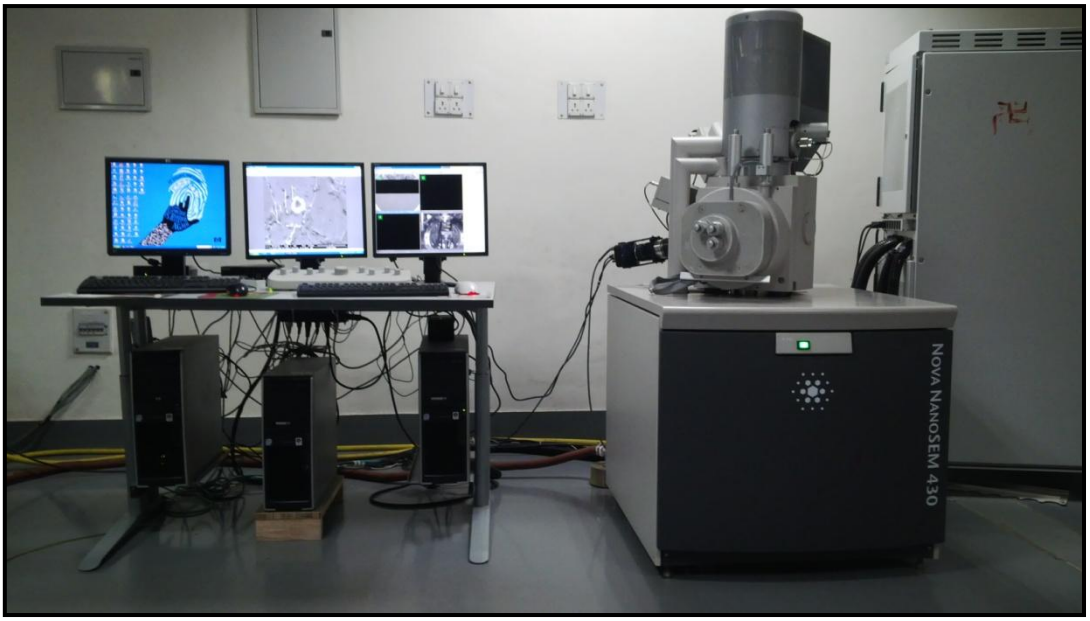

Figure 3.10 FE-SEM set-up used in the present work (Courtesy: NML, Jamshedpur).

3.4.5 Nano Indenter

A Nano Indentation tester (Make: MTS Nano Indenter' XP, *USA*) was used in the present work to help characterize the ferrite and globular/ lath marteniste. It is software-controlled and simple to use so as to allow the users to identify the exact location, where to make an indent.

Figure 3.11 Nano indenter tester used in the present work (Courtesy: NML, Jamshedpur).

In the present study, nano-hardness testing was done with an indentation depth of 150 nm. The surface approach velocity was 10 nm/s. Figure 3.11 shows the nano-indentation hardness testing machine used in the present work.

3.4.6 Tensile Testing Machine

The tensile testing machine (Make: Instron 8501 System, *Instron Engineering Corporation*, Norwood, USA) with a loading capacity of 100 kN was used for stress-strain analysis. The machine provides data in the form of values of load corresponding to extension. The data when plotted can be used to calculate the yield strength, ultimate tensile strength, and total elongation. Figure 3.12 shows the tensile testing machine used for the current study.

Figure 3.12 Tensile testing machine used in the present work (Courtesy: NML, Jamshedpur).

3.5 Summary of the Chapter

This chapter presented the design of the current research work. In this chapter of the report, the objective function with key issues was discussed. An overview of the research methodology and equipment to be used during the research work was briefly discussed.

Chapter 4
Results and Discussion

4.1 General

This chapter presents the details of results of the present study in a systematic manner. The results pertaining to the dilation studies, annealing simulations, microstructure characterisation and quantification etc. have been discussed in detail along with the evaluation of mechanical properties.

Various strategies are employed to manoeuvre the microstructure of DP steels for improved mechanical properties. Based on the annealing parameters (inter-critical annealing (IA) temperature, annealing time, and prior cold rolling conditions), either ferrite recrystallization dominates over phase transformation or phase transformation is the controlling phenomenon in microstructure evolution. So, depending upon the annealing parameters utilized, the interactions of these physical phenomena (i.e. ferrite recrystallization, and phase transformation) can fall into one of the following categories:

a) Deformed ferrite recrystallization is predominant. This occurs when annealing is done at temperatures close to the lower critical temperature [40,42–46].
b) Recrystallization and phase transformation is overlapping. This occurs when annealing is done at intermediate temperatures in the inter-critical range [38,43,47,48].
c) Phase transformation is predominant. This occurs when annealing is done at temperatures close to upper critical temperature [38,43,45,49].

It is clearly reported in literature that when annealing is carried out at low inter-critical annealing temperatures, ferrite recovery and recrystallization are the dominating phenomenon in microstructure evolution. The rate of pearlite dissolution is slow at low annealing temperatures and the extent of its dissolution can be increased by decreasing the heating rate for reaching Ac_1. On the other hand, when annealing is carried out at high annealing temperatures (close to Ac_3), phase transformation is the dominating phenomena. Furthermore, the pearlite dissolution is high and almost instantaneous (due to the high temperature). However, at intermediate temperatures during inter-critical annealing, recrystallization and phase transformation substantially overlap and occur concurrently [40,44,45].

In the present study, the effects of the above discussed parameters have been investigated on the kinetics of ferrite recrystallization, pearlite dissolution, and austenite transformation to

arrive at an industrially feasible continuous annealing process providing improved mechanical properties. This was important as DP steels are produced through a continuous annealing line (CAL) route owing to high production rates, uniformity in properties, and feasibility of leaner chemistry design [50]. Thus, the main aim of the present work was to modify the existing continuous annealing line (CAL) process for improved mechanical properties.

4.2 Characterization of the Starting Material

In the present study, a low carbon steel sheet (67 % cold rolled) containing ferrite and pearlite in the microstructure was used as a starting material.

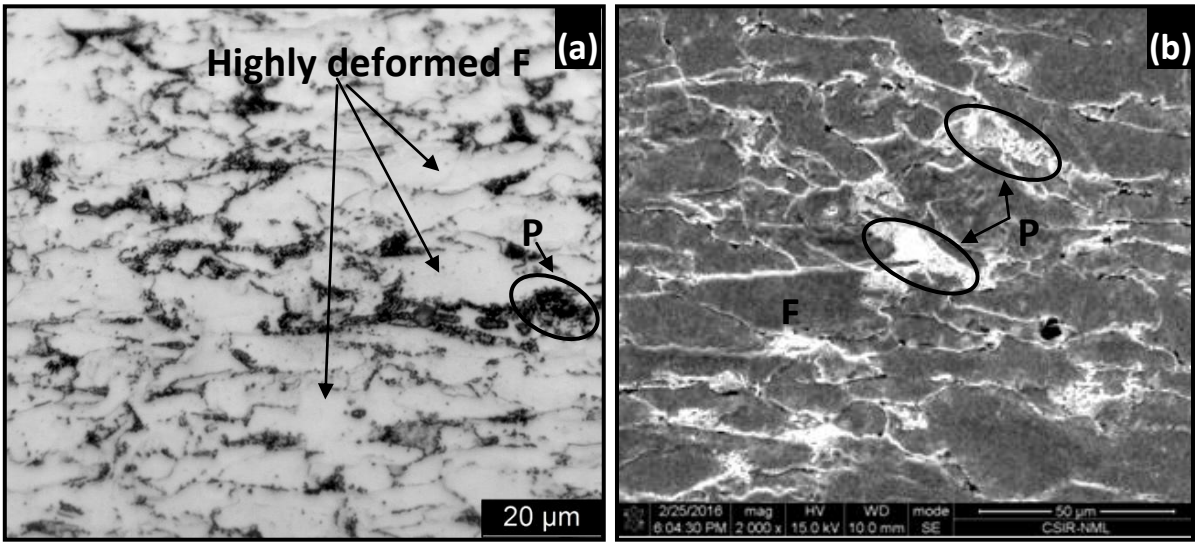

Figure 4.1 Microstructure of the as-received steel sheet (a) optical micrograph, (b) SEM micrograph. F = Ferrite, P = Pearlite.

The initial microstructure is shown in Figure 4.1a–b. As a result of cold deformation, the microstructure showed highly deformed ferrite and pearlite grains. The pearlite was non-uniformly distributed and was present as highly deformed colonies. This kind of distribution results in non-uniform pearlite dissolution during annealing. The quantitative analysis of the microstructure was done using "analySIS FIVE" commercial software. The volume fraction results showed 84% ferrite and 16% pearlite in microstructure.

4.3 Gleeble Dilation Study

In the present work, the main objective was to modify the martensite morphology and distribution in the given DP steel when processed under actual industrial CAL conditions to

obtain improved strength-ductility combination. This objective was achieved by modifying the existing CAL process (to a newly developed process called CHAP). The entire experimentation was carried out in an indigenously developed annealing simulator. In most of the experiments conducted in the annealing simulator, heating rates of the order of 10–15 ℃/s were used (as are used in the actual CAL process). In the present work, prior to the actual experimentation in the annealing simulator, preliminary experimentation was conducted in the standard and very sophisticated Gleeble 3800 set-up. The purpose of Gleeble dilation study was to establish that for the range of heating rates followed during inter-critical annealing for processing of DP steels, there is no significant shift in the inter-critical temperature values with change in heating rate. Gleeble experiments were conducted at two different heating rates of 5 ℃/s and 20 ℃/s.

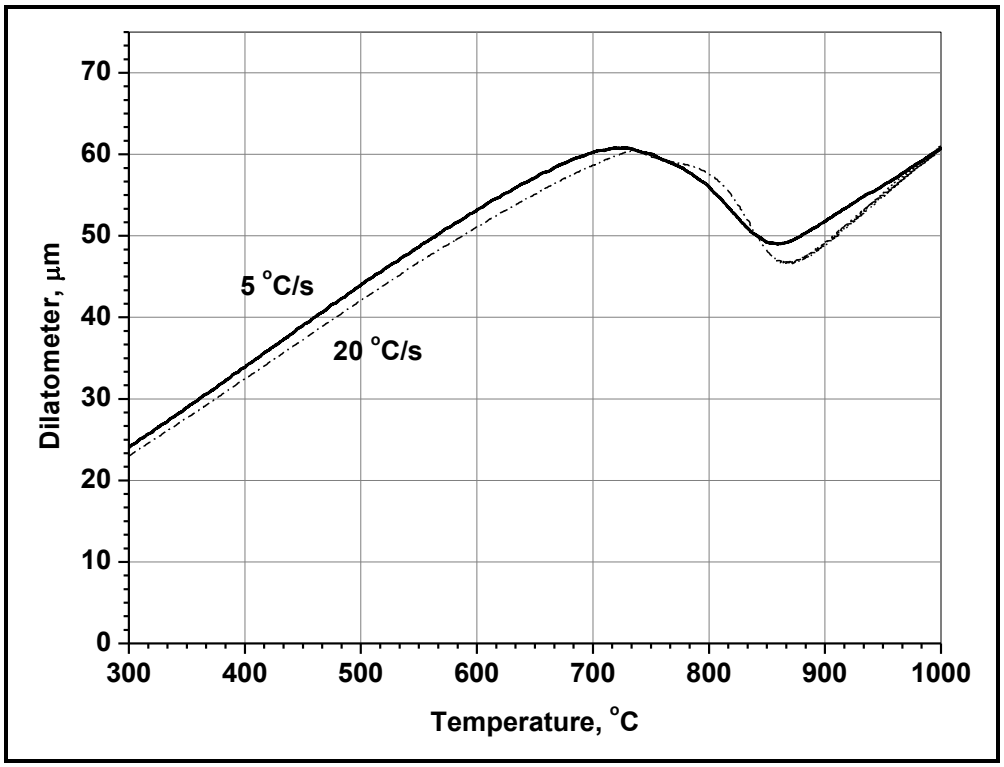

Figure 4.2 Gleeble dilation experiments showing the effect of heating rate on the inter-critical temperatures.

Figure 4.2 shows the dilation curves (only heating cycle portion shown) for the given steel when heated separately with these heating rates. For heating rate of 5 ℃/s, the estimated critical temperatures were, Ac_1 = 743 ℃ and Ac_3 = 860 ℃. For heating rate of 20 ℃/s, the predicted critical temperatures were, Ac_1 = 745 ℃ and Ac_3 = 873 ℃. Hence, it was noted that

for the heating rate range to be used in the present work, with change in heating rate, no significant change in the inter-critical temperatures occurred.

4.4 Effect of Heating Rate on Ferrite Recrystallization

The previous section established that for the range of heating rates followed during the present experimental work, no major change in the inter-critical temperatures was observed with change in heating rate. However, there was a need to further investigate the influence of change in heating rate on the ferrite recrystallization and pearlite dissolution. In this section, experiments were conducted (in the annealing simulator) at different heating rates (10 $℃/s$, normally used in industrial practice; and a slower rate than the normal, 3.5 $℃/s$ respectively). The specimens were subjected to an annealing cycle for each heating rate. In the annealing cycle, specimens were heated to a sub-critical temperature of 710 ℃ (sub-critical temperature was chosen because here the interest was only in ferrite recrystallization) at a given heating rate (10 $℃/s$ or 3.5 $℃/s$) and immediately quenched to room temperature. Figure 4.3a shows the typical annealing cycle with two different heating rates of 3.5 $℃/s$ and 10 $℃/s$ respectively. The effect of heating rate on ferrite recrystallization is shown in Figure 4.3c–d and is very well captured by grain aspect ratio (w/l) analysis shown in Figure 4.3b. Figure 4.3b shows that at a lower heating rate (here, 3.5 $℃/s$), the peak of the aspect ratio shifts towards a higher value (towards 1). This means that with decrease in heating rate, the grains tend to recrystallize more. Thus, it is clear that use of a lower heating rate to reach the sub-critical temperature promotes ferrite recrystallization. This is also clear from Figure 4.3c–d, where SEM micrograph corresponding to slower heating rate of 3.5 $℃/s$ shows better ferrite recrystallization.

Further, it may be noted that change in heating rate also affects the rate of dissolution of distorted pearlite colonies of the initial cold rolled steel. It can be observed that a slower heating rate (here, 3.5 $℃/s$) results in more uniform distribution of cementite/ carbide particles of pearlite. This uniform distribution of carbide particles provides better scope for controlling the spatial distribution of nucleation sites for austenite formation.

Speich et al. [49] demonstrated that austenite preferentially nucleates at the ferrite/cementite interfaces in the pearlite colonies. The authors [49] also concluded that rate of austenite growth was controlled by carbon diffusion from cementite. So, closer the cementite particles more will be the growth of austenite due to small carbon diffusion distance.

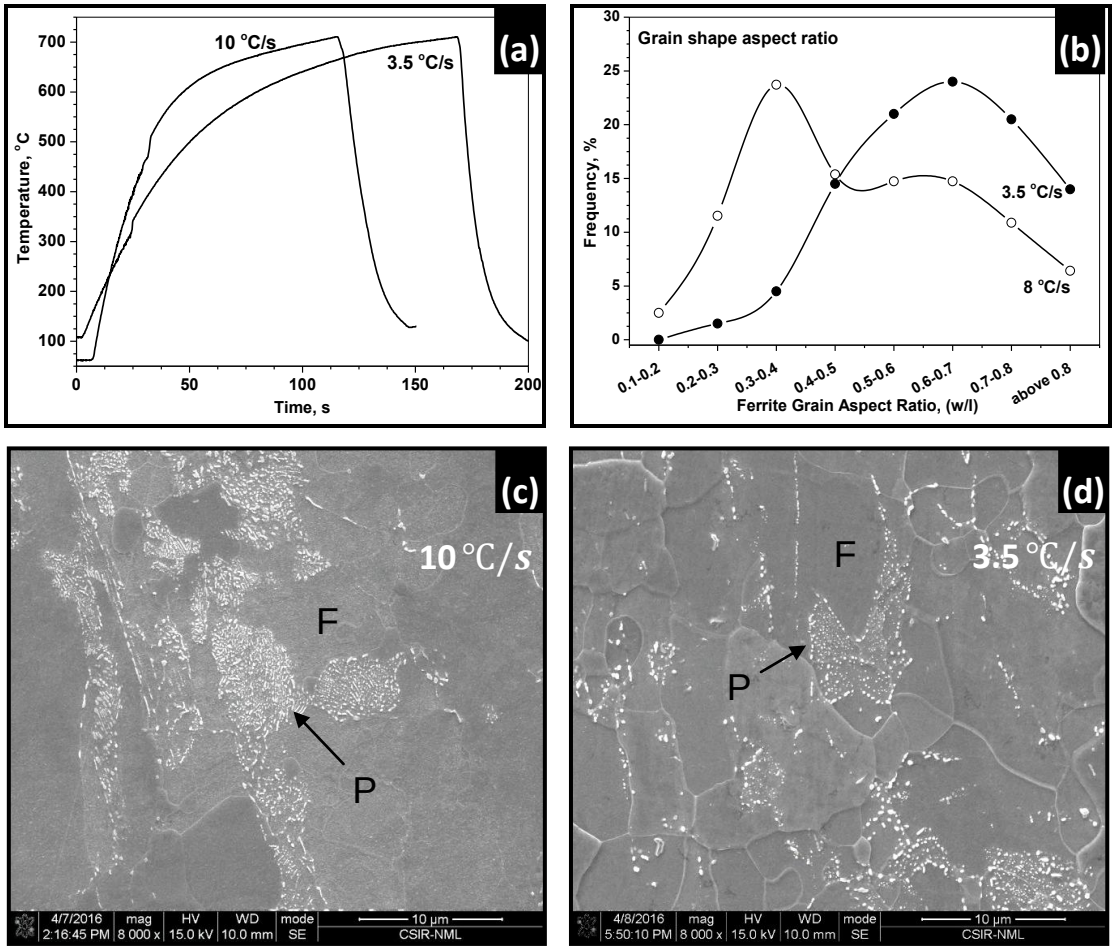

Figure 4.3 Effect of heating rate on ferrite recrystallization (a) time-temperature profile for annealing cycles, (b) grain shape aspect ratio curves, (c) SEM micrographs showing ferrite recrystallization at 10 ℃/s, and at (d) 3.5 ℃/s. F = Ferrite, P = pearlite.

Thus, the fine cementite particle dispersion obtained in the ferrite matrix (at slower heating rates) is expected to impose restriction on austenite growth. Hence, the martensite size distribution was also expected to be influenced by the above factors. Therefore, initial heating (heating rate followed) to reach the heat treatment temperature (just below Ac_1) tends to modify the ferrite and pearlite morphologies. Hence, altering (slowing down) the heating rate to reach the annealing temperature provides an opportunity to modify the DP microstructure.

4.5 Effect of Multiple Heating and Cooling Cycles on Ferrite/ Pearlite Structure

From the previous section, it was noted that variation in the heating rate affects the kinetics of ferrite recrystallization and pearlite dissolution (without phase transformation). Further, it is reported in literature that repetitive thermal cycling influences the ferrite recrystallization and pearlite dissolution process [51]. To investigate the effect of rapid and repetitive heating cycles on ferrite and pearlite morphologies, several variations of thermal cycles were applied

to the said steel. A typical example of such cycles is shown in Figure 4.4a and the resulting microstructure is shown in Figure 4.4b.

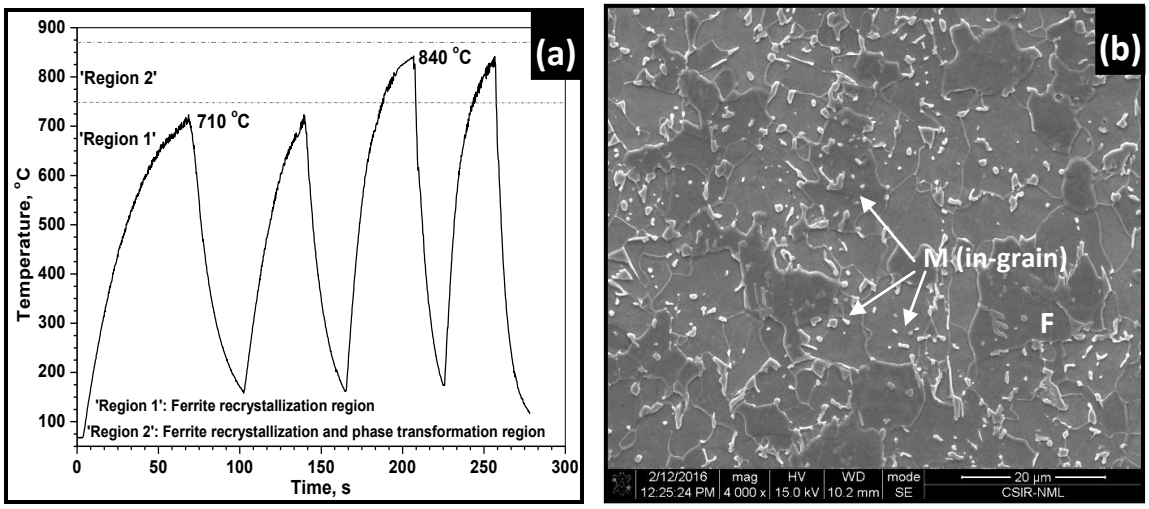

Figure 4.4 (a) Temperature-time profile of repeated annealing process, and (b) SEM micrograph showing finely dispersed second phase. F = Ferrite, M = Martensite.

The first two thermal cycles were conducted at a sub-critical temperature of 710 ℃, which was expected to predominantly facilitate recrystallization of deformed ferrite/ pearlite microstructure. Thereafter, this recrystallized microstructure with dispersed pearlite was subjected to high temperature heating (at 840 ℃) wherein phase transformation was anticipated (see Figure 4.4a). The resulting microstructure showed well dispersed fine globular and lath martensite in a ferrite matrix (see Figure 4.4b). From the above simulations, it was confirmed that repetitive thermal cycling affects the final dual phase microstructure.

Martin et al [22] and Yang et al [38] reported that during inter-critical annealing, if the microstructure consists of elongated/ deformed ferrite grains, before start of phase transformation, grain boundaries becomes the preferential nucleation sites for austenite and thus result in coarse austenite and hence martensite in final DP microstructure. However, by facilitating ferrite recrystallization and pearlite dissolution before the onset of phase transformation, the austenite nucleates primarily at the dispersed cementite particles, resulting in fine austenite.

In the present study also, it seems that the first two thermal cycles resulted in ferrite recrystallization and pearlite dispersion which facilitated austenite nucleation at cementite particles in the subsequent cycle. This could be the reason for the in-grain martensite formation (see Figure 4.4b).

4.6 Simulation of the Industrial Continuous Annealing Process Line

Figure 4.5 illustrates the industrially used continuous annealing line process (CAL) simulated by using annealing simulator. The process parameters shown for CAL in Figure 4.5 are similar to as are used in the industrial annealing practice [13,37].

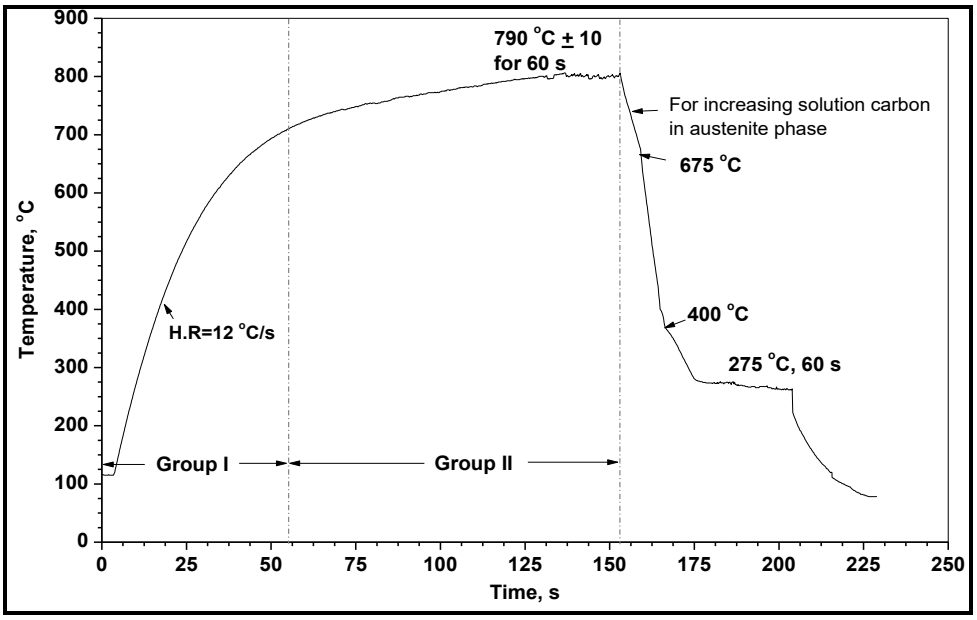

Figure 4.5 Typical temperature-time profile of industrial continuous annealing line (CAL) process [13,37,41].

The conventional CAL process (as is used in the industry; [13,37,41]) comprises of initial heating of the sample to the inter-critical temperature (here, 790 ℃), followed by isothermal holding (here, 60 s) and finally cooling to room temperature (along the route as described by Figure 4.5). The scope of the present work lies in modifying the heating and soaking steps (without any modification in the cooling route) for improved martensite morphology. The "heating and soaking" during CAL can be viewed as comprising of:

(i) Fast heating in the recrystallization zone (Group I; region where ferrite recrystallization is predominant). For example, in the present work (see Figure 4.5), the sample was initially heated to about 710 ℃ at a rate of 10–15 $℃/s$ (here, avg. heating rate was approximately 12 $℃/s$).

(ii) Moderate heating followed by isothermal soaking in the overlapping, 'phase transformation and recrystallization' zone (Group II; region where the two phenomena overlap). Here, it can be noted that beyond 710 ℃ and up to the peak temperature of 790 ℃, the heating rate was slow (about 1.06 ℃/s) followed by isothermal holding of 60 s.

One of the limitations of the existing CAL process is that due to the initial rapid heating till Ac_1, ferrite recrystallization and cementite/ carbide particles dispersion of pearlite is not able to complete during the heating step of annealing. Figure 4.6a shows the SEM micrograph of the CAL processed steel. The resulting microstructure was dual phase with ferrite and martensite phases. Martensite phase fraction was quantified by microstructure analysis (through 'analySIS FIVE' software) and was found to be around 17%. Further, it was noted that martensite was mostly associated with ferrite grain boundaries. The grain size distribution of the two phases is shown in Figure 4.6b–c.

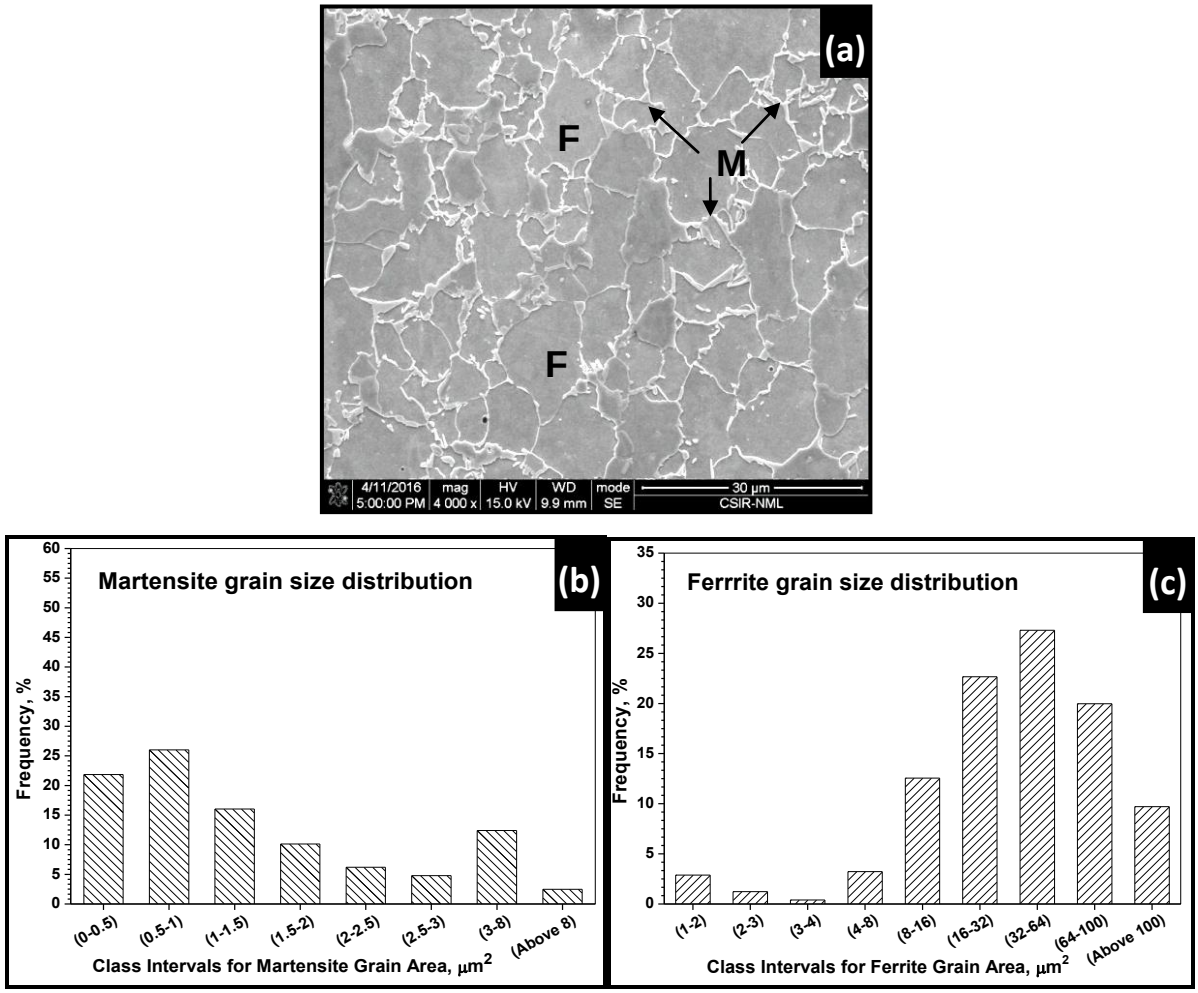

Figure 4.6 Microstructure of CAL processed DP590 steel (a) grain boundary network of martensite phase, (b) grain size distribution of martensite, and (c) ferrite. F = ferrite and M = martensite.

Martensite showed a large fraction of fine grains (see Figure 4.6b), whereas ferrite showed a recrystallized (comparing Figure 4.1a and Figure 4.6a) random distribution pattern (Figure 4.6c). CAL processed steel showed an ultimate tensile strength of 590 MPa (see Figure 4.9), which was as per the DP590 grade steel. This result of tensile testing also

validated the CAL simulation process. The above CAL process showed preferential formation of grain boundary martensite. The presence of martensite phase at grain boundaries is reported to affect the mechanical properties of steels under strain path changes [52].

From the previous sections, it was noted that by varying the heating rate, it is possible to engineer the austenite nucleation sites (and hence martensite distribution in the final DP microstructure). Also, it was noted that through rapid heating and cooling cycles (i.e. thermal cycling), a better dispersion of austenite nucleation sites (and hence better dispersion of martensite phase in the final DP microstructure) could be obtained. Thus, in order to obtain a starting microstructure with well dispersed cementite/ carbides (of initial pearlite) for the CAL process, it was decided to subject the as-received cold deformed steel to thermal cycling before subjecting it to CAL.

4.7 Simulations with Thermal Cycling as Pre-treatment to CAL

Initial rapid heating and cooling cycles were applied to the as-received steel before subjecting it to CAL. Several combinations of heating and cooling cycles (as pre-treatment), details of which are shown in Table 4.1 were applied to steel before subjecting it to CAL. All these efforts were classified into three main groups, depending upon the different physical phenomenon involved.

Table 4.1 Details of pre-heating rates, annealing temperatures, and ensuing mechanisms of annealing simulation process.

S. No	Annealing Process		Category/ Ensuing Mechanisms
	Initial Annealing Cycle	Final Annealing and Cooling Cycle	
1.	TC at 710 ℃ with two cycles at a heating rate of 10 ℃/s + TC at 840 ℃ with two cycles at a heating rate of 15 ℃/s.	CAL	**Group I:** Predominant deformed ferrite recrystallization phenomenon
2.	TC at 750 ℃ with two cycles at a heating rate of 10 ℃/s + TC at 840 ℃ with two cycles at a heating rate of 15 ℃/s.	CAL	**Group II:** Overlapping deformed ferrite recrystallization and phase transformation phenomena
3.	TC at 860 ℃ with four cycles at a heating rate of 10 ℃/s.	CAL	**Group III:** Predominant phase transformation phenomenon

Group I is classified as the zone of predominant ferrite recrystallization and consists of preferential ferrite recrystallization and pearlite dissolution (without phase transformation)

during controlled heating. Therefore, microstructure input for CAL (after the initial annealing cycle of Group 1) was recrystallized ferrite and well dispersed fine martensite. The resulting microstructure after the complete simulation is shown in Figure 4.7a. It may be noted from the microstructure that the initial ferrite recrystallization and pearlite dissolution (because of initial annealing cycle) lead to formation of well dispersed fine martensite (V_f=13%), mostly within the ferrite grains (as discussed in Section 4.5; shown in black circles in Figure 4.7a). Figure 4.8 shows ferrite grain size distribution pattern which is a random mono-modal distribution (for Group I) indicating complete ferrite recrystallization [46,53], as expected.

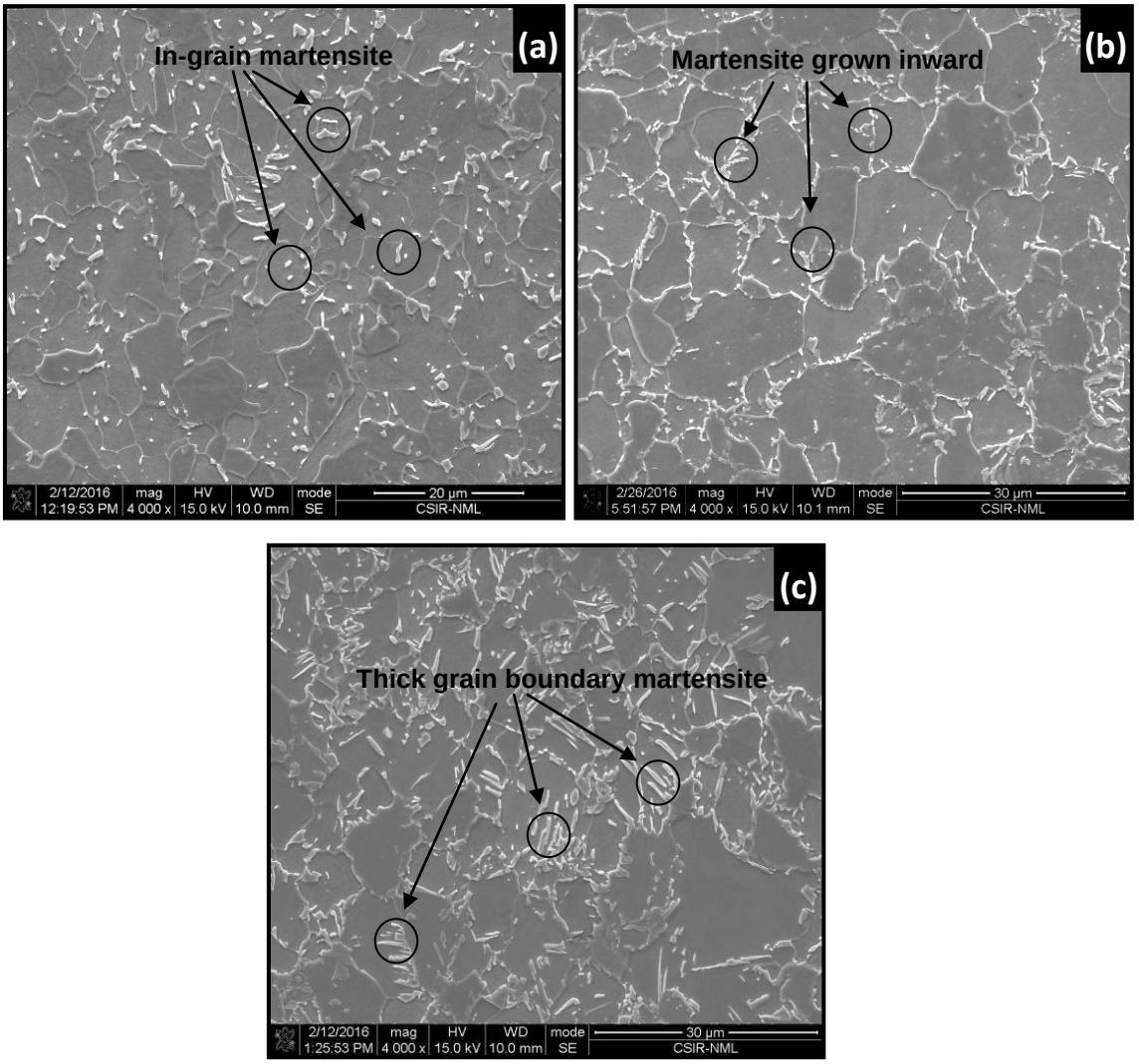

Figure 4.7 SEM micrographs showing distribution of martensite phase after the complete annealing based on thermal cycling pre-treatment (a) Group I showing in-grain martensite, (b) Group II showing necklace type martensite morphology with rapid grain growth, and (c) Group III showing thicker martensite.

For Group II, ferrite recrystallization and phase transformation are overlapping, causing austenite nucleation to occur concurrently with pearlite dissolution and ferrite recrystallization. Interestingly, martensite appeared to have nucleated mainly at the ferrite grain boundaries and also grew inwards into the grains (as shown in black circles in Figure 4.7b). Also, a necklace type martensite structure was observed under this condition which is consistent with observations reported by others [40,43]. Further, the fraction of martensite slightly increased (V_f=15%). It may be noted from Figure 4.8 that ferrite grain size distribution showed tendency for transition from mono-modal to bimodal distribution (for Group II) with small peak at smaller grain size values. This indicates heterogeneous grain growth behaviour with accelerated grain growth. Ferrite grain growth could be observed from the microstructure, as shown in Figure 4.7b. Peranio et al [44] reported that austenite nucleation and growth kinetics can be affected by recrystallization of ferrite grains at intermediate temperatures when grain boundary migration occurs rapidly. This may be reason for the observed fine martensite formation (thin laths) at ferrite grain boundary during this annealing cycle.

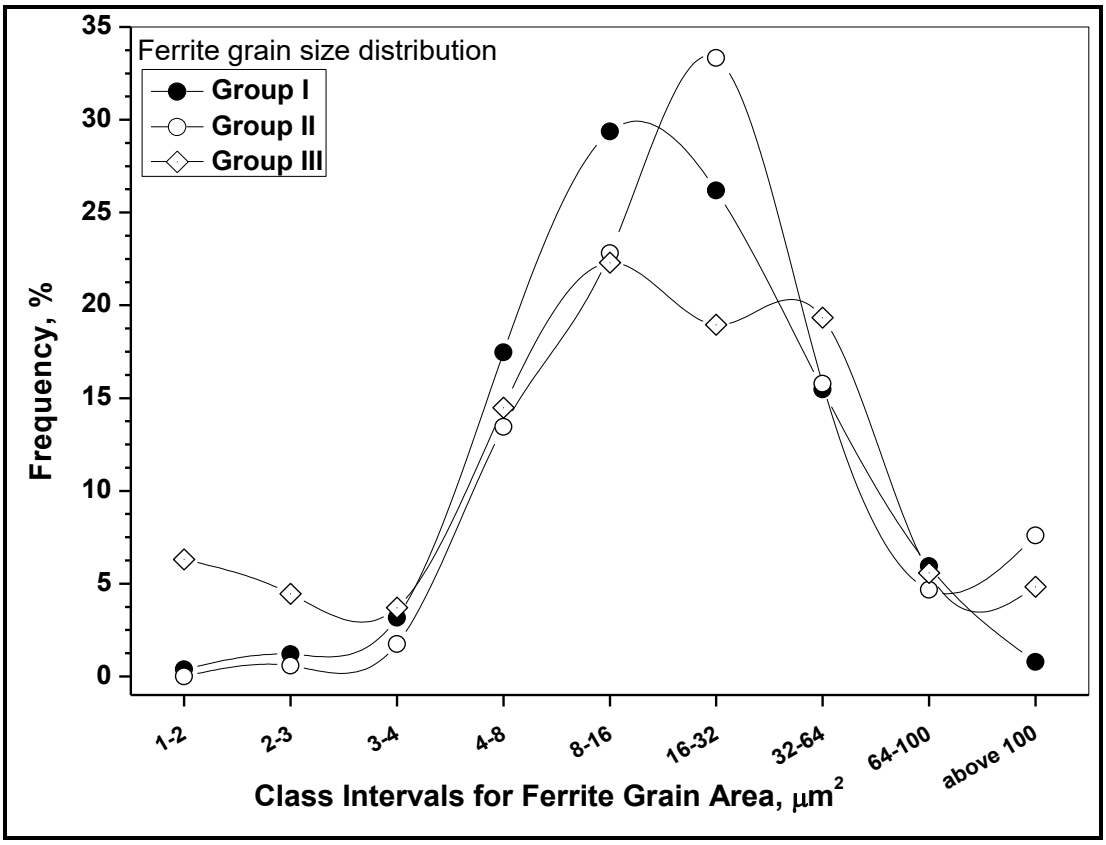

Figure 4.8 Ferrite grain size distributions for various annealing cycles with thermal cycling used as a pre-treatment for CAL.

Group III zone falls in the region where phase transformation is favoured over ferrite recrystallization due to high peak annealing temperature. It is well reported that increasing the annealing temperatures drastically accelerates the pearlite dissolution and results in instantaneous austenite nucleation and growth [49]. Figure 4.7c shows the microstructure obtained after subjecting the steel to CAL (with Group III as the initial annealing cycle). It can be noted from the micrographs that martensite fraction and its size increased due to increase in fraction of austenite formed resulting in a thick martensite network mainly at the grain boundaries (as shown in black circles in Figure 4.7c). Martensite fraction obtained at this annealing temperature was even more (V_f=19%). It is important to note (from Figure 4.8) that with annealing temperature close to Ac_3, a very distinct shift from mono-modal to bimodal grain size distribution in ferrite grain size results.

4.7.1 Mechanical Properties with Thermal Cycling as Pre-treatment to CAL

The engineering stress-strain curves of tensile samples subjected to processing as per Group I, II, and III (of Table 4.2) are shown in Figure 4.9.

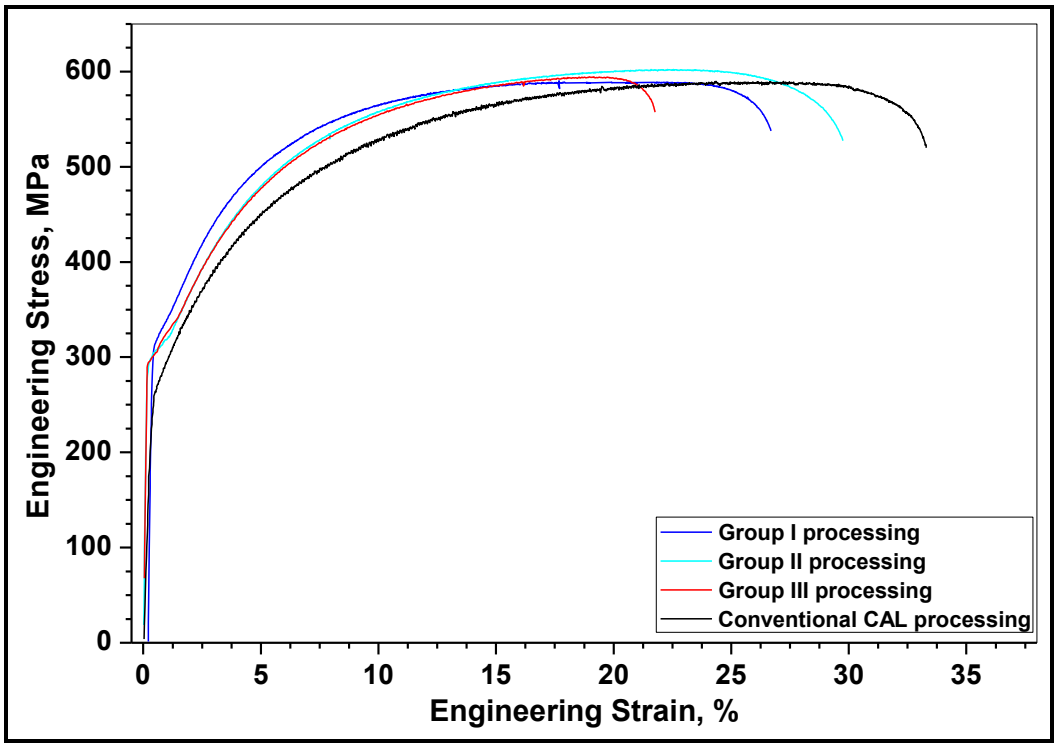

Figure 4.9 Stress-strain curves of steel specimens processed through CAL route with thermal cycling pre-treatment.

Steel samples subjected to Group I processing showed slightly better strength level as compared to CAL processed specimens despite the fact that martensite volume fraction in the

former case was lower than the latter case. Slight improvement in strength even with less martensite was attributed to the presence of finer ferrite grain size (because of better recrystallization) in the Group I processed specimen. However, these finer ferrite grains led to some loss in ductility also. An increase in strain hardening exponent was also observed by incorporating preferential ferrite recrystallization and pearlite dissolution before subjecting the steel to CAL (i.e. Group I processing). This could be the result of better strain partitioning due to fine in-grain martensite [54–58]. For sample processed using Group II processing, a slight improvement in strength and strain hardening exponent and a marginal decrease in ductility, as compared to the conventional CAL processed specimen was observed. The tendency of martensite grains to grow inwards into the ferrite grains could be the reason for slight improvement observed in strength and strain hardening for Group II processed samples.

For sample processed using Group III processing, ductility decreased severely as compared to the conventional CAL processed specimen with an improvement in strength. This can be attributed to the fact that with repetitive annealing cycles at high peak temperatures, instantaneous pearlite dissolution makes ferrite grain boundaries a preferential nucleation site for austenite [35,45]. This caused a network like thick martensite at ferrite grain boundaries resulting in excessive strain hardening with poor strain distribution and hence loss of ductility.

From the above studies, it was noted that significant improvements in mechanical properties were not observed with complete thermal cycling used as a pre-treatment to the conventional CAL cycle. Though, Group I processing route showed better strain hardening exponent and strength levels compared to CAL processed specimen, but the problem of ductility loss was to be addressed. Also, Group II showed best ductility values among the three processing routes. However, for Group III processed specimen, the ductility deteriorated severely. Since, Group I and Group II processing showed some promise, it was decided to modify them further.

4.8 Simulations with Modified Thermal Cycling as Pre-treatment to Modified CAL

The simulation effort of combining CAL with the thermal cycling pre-treatment (routes discussed in Table 4.1) did not bring significant improvements in the desired mechanical

properties. Out of the three main annealing routes (Group I, II, and III) discussed in the last section, it was observed that:

- With Group I processing, strain hardening exponent and strength improved as compared to conventional CAL process. However, a loss in ductility was observed.
- With Group II processing, strain hardening exponent improved slightly but the improvement was not as much as was with Group I processing. Strength also improved as compared to CAL. However, a slight loss in ductility was observed as compared to CAL.
- With Group III processing, strength level and strain hardening exponent were better than what were obtained through CAL. However, processing through this route led to severe loss in ductility. As a result, this route was not considered for further modification.

Keeping the above discussed points in view, processes in Group I and Group II (as shown in Table 4.1) were modified further. It was decided that for Group I and Group II processes, there was no need to utilize the complete CAL cycle after the initial annealing cycle (as was the case in Table 4.1). The modification proposed was that, after the initial annealing cycle, only the cooling route of the conventional CAL should be used (and not the complete heating, holding, and cooling route of CAL).

Table 4.2 Process parameters of modified annealing process based on thermal cycling.

S. No	Annealing Process		Category/ Ensuing Mechanism
	Initial Annealing Cycle	Final Annealing and Cooling Cycle	
1.	TC at 710 ℃ with two cycles at heating rate of 10 ℃/s + TC at 860 ℃ with two cycles at heating rate of 15 ℃/s (without quenching in the last cycle).	Cooling route of CAL process	**Group I:** Predominant deformed ferrite recrystallization phenomenon
2.	TC at 750 ℃ with two cycles at heating rate of 10 ℃/s + TC at 860 ℃ with two cycles at heating rate of 15 ℃/s (without quenching in the last cycle).	Cooling route of CAL process	**Group II:** Overlapping deformed ferrite recrystallization and phase transformation phenomenon

The detail of the modified processes is shown in Table 4.2. It can be noted that as compared to the earlier processing (as shown in Table 4.1), in the modified processing (as shown in Table 4.2), the final cooling step of the fourth thermal cycle, the initial heating step of the CAL cycle, and also the holding step of the CAL cycle have been eliminated. To compensate for the elimination of soaking step of CAL (to avoid any grain coarsening which holding can cause), the peak temperatures during the third and the fourth thermal

cycles of the initial annealing cycle were raised from 840 to 860 ℃. Figure 4.10 depicts the typical temperature-time profiles for the modified cycles. Figure 4.11a–b shows the SEM micrographs of the samples processed through the modified annealing process based on thermal cycling. For the Group I based processed specimen (see Table 4.2), the micrograph (see Figure 4.11a) showed an almost recrystallized microstructure, with fine ferrite grains and martensite largely at ferrite grain boundaries and few martensite needles within the ferrite grains (shown in black circles in Figure 4.11a).

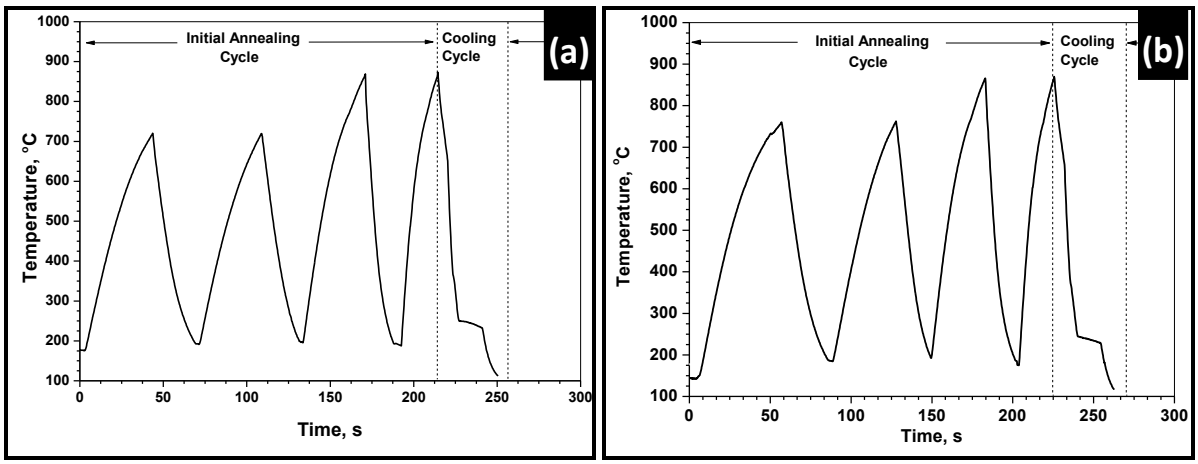

Figure 4.10 Typical temperature-time profile of the modified cycle based on thermal cycling (a) Group I, and (b) Group II.

For the Group II based processed specimen (see Table 4.2), the microstructure (see Figure 4.11b) showed slightly lesser recrystallization compared to Group I processed sample. It is very clearly visible from micrographs (Figure 4.11a–b) as well as grain size distribution curves (Figure 4.12a) that for Group I based specimen, finer ferrite grains were obtained. However, steel subjected to Group II based processing, showed relatively larger ferrite grain growth. The martensite volume fraction for Group I, and Group II based samples was 15% and 16% respectively.

It is evident that for both the processes, strength of steel increased (see Figure 4.12b) with better (or comparable) elongation as compared to CAL processed specimen. In addition, strain hardening also appeared to increase for both the processes, when continuous heating without isothermal holding was used. For modified Group I processed sample, the increased strength (as compared to CAL processed) could be due to the finer ferrite grain size with comparable martensite volume fraction (see Figure 4.6c and Figure 4.12a). Further, comparable ductility could be obtained, may be because of less dense martensite network at grain boundaries along with some in-grain martensite obtained through this processing route.

However, for Group II processed sample, the strength, and ductility were more than that for CAL processed specimen. On comparing Figure 4.6c and 4.12a, it may be noted that Group II processed sample showed finer ferrite grain size as compared to conventional CAL processed sample. Moreover, as compared to CAL processed samples, martensite formed for Group II processing was finer with less dense martensite network at ferrite grain boundaries (see Figure 4.6a and Figure 4.12b). Also some in-grain martensite can be observed for Group II processed samples (see Figure 4.12b). The above mentioned facts could be the reason for improved strength and ductility for Group II processed sample.

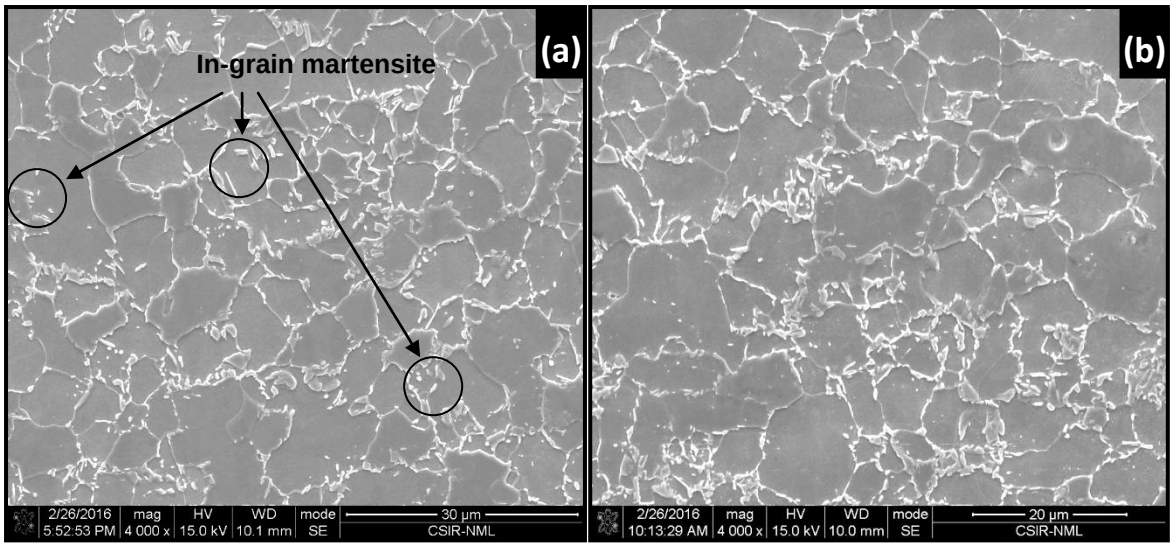

Figure 4.11 SEM micrographs showing distribution of martensite phase after complete annealing based on modified thermal cycling pre-treatment (a) Group I, and (b) Group II processing.

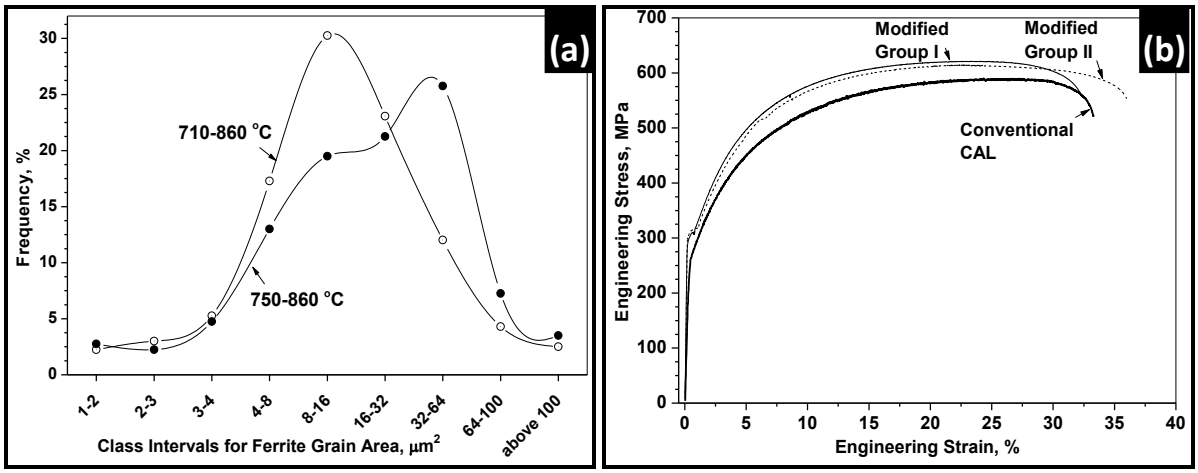

Figure 4.12 (a) Effect of annealing process parameters in continuous cycle on ferrite grain size distribution, (b) Tensile engineering stress-strain curves of steel process by continuous cycle with cooling regime similar to CAL.

Experiments were performed in the previous sections to develop a modified CAL processing route for improved mechanical properties of a given DP steel. The aim was to obtain superior mechanical properties by altering the martensite morphology and distribution through the modified annealing route. The following main observations with regards to the experimental simulations and the consequent results obtained were made. These observations were used as a means for further modification of the existing CAL route to develop a new processing route.

(i) It was observed that, allowing for more ferrite recrystallization and better cementite dispersion (of pearlite) before entering the inter-critical temperature range during heating step (of annealing) promotes formation of relatively more fine grained ferrite and martensite phases. It also results in formation of in-grain martensite (or at least a tendency of grain boundary martensite to start growing in towards inside of ferrite grains). Now, this all can be achieved either by slower heating (by slowing down the initial heating; see Figure 4.3a–d) to reach the inter-critical temperature range (as discussed in Section 4.4) or by subjecting the samples to repeated heating and cooling cycles (thermal cycling) with a subcritical peak temperature for the initial cycles (as discussed in Section 4.5).

(ii) During the conventional CAL processing, a soaking period is always provided as a part of Group II processing. The purpose of this soaking is to ensure the completion of recrystallization (which remains incomplete due to the fast heating rate during Group I processing of conventional CAL cycle), austenite nucleation and growth. The soaking period during CAL processing undertakes these three main activities. However, in light of point (i) as mentioned above, soaking time period provided during Group II processing can be eliminated. This is because, if slow heating rate is followed (during Group I processing; as discussed in point (i)), ferrite recrystallization would be almost complete before start of Group II processing. So, now if during Group II processing, any soaking is given, it will lead to grain growth of recrystallized ferrite and will also promote the tendency of austenite grains to nucleate at ferrite grain boundaries [37,45,49,59–61]. Thus, it was concluded that soaking step of conventional CAL processing can be eliminated. But, in order to obtain the same austenite and hence martensite volume fraction (as is in CAL), a higher peak temperature during Group III processing needs to be taken.

4.9 Development of the New Annealing Cycle

A review of the above conjecture formed the basis for the development of a novel continuous annealing cycle wherein different heating rates were employed during heating stage to modify the resulting morphology of martensite in the final dual phase microstructure.

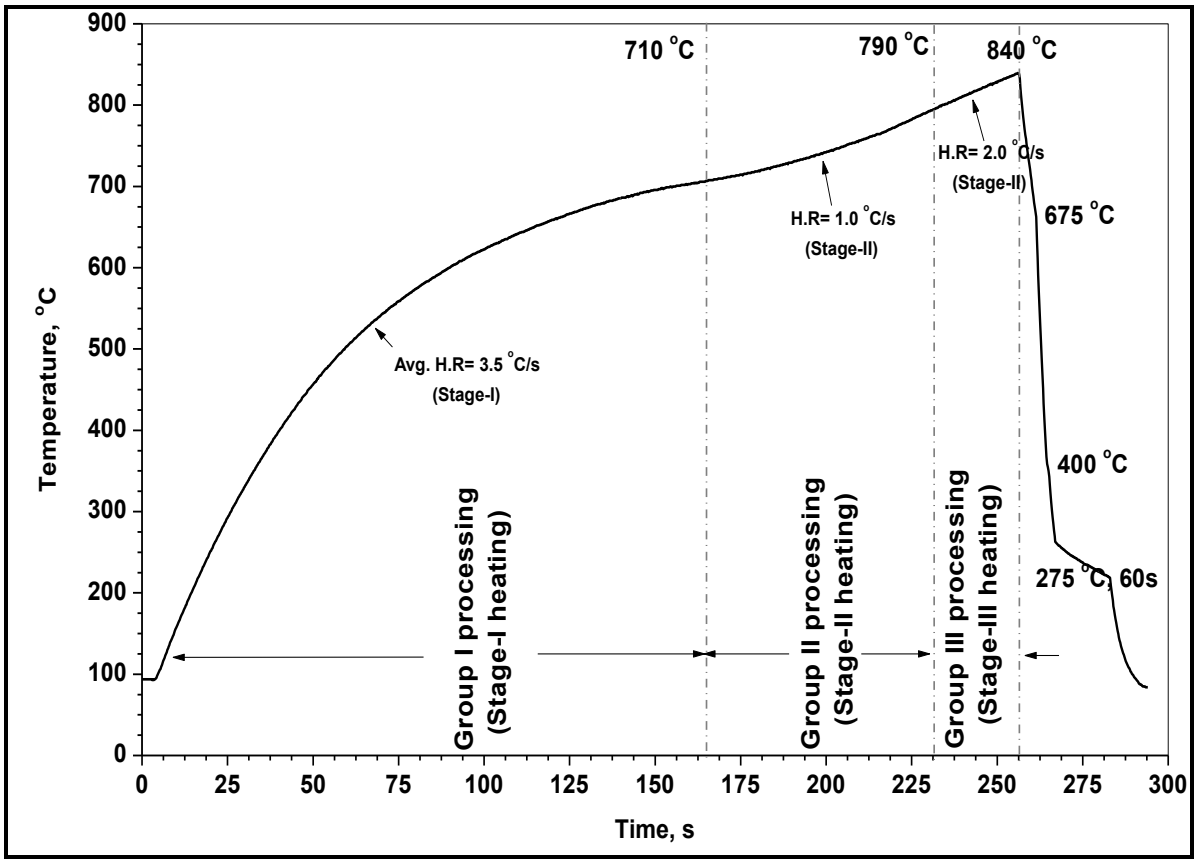

Figure 4.13 Typical temperature-time profile of the newly developed continuous heating annealing process (CHAP).

From the experimentation performed in previous sections, it was clear that allowing ferrite recrystallization before entering the inter-critical temperature range led to formation of fine ferrite as well as well dispersed martensite (which was also of small size). Therefore, in the proposed modified cycle, an attempt was made to slow down the heating rate during 'Stage-I' (Group I processing) of the continuous heating cycle. The motive was to allow for more ferrite recrystallization and better dispersion of cementite present in the original pearlite. So, in the modified cycle, the 'Continuous Annealing Heating Process (CHAP)', the temperature of 710 ℃ was reached at a relatively slower rate (an average heating rate of about 3.5 $℃/s$; see Figure 4.13) to allow for more ferrite recrystallization and better cementite dispersion (as compared to a faster heating rate of about 12 $℃/s$ during CAL; see Figure 4.5). Following this, during the second stage of continuous heating in the inter-critical range (i.e Group II

processing), a similar heating rate of 1 ℃/s was applied to reach the temperature of 790 ℃. This heating stage allowed further recrystallization of the remaining unrecrystallized grains, if any, (after the first stage of heating) along with slight growth of newly recrystallized ferrite grains (which formed during Stage-I heating). Also, during this Stage-II heating, it was expected that some austenite grains start to nucleate. The austenite nucleation was expected to occur at the dispersed carbide particles (of pearlite) due to the presence of high carbon concentration at these locations. Here, it should be noted that since cementite/ carbide particles are well dispersed, this effective dispersion may promote formation of austenite with fine grains. Also, in the CHAP processing, holding during Stage-II heating was eliminated. This was done to avoid ferrite and austenite grain growth. Therefore, during CHAP, instead of holding at the inter-critical annealing temperature of 790 ℃, heating was continued into the third stage (Stage-III heating) to a higher temperature of 840 ℃ at a heating rate of 2 ℃/s. The Stage-III temperature was chosen in a manner which would achieve similar austenite fraction (as in CAL) and without any grain coarsening. Peak annealing temperature of 840 ℃ met both these objectives effectively. Finally, cooling regime similar to CAL was used to complete the annealing cycle. Figure 4.13 depicts a typical CHAP annealing cycle utilized to produce DP microstructure. The ferrite-martensite dual phase microstructure obtained as a result of CHAP processing is shown in Figure 4.14a–c. Quantitative analysis showed about 18% martensite fraction in the final microstructure which was comparable to that obtained using CAL. The grain size distribution of phases present in the CHAP processed specimen is shown in Figure 4.15a–b.

The difference in morphology, distribution, and size of martensite phase obtained in the two DP microstructures (CAL and CHAP processed respectively) is evident from comparison of Figure 4.6a–c and Figure 4.14a–b/ Figure 4.15a–b respectively. It can be noted that for the CHAP processed specimen, the martensite phase was more uniformly distributed (see Figure 4.14a–b). Further, the martensite phase in the CHAP processed specimen was present both at the ferrite grain boundary regions and also within the ferrite grains (i.e. in-grain martensite; see Figure 4.14a–b) while only grain boundary martensite in CAL processed specimen (see Figure 4.6a). With regards to grain size, the CAL processed specimen showed a mixture of fine to medium sized martensite (see Figure 4.6b), whereas CHAP processed specimen showed a peak distribution of relatively finer martensite (see Figure 4.15a). The ferrite grain size distribution in the two cases was almost similar with slightly finer grains in CHAP processed specimen.

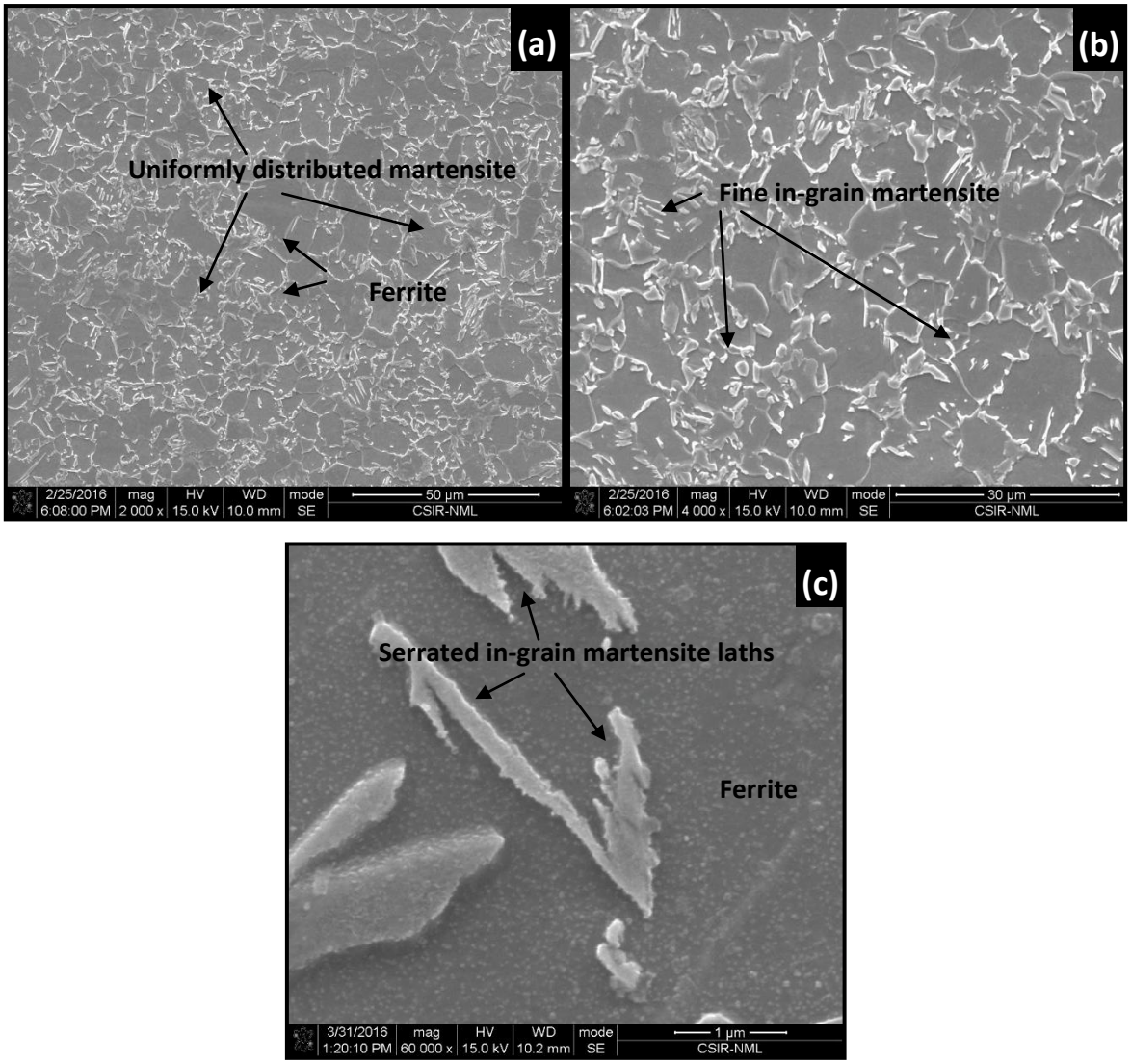

Figure 4.14 Microstructure evolution during continuous heating annealing cycle (CHAP) showing (a) uniform distribution of martensite phase (b) preferential in-grain martensite, and (c) serrated martensite lath interfaces.

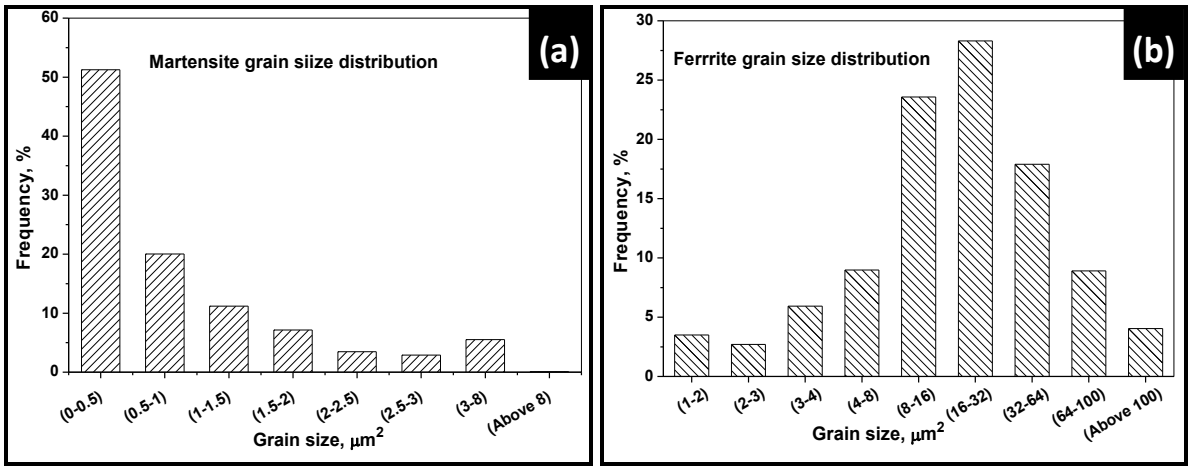

Figure 4.15 Grain size distribution of martensite and ferrite in specimens processed CHAP.

Further, the interface of in-grain martensite laths showed a serrated feature, which was unique to CHAP processed specimens (see Figure 4.14c). This could be due to the multi-variant austenite growth (tendency of austenite to grow in multiple directions). It is predicted that since during CHAP processing there was no soaking in the inter-critical temperature range, so austenite growth was non-uniform. This non-uniform growth did not allow different austenite growth fronts to merge properly thereby resulting in a serrated lath interface for martensite formed during subsequent quenching [62]. However, for the CAL processed samples, a definite soaking period in the inter-critical temperature range (Group II processing; see Figure 4.5) allowed the austenite growth fronts to merge and form into a sharp ferrite-martensite interface.

4.9.1 Nano-Indentation Analysis

Further, the phases present were characterized using nano-indentation hardness measurements (ferrite grains as well as globular/ lath shaped martensite grains). Figure 4.16 shows the results (one typical measurement) for both CAL and CHAP processed steel.

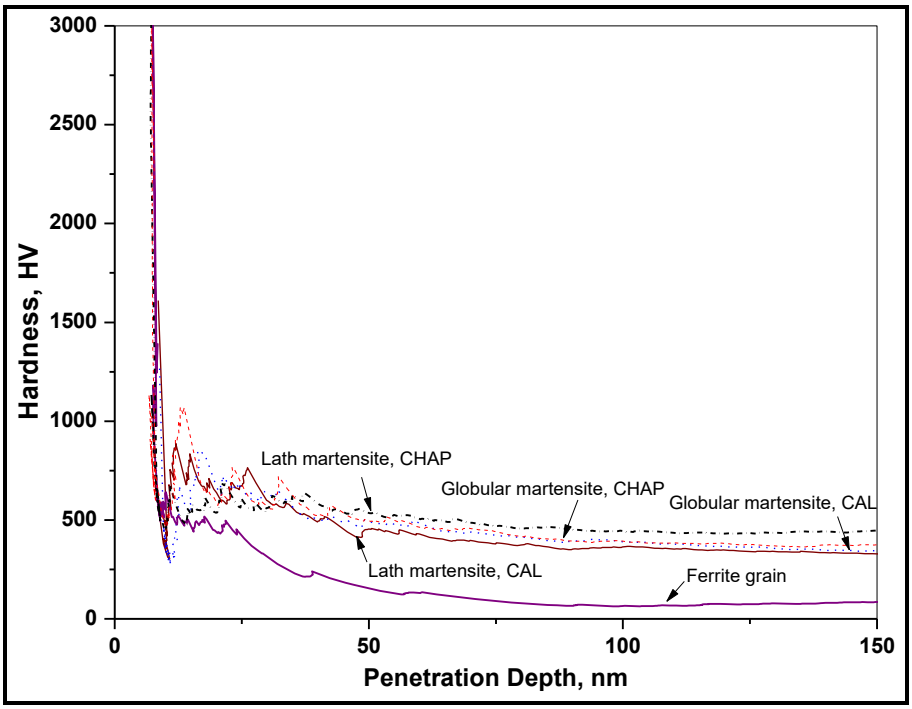

Figure 4.16 Hardness versus penetration depth plots for CAL and CHAP.

The average hardness (8 measurements for each phase) of martensite phase (globular and lath type) for the CHAP processed specimen was observed to be slightly higher (384 HV) than for the CAL processed specimen (348 HV). However, these values confirmed the presence of

martensite phase [63–65]. The relatively higher martensite hardness for CHAP processed specimen was attributed to the increase in carbon in martensite phase. The elimination of soaking time period (as was in CAL) and consequently heating to higher annealing temperature (840 ℃) during CHAP process resulted in formation of carbon rich austenite. This happened because of the high peak temperature which enhanced the carbon partitioning in the austenite, and resulted in more carbon in martensite formed on subsequent quenching (as compared to that obtained during CAL processing) [13]. This carbon rich martensite increased the tetragonality of body-centered tetragonal lattice of martensite, which resulted in higher hardness for martensite phase [66]. Further, ferrite grains showed an average hardness of about 150 HV for both the processes. This value confirmed the presence of ferrite phase [63,64].

4.10 Comparison of Mechanical Properties of CAL and CHAP Processed Specimens

This section evaluates and compares the mechanical properties of specimens processed through the conventional CAL process and the newly developed CHAP cycle. Figure 4.17 shows the tensile curves of the two processes.

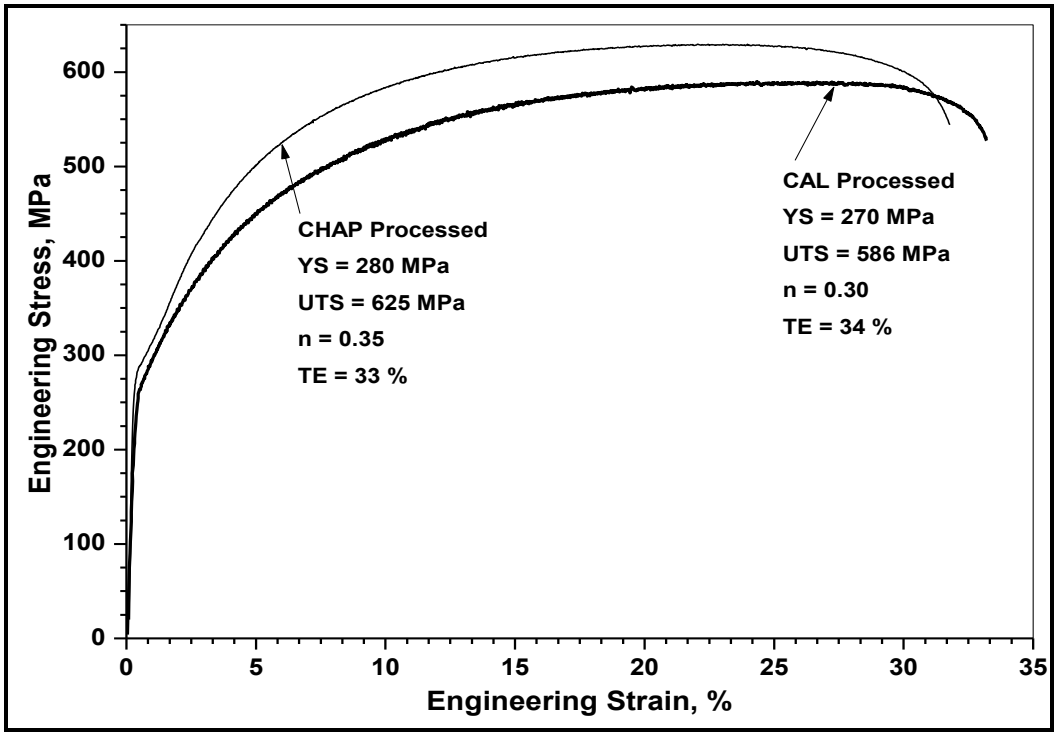

Figure 4.17 Comparison of tensile properties of steel specimens processed through the CAL and CHAP processing routes.

It can be observed from the tensile flow curves that CHAP processing resulted in a significantly improved strength of about 625 MPa along with increase in the strain hardening exponent without any significant loss in ductility. The increase in ultimate tensile strength for the specimen processed through CHAP processing route was attributed to the better distribution of martensite throughout the ferrite matrix, thus strengthening the ferrite phase [17,56]. Moreover, the increase in martensite hardness also contributed towards the increased strength [28,67,68]. Further, the presence of a considerable fraction of in-grain martensite in the CHAP processed specimen resulted in better strain partitioning between ferrite and martensite phases, and thus, helped in achieving better strain hardening properties with good ductility [54,56,57]. Also, the serrated nature of martensite lath interface could be the reason for achieving good combination of strength and ductility for the CHAP processed specimen compared to the CAL processed specimen (with typical sharp martensite interface). It is predicted that presence of serrated ferrite-martensite interface makes it difficult for the voids to nucleate and grow. This is because with the serrated type interface in CHAP processed specimen, the change in hardness occurs less abruptly, thus delaying the possibility of interface delamination [56,69] and therefore providing better strength-ductility combination.

Chapter 5
Conclusions

5.1 General

Dual-phase steels derive their properties via the second hard phase, namely; martensite and bainite present in a ferrite matrix. Their composite nature of the microstructure offers very attractive mechanical properties which is suitable to automotive industry. These steels are mostly produced through continuous annealing route in the industry because of high production rates, uniformity in properties, and leaner chemistry design feasibility.

In the present study, experimental simulation of various annealing parameters was carried out on cold rolled steel using a custom designed annealing simulator. The evolution of microstructure was studied using field emission scanning electron microscopy. The evolving microstructures were correlated with governing mechanisms viz. recrystallization, pearlite dissolution, and phase transformation. Through these simulations it was possible to tailor the microstructure and consequently tensile properties of the investigated dual phase steel.

5.2 Results and Conclusions

The main results from the present study are:

Starting Material

- The starting cold rolled material was composed of deformed ferrite and destructed pearlite colonies distributed non-uniformly in the ferrite matrix. Pearlite was present as big chunks at martensite grain boundaries.
- Quantitative analysis of microstructure showed volume fraction of phases as 84% ferrite and 16% pearlite.

Gleeble Dilation Study

- At slower heating rate of 5 ℃/s, the estimated inter-critical temperatures were Ac_1 = 743 ℃ and Ac_3 = 860 ℃. At higher heating rate of 20 ℃/s, a small shift was observed in Ac_3 (873 ℃) without any significant change in Ac_1 (745 ℃). Thus, with change in heating rate, significant changes in the inter-critical temperatures were not observed.

Annealing Simulations and Microstructure Analysis

Effect of heating rate on ferrite recrystallization and pearlite dissolution

- Although, heating rate used for the present work did not change the inter-critical temperature range, its effect on the ferrite recrystallization and pearlite dissolution (without phase transformation) had to be investigated. This was done by heating the specimen to a sub-critical temperature (of 710 ℃) with two different heating rates (3.5 $℃/s$ and 10 $℃/s$) and subsequently quenching to room temperature.
- It was observed from microstructure analysis and ferrite grain aspect ratio (w/l) that by slowing down the initial heating rate before entering the inter-critical temperature range, better cementite dispersion and ferrite recrystallization was achieved. This ferrite recrystallization before austenite nucleation promoted in-grain martensite formation. Also, during further heating to high annealing temperatures, grain boundary martensite formation was minimized by facilitating ferrite recrystallization and pearlite dispersion during the initial heating stage.

Thermal cycling as pre-treatment

- Thermal cycling can be used as a pretreatment to the conventional continuous annealing process. This pretreatment (if done at subcritical temperature; 710 ℃ in the present work) facilitates ferrite recrystallization and better carbide dispersion of pearlite, thus providing a well recrystallized microstructure as an input to CAL process.
- When thermal cycling at intermediate (750 ℃ in the present work; Group II processing) and high peak temperatures (840 ℃ in the present work; Group III processing) was combined with CAL cycle, no significant improvement in final microstructure was observed. It was predicted that the benefit of initial thermal cycles was lost during CAL heating and isothermal soaking.
- However, using thermal cycling as a pre-treatment to CAL by eliminating the heating and soaking stages of CAL showed promising results and a good combination of strength and ductility was achieved (UTS>600 MPa with ductility similar to CAL).

Continuous heating annealing process (CHAP) cycle

- A new continuous annealing process was developed which involved continuous heating to peak temperature of 840 ℃ with a slow heating rate of 3.5 $℃/s$ in subcritical region

(up to 710 ℃) to facilitate ferrite recrystallization and carbide dispersion. No isothermal soaking was given during this annealing cycle and specimens were quenched using the cooling regime of conventional CAL cycle. This new annealing route resulted in in-grain martensite formation with serrated lath interfaces. This type of martensite was observed to improve the tensile properties of dual phase microstructure (UTS = 625MPa and TE = 33%).

Tensile Properties

- Steel specimen in which recrystallization was complete before the onset of phase transformation (Group I, modified Group I) showed strength levels similar/ or higher than CAL processed specimen with comparable uniform elongation. An increase in strain hardening was also observed by incorporating preferential ferrite recrystallization and pearlite dissolution.
- For Group II (zone of overlapping ferrite recrystallization and phase transformation), strength was similar to that for CAL processed specimen with slightly lower ductility. Also, a slight increase in strain hardening exponent was observed due to the presence of martensite growing into the ferrite grains.
- However, for Group III, strength was slightly better whereas, ductility decreased severely compared to CAL. This was because repeated annealing cycles at a high peak temperature led to instantaneous pearlite dissolution and austenite nucleation. This made ferrite grain boundaries a preferential nucleation site for austenite (and hence martensite formation), thereby deteriorating the ductility.
- For annealing routes (modified Group I, and modified Group II) involving thermal cycling as pre-treatment to a peak temperature of 860 ℃ followed by cooling regime similar to conventional CAL process (without isothermal soaking) showed increase in strength (above 600 MPa), increase in strain hardening exponent, with comparable or better elongation than CAL processed specimen.
- The new annealing route (CHAP) resulted in significant fraction of in-grain martensite with serrated lath interfaces. The presence of in-grain martensite improved the strain partitioning between ferrite and martensite phases. These changes in distribution, size, and morphology of second phase (martensite) resulted in improved tensile properties of dual phase microstructure (UTS = 625 MPa and TE = 33%) as compared to conventional CAL cycle (UTS = 586 MPa and TE = 34%).

5.3 Major Conclusions

- When a cold-rolled ferrite-pearlite steel is subjected to continuous annealing, the ferrite recrystallization, carbide dispersion, and phase transformation are vital mechanisms for formation of DP microstructure. These physical phenomena can occur successively or concurrently, depending upon heating rate, annealing temperature, and soaking time for a given composition of the steel. Especially, at intermediate inter-critical annealing temperatures, complex interactions of various physical phenomena occur. Owing to the complexity of these mechanisms, minor variation in the annealing parameters (which control these interactions) can significantly affect the resulting dual phase microstructure. Therefore, understanding the interactions of these mechanisms can pave way for microstructure tailoring of dual phase steels according to specific strength-ductility requirements.
- A significant fraction of fine grain boundary martensite and in-grain martensite can be achieved by enabling ferrite recrystallization and pearlite dissolution (without phase transformation) during the initial stage of continuous annealing process. This in-grain martensite can improve strain partitioning between the ferrite and martensite phases, thus providing better mechanical properties.
- The newly developed, Continuous Heating Annealing Process (CHAP) resulted in changes in the second phase distribution, size, and morphology. As compared to the conventional CAL process (where second phase was mainly present at ferrite grain boundaries, and interface was typically sharp), the second phase (martensite) in CHAP process was distributed both at grain boundaries and within ferrite grains. Also, martensite was relatively finer and the martensite lath interfaces were serrated in nature. These changes in the second phase resulted in improved strength-ductility combination in the DP steel processed through CHAP route.

5.4 Scope for Future Work

In the present study, the influence of ferrite recrystallization and pearlite dissolution during the initial heating stage of continuous annealing process was investigated. An attempt was made to control the austenite nucleation and growth kinetics during inter-critical annealing by simulating conditions similar to industrial continuous annealing lines used for production of commercial DP590 grade steel. By incorporating preferential ferrite recrystallization and pearlite dissolution, dual phase microstructure with fine martensite distributed uniformly

throughout the microstructure with a significant fraction of in-grain martensite was achieved. Interestingly, a significant fraction of martensite showed serrated interface.

- However, further investigations are needed to explain the origin of serrated martensite interface which was essentially responsible for improved mechanical properties. TEM analysis could provide an insight into the interfacial properties of ferrite-martensite interface.
- Moreover, the strain hardening behaviour and deformation mechanisms can be studied in detail. Further research can focus on the hole expansion properties of steel produced through this new processing route (CHAP).
- The current investigation used a cold rolled low carbon Si based ferrite-pearlitic steel. The investigations with regards to effect of different annealing parameters and physical phenomena on microstructure evolution can be done with a hot rolled low carbon steel as the starting material.

References

[1] Baluch N, Udin ZM, Abdullah CS. Advanced high strength steel in auto industry: An overview. J Eng Technol Appl Sci Res 2014;4:686–9.

[2] Fish M.P. The international steel trade. 1st ed. Woodhead Publishing Limited; 1995.

[3] Demeri YM. Advanced high strength steels: science, technology, and applications. 1st ed. ASM Internationals; 2013.

[4] Matlock DK, Speer JG, Moor E De, Gibbs PJ. Recent developments in advanced high strength sheet steels for automotive applications: An overview. J Eng Sci Technol 2012;15:1–12.

[5] Mittal A. Dual phase steels. http://automotive.arcelormittal.com (accessed June 10, 2016).

[6] Mesplont C. Phase transformations and microstructure-mechanical properties relations in complex phase high strength steels. Ghent University, 2002.

[7] Cornet X, Herman JC. Method for making a multiphase hot-rolled steel strip. US20030041933 A1, 2003.

[8] Saleh MH, Priestner R. Retained austenite in dual-phase silicon steels and its effect on mechanical properties. J Mater Process Technol 2001;113:587–93. doi:10.1016/S0924-0136(01)00638-0.

[9] Erdogan M, Tekeli S. The effect of martensite particle size on tensile fracture of surface-carburised AISI 8620 steel with dual phase core microstructure. Mater Des 2002;23:597–604. doi:10.1016/S0261-3069(02)00065-1.

[10] Demir B, Erdogan M. The hardenability of austenite with different alloy content and dispersion in dual-phase steels. J Mater Process Technol 2008;208:75–84.

[11] Adamczyk J, Grajcar A. Structure and mechanical properties of DP-type and TRIP-type sheets obtained after the thermomechanical processing. J Mater Process Technol 2005;162–163:267–74. doi:10.1016/j.jmatprotec.2005.02.032.

[12] Meng Q, Li J, Wang J, Zhang Z, Zhang L. Effect of water quenching process on microstructure and tensile properties of low alloy cold rolled dual-phase steel. Mater Des 2009;30:2379–85. doi:10.1016/j.matdes.2008.10.026.

[13] Tasan CC, Diehl M, Yan D, Bechtold M, Roters F, Schemmann L, et al. An overview of dual-phase steels: Advances in microstructure oriented processing and micromechanically guided design. Annu Rev Mater Sci 2015;45:391–431.

[14] Kuziak R, Kawalla R, Waengler S. Advanced high strength steels for automotive

industry. Arch Civ Mech Eng 2008;8:103–17. doi:10.1016/S1644-9665(12)60197-6.

[15] Zhang H, Johansson B, Ahuja R, Vitos L. First-principles study of solid-solution hardening in steel alloys. Comput Mater Sci 2012;55:269–72. doi:10.1016/ j.commatsci.2011.12.020.

[16] Callister WD, Rethwisch DG. Materials science and engineering: An introduction. 9th ed. Wiley; 2013.

[17] Calcagnotto M, Ponge D, Raabe D. Effect of grain refinement to 1μm on strength and toughness of dual-phase steels. Mater Sci Eng A 2010;527:7832–40. doi:10.1016/ j.msea.2010.08.062.

[18] Avner SH. Introduction to physical metallurgy. 2nd ed. Tata McGraw Hill Education Private Limited; 2007.

[19] ULSAB-AVC: safe, affordable, fuel efficient vehicle concepts for the 21st century designed in steel. 2002.

[20] Patel J, Klinkenberg C, Hulka K. Hot rolled HSLA strip steels for automotive and construction applications. Niobium Sci Technol 2001;100:647–74.

[21] Erdogan M, Tekeli S. The effect of martensite volume fraction and particle size on the tensile properties of a surface-carburized AISI 8620 steel with a dual-phase core microstructure. Mater Charact 2002;49:445–54. doi:10.1016/S1044-5803(03)00070-6.

[22] Adamczyk J, Grajcar A. Effect of heat treatment conditions on the structure and mechanical properties of DP-type steel. J Achiev Mater Manuf Eng 2006;17:305–8.

[23] Santofimia MJ, Zhao L, Petrov R, Sietsma J. Characterization of the microstructure obtained by the quenching and partitioning process in a low-carbon steel. Mater Charact 2008;59:1758–64. doi:10.1016/j.matchar.2008.04.004.

[24] Sudersanan PD, Kori N, Aprameyan S, Kempaiah UN. The effect of carbon content in martensite on the strength of dual phase steel. Int J Ind Eng Manag Sci 2012;2:1–4.

[25] Mittal M. Effect of inter-critical annealing parameters on the recrystallization, austenite formation and stabilization in a dual phase steel. Thapar university, 2014.

[26] Sebek M, Hornak P, Zimovcak P, Longauer S. Microstructure evolution and mechanical properties of C-Mn cold rolled dual phase steel after continuous annealing process in laboratory conditions. Arch Metall Mater 2014;59:821–4.

[27] Kalashami GA, Kermanpur A, Najafizadeh A, Mazaheri Y. The effect of intercritical annealing time on the microstructures and mechanical properties of an ultrafine grained dual phase steel containing niobium. Int J ISSI 2014;11:7–11.

[28] Concepción VL, Lorusso HN, Svoboda HG. Effect of carbon content on

microstructure and mechanical properties of dual phase steels. Procedia Mater Sci 2015;8:1047–56. doi:10.1016/j.mspro.2015.04.167.

[29] Zhang J, Di H, Deng Y, Misra RDK. Effect of martensite morphology and volume fraction on strain hardening and fracture behavior of martensite-ferrite dual phase steel. Mater Sci Eng A 2015;627:230–40. doi:10.1016/j.msea.2015.01.006.

[30] Li C, Li Z, Cen Y, Biao M, Huo G. Microstructure and mechanical properties of dual phase strip steel in the overaging process of continuous annealing. Mater Sci Eng A 2015;627:281–9.

[31] Maresca F, Kouznetsova VG, Geers MGD. Deformation behaviour of lath martensite in multi-phase steels. Scr Mater 2016;110:74–7. doi:10.1016/j.scriptamat.2015.08.004.

[32] Zhang F, Ruimi A, Ching P, Field DP. Morphology and distribution of martensite in dual phase (DP980) steel and its relation to the multiscale mechanical behavior. Mater Sci Eng A 2016;659:93–103.

[33] Ayatollahi MR, Darabi AC, Chamani HR, Kadkhodapo J. 3D micromechanical modeling of failure and damage evolution in dual phase steel based on a real 2D microstructure. Acta Mech Solida Sin 2016;29:95–110. doi:10.1016/S0894-9166(16) 60009-5.

[34] Matlock DK, Speer JG. Processing opportunities for new advanced high-strength sheet steels. Mater Manuf Process 2010;25:7–13. doi:10.1080/10426910903158272.

[35] Li P, Li J, Meng Q, Hu W, Xu D. Effect of heating rate on ferrite recrystallization and austenite formation of cold-roll dual phase steel. J Alloys Compd 2013;578:320–7. doi:10.1016/j.jallcom.2013.05.226.

[36] Kwon OJ, Lee KY, Kim GS, Chin KG. New trends in advanced high strength steel developments for automotive application. Mater Sci Forum 2010;638-642:136–41. doi:10.4028/www.scientific.net/MSF.638-642.136.

[37] Li P, Li J, Meng Q, Hu W, Xu D. Effect of heating rate on nucleation and growth of austenite in cold rolled dual phase steel. Ironmak Steelmak 2015;42:81–7. doi:10.1179/1743281214Y.0000000228.

[38] Zheng C, Raabe D. Interaction between recrystallization and phase transformation during intercritical annealing in a cold-rolled dual-phase steel: A cellular automaton model. Acta Mater 2013;61:5504–17. doi:10.1016/j.actamat.2013.05.040.

[39] Ogawa T, Maruyama N, Sugiura N, Yoshinaga N. Incomplete recrystallization and subsequent microstructural evolution during intercritical annealing in cold-rolled low carbon steels. ISIJ Int 2010;50:469–75. doi:10.2355/isijinternational.50.469.

[40] Huang J, Poole WJ, Militzer M. Austenite formation during intercritical annealing. Metall Mater Trans A 2004;35:3363–75. doi:10.1007/s11661-004-0173-x.

[41] Ghaheri A, Shafyei A, Honarmand M. Effects of inter-critical temperatures on martensite morphology, volume fraction and mechanical properties of dual-phase steels obtained from direct and continuous annealing cycles. Mater Des 2014;62:305–19. doi:10.1016/j.matdes.2014.04.073.

[42] Peranio N, Li YJ, Roters F, Raabe D. Microstructure and texture evolution in dual-phase steels: Competition between recovery, recrystallization, and phase transformation. Mater Sci Eng A 2010;527:4161–8. doi:10.1016/j.msea.2010.03.028.

[43] Masimov M, Peranio N, Springub B. EBSD study of substructure and texture formation in dual-phase steel sheets for semi-finished products. Solid State 2010;160:251–6. doi:10.4028/www.scientific.net/SSP.160.251.

[44] Peranio N, Roters F, Raabe D. Microstructure evolution during recrystallization in dual-phase steels. Recryst Grain Growth IV 2012;715–716:13–22. doi:10.4028/www.scientific.net/MSF.715-716.13.

[45] Yang DZ, Brown EL, Matlock DK, Krauss G. Ferrite recrystallization and austenite formation in cold-rolled intercritically annealed steel. Metall Trans A 1985;16:1385–92. doi:10.1007/BF02658671.

[46] Azizi-Alizamini H, Militzer M, Poole WJ. Austenite formation in plain low-carbon steels. Metall Mater Trans A 2011;42:1544–57. doi:10.1007/s11661-010-0551-5.

[47] Krielaart G, Sietsma J, Zwaag S Van Der. Ferrite formation in Fe-C alloys during austenite decomposition under non-equilibrium interface conditions. Mater Sci Eng A 1997;237:216–23. doi:10.1016/S0921-5093(97)00365-1.

[48] Militzer M. Phase field modeling of microstructure evolution in steels. Curr Opin Solid State Mater Sci 2011;15:106–15. doi:10.1016/j.cossms.2010.10.001.

[49] Speich GR, Demarest VA, Miller RL. Formation of austenite during intercritical annealing of dual-phase steels. Metall Trans A 1981;12:1419–28. doi:10.1007/BF02643686.

[50] Nakaoka K, Hosoya Y, Ohmura M, Nishimoto A. Structure and properties of dual phase steels. In: Kot RA, Morris JW, editors. Struct. Prop. dual phase steels, New York: 1979, p. 330–45.

[51] Kar M. Effect of thermal cycling on the structure mechanical properties and texture of a dual phase steel. Indian Institute of Technology, Kanpur, 1991.

[52] Nesterova EV, Bouvier S, Bacroix B. Microstructure evolution and mechanical

behavior of a high strength dual-phase steel under monotonic loading. Mater Charact 2015;100:152–62. doi:10.1016/j.matchar.2014.11.031.

[53] Patra S, Hasan SM, Narasaiah N, Chakrabarti D. Effect of bimodal distribution in ferrite grain sizes on the tensile properties of low-carbon steels. Mater Sci Eng A 2012;538:145–55. doi:10.1016/j.msea.2011.12.114.

[54] Colla V, De Sanctis M, Dimatteo A, Lovicu G, Solina A, Valentini R. Strain hardening behavior of dual-phase steels. Metall Mater Trans A 2009;40:2557–67. doi:10.1007/ s11661-009-9975-1.

[55] Fang XF, Gusek CO, Dahl W. Strain hardening of pearlitic and austenitic steels and the estimation of mechanical properties. Mater Sci Eng A 1995;203:26–35. doi:10.1016/0921-5093(95) 09842-9.

[56] Curtze S, Kuokkala VT, Hokka M, Peura P. Deformation behavior of TRIP and DP steels in tension at different temperatures over a wide range of strain rates. Mater Sci Eng A 2009;507:124–31. doi:10.1016/j.msea.2008.11.050.

[57] Sodjit S, Uthaisangsuk V. Microstructure based prediction of strain hardening behavior of dual phase steels. Mater Des 2012;41:370–9. doi:10.1016/j.matdes.2012.05.010.

[58] Colla V, De Sanctis M, Dimatteo A, Lovicu G, Solina A, Valentini R. Strain hardening behavior of dual-phase steels. Metall Mater Trans A 2009;40:2557–67. doi:10.1007/ s11661-009-9975-1.

[59] Martín SD, De Cock T, García-Junceda A, Caballero FG, Capdevila C, De Andrés CG. Effect of heating rate on reaustenitisation of low carbon niobium microalloyed steel. Mater Sci Technol 2008;24:266–72. doi:10.1179/174328408X265640.

[60] Shtansky DV, Nakai K, Ohmori Y. Pearlite to austenite transformation in an Fe-2.6Cr-1C alloy. Acta Mater 1999;47:2619–32. doi:10.1016/S1359-6454(99)00142-1.

[61] Oliveira FLG, Andrade MS, Cota AB. Kinetics of austenite formation during continuous heating in a low carbon steel. Mater Charact 2007;58:256–61. doi:10.1016/ j.matchar.2006.04.027.

[62] Asadi M, Goodarzi M, Kheirandish S. Kinetics of austenite formation in dual phase steels. ISIJ Int 2008;48:1251–5. doi:10.2355/isijinternational.48.1251.

[63] Craig B, L.Pohlman S. Metals handbook, ninth edition: volume 13 - corrosion (ASM handbook). ASM Met. Handb., vol. 13, 1987, p. 77–189. doi:10.1002/jbm.b.31896.

[64] Davis JR. Metals handbook. Met Handb 1998:2571. doi:10.1017/CBO978110 7415324.004.

[65] Bramfitt BL, Corporation BS. Structure/ property relationships in irons and steels. Met

Handb Desk Ed 1998;20:153–73.

[66] Waterschoot T, Verbeken K, De Cooman BC. Tempering kinetics of the martensitic phase in DP steel. ISIJ Int 2006;46:138–46. doi:10.2355/isijinternational.46.138.

[67] Lai Q, Brassart L, Bouaziz O, Gounz M, Verdier M, Parry G, et al. Influence of martensite volume fraction and hardness on the plastic behavior of dual-phase steels: Experiments and micromechanical modeling. Int J Plast 2016;80:187–203. doi: 10.1016/j.ijplas.2015.09.006.

[68] Choi KS, Liu WN, Sun X, Khaleel MA. Influence of martensite mechanical properties on failure mode and ductility of dual-phase steels. Metall Mater Trans A Phys Metall Mater Sci 2009;40:796–809. doi:10.1007/s11661-009-9792-6.

[69] Taylor MD, Choi KS, Sun X, Matlock DK, Packard CE, Xu L, et al. Correlations between nanoindentation hardness and macroscopic mechanical properties in DP980 steels. Mater Sci Eng A 2014;597:431–9. doi:10.1016/j.msea.2013.12.084.

virender report

ORIGINALITY REPORT

13%	2%	9%	3%
SIMILARITY INDEX	INTERNET SOURCES	PUBLICATIONS	STUDENT PAPERS

PRIMARY SOURCES

1	de la Concepción, Valeria L., Hernán N. Lorusso, and Hernán G. Svoboda. "Effect of Carbon Content on Microstructure and Mechanical Properties of Dual Phase Steels", Procedia Materials Science, 2015. Publication	3%
2	Li, Chang-sheng, Zhen-xing Li, Yi-ming Cen, Biao Ma, and Gang Huo. "Microstructure and mechanical properties of dual phase strip steel in the overaging process of continuous annealing", Materials Science and Engineering A, 2015. Publication	2%
3	Zhang, Jiecen, Hongshuang Di, Yonggang Deng, and R.D.K. Misra. "Effect of martensite morphology and volume fraction on strain hardening and fracture behavior of martensite–ferrite dual phase steel", Materials Science and Engineering A, 2015. Publication	2%
4	Submitted to Lovely Professional University Student Paper	1%